CERN-PH-TH/2004-085
hep-ph/0405091

Flavour Physics and CP Violation

ROBERT FLEISCHER

Theory Division, Department of Physics, CERN, CH-1211 Geneva 23, Switzerland

Abstract

The starting point of these lectures is an introduction to the weak interactions of quarks and the Standard-Model description of CP violation, where the key element is the Cabibbo–Kobayashi–Maskawa matrix and the corresponding unitarity triangles. Since the B-meson system will govern the stage of (quark) flavour physics and CP violation in this decade, it will be – after a brief look at the kaon system – our main focus. We shall classify B-meson decays, introduce the theoretical tools to deal with them, explore the requirements for non-vanishing CP-violating asymmetries, and discuss B_q^0–$\bar{B}_q^0$ mixing ($q \in \{d, s\}$). We will then turn to B-factory benchmark modes, discuss the physics potential of B_s^0 mesons, which is particularly promising for B-decay experiments at hadron colliders, and emphasize the importance of studies of rare decays, which are absent at the tree level in the Standard Model, complement nicely the studies of CP violation, and provide interesting probes for new physics.

Lectures given at the 2003 European School of High-Energy Physics,
Tsakhkadzor, Armenia, 24 August – 6 September 2003
To appear in the Proceedings (CERN Report)

Contents

FLAVOUR PHYSICS AND CP VIOLATION

Robert Fleischer
CERN, Geneva, Switzerland

Abstract
The starting point of these lectures is an introduction to the weak interactions of quarks and the Standard-Model description of CP violation, where the key element is the Cabibbo–Kobayashi–Maskawa matrix and the corresponding unitarity triangles. Since the B-meson system will govern the stage of (quark) flavour physics and CP violation in this decade, it will be – after a brief look at the kaon system – our main focus. We shall classify B-meson decays, introduce the theoretical tools to deal with them, explore the requirements for non-vanishing CP-violating asymmetries, and discuss B_q^0–$\bar{B}_q^0$ mixing ($q \in \{d, s\}$). We will then turn to B-factory benchmark modes, discuss the physics potential of B_s^0 mesons, which is particularly promising for B-decay experiments at hadron colliders, and emphasize the importance of studies of rare decays, which are absent at the tree level in the Standard Model, complement nicely the studies of CP violation, and provide interesting probes for new physics.

1 INTRODUCTION

The violation of the CP symmetry, where C and P are the charge-conjugation and parity-transformation operators, respectively, is one of the fundamental and most exciting phenomena in particle physics. Although weak interactions are not invariant under P (and C) transformations, as discovered in 1957, it was believed for several years that the product CP was preserved. Consider, for instance, the process

$$\pi^+ \to e^+ \nu_e \;\xrightarrow{\mathcal{C}}\; \pi^- \to e^- \nu_e^{\rm C} \;\xrightarrow{\mathcal{P}}\; \pi^- \to e^- \bar{\nu}_e, \tag{1.1}$$

where the left-handed $\nu_e^{\rm C}$ state is not observed in nature; only after performing an additional parity transformation we obtain the usual right-handed electron antineutrino. Consequently, it appears as if CP was conserved in weak interactions. However, in 1964, it was discovered through the observation of $K_{\rm L} \to \pi^+\pi^-$ decays that weak interactions are *not* invariant under CP transformations [1].

After its discovery, CP violation was, for a very long time, only accessible in the neutral kaon system, where it is described by two complex parameters, ε and ε'; a non-zero value of the latter could only be established – after tremendous efforts – in 1999 [2, 3]. In 2001, CP violation could then also be observed in decays of neutral B mesons [4, 5], which represents the beginning of a new era in the exploration of this phenomenon. Despite this impressive progress, we still have few experimental insights into CP violation, which originates, within the Standard Model (SM) of electroweak interactions, from the flavour structure of the charged-current interactions [6]. One of the main motivations for the exploration of CP violation is that "new" physics (NP), i.e. physics lying beyond the SM, is typically also associated with new sources of CP violation and new flavour structures [7]–[9]. This is actually the case in many specific NP scenarios, for instance in supersymmetry (SUSY), left–right-symmetric models, and in models with extended Higgs sectors. In this context, it is also interesting to note that the evidence for non-vanishing neutrino masses that we obtained over the last years points towards on origin beyond the SM [10, 11], raising – among other issues – also the question of having CP violation in the neutrino sector, which could be studied, in the more distant future, at dedicated neutrino factories [12].

Interestingly, we may also obtain indirect information on CP violation from cosmology. One of the characteristic features of our Universe is the cosmological baryon asymmetry of $\mathcal{O}(10^{-10})$ [13, 14]. As was pointed out by Sakharov [15], one of the necessary conditions to generate such an asymmetry of the

Universe is – in addition to baryon-number violation and deviations from thermal equilibrium – that the elementary interactions violate CP (and C). Model calculations indicate, however, that the CP violation present in the SM is too small to generate the observed matter–antimatter asymmetry of $\mathcal{O}(10^{-10})$ [16]. It is conceivable that the particular kind of NP underlying the baryon asymmetry is associated with very short-distance scales. In this case, it could not be seen in CP-violating effects in weak meson decays. However, as we have noted above, there are also various scenarios for physics beyond the SM that would affect these processes. Moreover, we do not understand the observed patterns of quark and lepton masses, their mixings and the origin of flavour dynamics in general. It is likely that the NP required to understand these features is also related to new sources of CP violation.

The field of (quark) flavour physics and CP violation is very broad. In this decade, it will be governed by studies of decays of B mesons. The asymmetric e^+e^- B factories operating at the $\Upsilon(4S)$ resonance [17], with their detectors BaBar (SLAC) and Belle (KEK), have already been taking data for a couple of years and have produced plenty of exciting results. Moreover, also hadron colliders have a very promising potential for the exploration of B-meson decays. We may expect first interesting results on several processes from run II of the Tevatron soon [18]. The corresponding channels can then be fully exploited in the era of the LHC, in particular by LHCb (CERN) and BTeV (FNAL) [19]. The great interest in B physics – our main topic – originates from the fact that it provides a very fertile testing ground for the SM picture of flavour physics and CP violation, as we will see in these lectures. The outline is as follows: in Section 2, we have a closer look at the weak interactions of quarks, discuss the quark-mixing matrix, and introduce the unitarity triangle(s). After giving a brief introduction to the CP violation in the kaon system and making first contact with "rare" K decays in Section 3, we enter the world of the B mesons in Section 4, where we shall classify their decays, discuss the theoretical tools to deal with them, and investigate the requirements for non-vanishing CP asymmetries. In Section 5, we discuss features of neutral B_q mesons ($q \in \{d, s\}$), including the very important phenomenon of B_q^0–$\bar{B}_q^0$ mixing, and introduce the corresponding CP-violating observables. These considerations then allow us to have a closer look at important benchmark modes for the B factories in Section 6, where we will also address the current experimental status. In Section 7, we discuss the exploration of CP violation with the help of amplitude relations, whereas we shall focus on the B_s-meson system, which is particularly interesting for B-decay studies at hadron colliders, in Section 8. In Section 9, we emphasize the importance of studies of "rare" B- and K-meson decays, which are absent at the tree level in the SM, and offer important probes for the search of NP. Finally, we summarize our conclusions in Section 10.

For a collection of detailed textbooks and reviews on CP violation and flavour physics, the reader is referred to [20]–[26]. Since this field is evolving quickly, I will also address recent developments that took place after the school in Tsakhkadzor in order to complement the material that I presented there. The data refer to the experimental situation in early 2004.

2 CP VIOLATION IN THE STANDARD MODEL

2.1 Weak Interactions of Quarks and the Quark-Mixing Matrix

In the framework of the Standard Model of electroweak interactions [6, 27], which is based on the spontaneously broken gauge group

$$SU(2)_{\rm L} \times U(1)_{\rm Y} \xrightarrow{\rm SSB} U(1)_{\rm em}, \tag{2.1}$$

CP-violating effects may originate from the charged-current interactions of quarks, having the structure

$$D \to U W^-. \tag{2.2}$$

Here $D \in \{d, s, b\}$ and $U \in \{u, c, t\}$ denote down- and up-type quark flavours, respectively, whereas the W^- is the usual $SU(2)_{\rm L}$ gauge boson. From a phenomenological point of view, it is convenient to

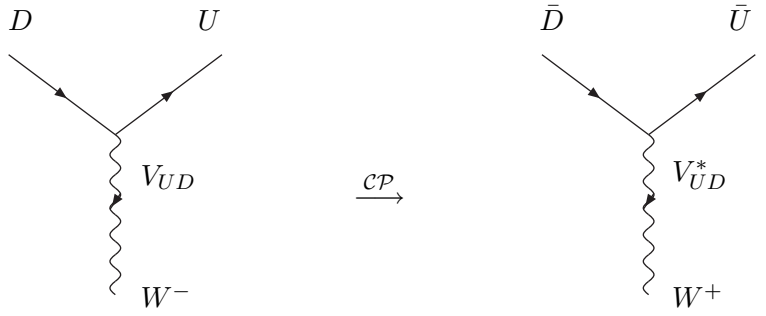

Fig. 1: CP-conjugate charged-current quark-level interaction processes in the SM.

collect the generic "coupling strengths" V_{UD} of the charged-current processes in (2.2) in the form of the following matrix:

$$\hat{V}_{\rm CKM} = \begin{pmatrix} V_{ud} & V_{us} & V_{ub} \\ V_{cd} & V_{cs} & V_{cb} \\ V_{td} & V_{ts} & V_{tb} \end{pmatrix}, \tag{2.3}$$

which is referred to as the Cabibbo–Kobayashi–Maskawa (CKM) matrix [28, 29].

From a theoretical point of view, this matrix connects the electroweak states (d', s', b') of the down, strange and bottom quarks with their mass eigenstates (d, s, b) through the following unitary transformation [6]:

$$\begin{pmatrix} d' \\ s' \\ b' \end{pmatrix} = \begin{pmatrix} V_{ud} & V_{us} & V_{ub} \\ V_{cd} & V_{cs} & V_{cb} \\ V_{td} & V_{ts} & V_{tb} \end{pmatrix} \cdot \begin{pmatrix} d \\ s \\ b \end{pmatrix}. \tag{2.4}$$

Consequently, $\hat{V}_{\rm CKM}$ is actually a *unitary* matrix. This feature ensures the absence of flavour-changing neutral-current (FCNC) processes at the tree level in the SM, and is hence at the basis of the famous Glashow–Iliopoulos–Maiani (GIM) mechanism [30]. We shall return to the unitarity of the CKM matrix in Subsection 2.6, discussing the "unitarity triangles". If we express the non-leptonic charged-current interaction Lagrangian in terms of the mass eigenstates appearing in (2.4), we arrive at

$$\mathcal{L}^{\rm CC}_{\rm int} = -\frac{g_2}{\sqrt{2}} \left(\begin{array}{ccc} \bar{u}_{\rm L}, & \bar{c}_{\rm L}, & \bar{t}_{\rm L} \end{array} \right) \gamma^\mu \hat{V}_{\rm CKM} \begin{pmatrix} d_{\rm L} \\ s_{\rm L} \\ b_{\rm L} \end{pmatrix} W^\dagger_\mu \; + \; \text{h.c.}, \tag{2.5}$$

where the gauge coupling g_2 is related to the gauge group $SU(2)_{\rm L}$, and the $W^{(\dagger)}_\mu$ field corresponds to the charged W bosons. Looking at the interaction vertices following from (2.5), we observe that the elements of the CKM matrix describe in fact the generic strengths of the associated charged-current processes, as we have noted above.

In Fig. 1, we show the $D \to UW^-$ vertex and its CP conjugate. Since the corresponding CP transformation involves the replacement

$$V_{UD} \xrightarrow{\mathcal{CP}} V^*_{UD}, \tag{2.6}$$

CP violation could – in principle – be accommodated in the SM through complex phases in the CKM matrix. The crucial question in this context is, of course, whether we may actually have physical complex phases in that matrix.

2.2 Phase Structure of the CKM Matrix

We have the freedom to redefine the up- and down-type quark fields in the following manner:

$$U \to \exp(i\xi_U) U, \quad D \to \exp(i\xi_D) D. \tag{2.7}$$

If we perform such transformations in (2.5), the invariance of the charged-current interaction Lagrangian implies the following phase transformations of the CKM matrix elements:

$$V_{UD} \to \exp(i\xi_U) V_{UD} \exp(-i\xi_D). \tag{2.8}$$

Using these transformations to eliminate unphysical phases, it can be shown that the parametrization of the general $N \times N$ quark-mixing matrix, where N denotes the number of fermion generations, involves the following parameters:

$$\underbrace{\frac{1}{2}N(N-1)}_{\text{Euler angles}} + \underbrace{\frac{1}{2}(N-1)(N-2)}_{\text{complex phases}} = (N-1)^2. \tag{2.9}$$

If we apply this expression to the case of $N = 2$ generations, we observe that only one rotation angle – the Cabibbo angle $\theta_{\rm C}$ [28] – is required for the parametrization of the 2×2 quark-mixing matrix, which can be written in the following form:

$$\hat{V}_{\rm C} = \begin{pmatrix} \cos\theta_{\rm C} & \sin\theta_{\rm C} \\ -\sin\theta_{\rm C} & \cos\theta_{\rm C} \end{pmatrix}, \tag{2.10}$$

where $\sin\theta_{\rm C} = 0.22$ can be determined from $K \to \pi\ell\bar{\nu}$ decays. On the other hand, in the case of $N = 3$ generations, the parametrization of the corresponding 3×3 quark-mixing matrix involves three Euler-type angles and a single *complex* phase. This complex phase allows us to accommodate CP violation in the SM, as was pointed out by Kobayashi and Maskawa in 1973 [29]. The corresponding picture is referred to as the Kobayashi–Maskawa (KM) mechanism of CP violation.

In the "standard parametrization" advocated by the Particle Data Group (PDG) [31], the three-generation CKM matrix takes the following form:

$$\hat{V}_{\rm CKM} = \begin{pmatrix} c_{12}c_{13} & s_{12}c_{13} & s_{13}e^{-i\delta_{13}} \\ -s_{12}c_{23} - c_{12}s_{23}s_{13}e^{i\delta_{13}} & c_{12}c_{23} - s_{12}s_{23}s_{13}e^{i\delta_{13}} & s_{23}c_{13} \\ s_{12}s_{23} - c_{12}c_{23}s_{13}e^{i\delta_{13}} & -c_{12}s_{23} - s_{12}c_{23}s_{13}e^{i\delta_{13}} & c_{23}c_{13} \end{pmatrix}, \tag{2.11}$$

where $c_{ij} \equiv \cos\theta_{ij}$ and $s_{ij} \equiv \sin\theta_{ij}$. Performing appropriate redefinitions of the quark-field phases, the real angles θ_{12}, θ_{23} and θ_{13} can all be made to lie in the first quadrant. The advantage of this parametrization is that the generation labels $i, j = 1, 2, 3$ are introduced in such a manner that the mixing between two chosen generations vanishes if the corresponding mixing angle θ_{ij} is set to zero. In particular, for $\theta_{23} = \theta_{13} = 0$, the third generation decouples, and the 2×2 submatrix describing the mixing between the first and second generations takes the same form as (2.10).

Another interesting parametrization of the CKM matrix was proposed by Fritzsch and Xing [32]:

$$\hat{V}_{\rm CKM} = \begin{pmatrix} s_{\rm u}s_{\rm d}c + c_{\rm u}c_{\rm d}e^{-i\varphi} & s_{\rm u}c_{\rm d}c - c_{\rm u}s_{\rm d}e^{-i\varphi} & s_{\rm u}s \\ c_{\rm u}s_{\rm d}c - s_{\rm u}c_{\rm d}e^{-i\varphi} & c_{\rm u}c_{\rm d}c + s_{\rm u}s_{\rm d}e^{-i\varphi} & c_{\rm u}s \\ -s_{\rm d}s & -c_{\rm d}s & c \end{pmatrix}. \tag{2.12}$$

It is inspired by the hierarchical structure of the quark-mass spectrum and is particularly useful in the context of models for fermion masses and mixings. The characteristic feature of this parametrization is that the complex phase arises only in the 2×2 submatrix involving the up, down, strange and charm quarks.

Let us finally note that physical observables, for instance CP-violating asymmetries, *cannot* depend on the chosen parametrization of the CKM matrix, i.e. have to be invariant under the phase transformations specified in (2.8).

2.3 Further Requirements for CP Violation

As we have just seen, in order to be able to accommodate CP violation within the framework of the SM through a complex phase in the CKM matrix, at least three generations are required. However, this feature is not sufficient for observable CP-violating effects. To this end, further conditions have to be satisfied, which can be summarized as follows [33, 34]:

$$(m_t^2 - m_c^2)(m_t^2 - m_u^2)(m_c^2 - m_u^2)(m_b^2 - m_s^2)(m_b^2 - m_d^2)(m_s^2 - m_d^2) \times J_{\rm CP} \neq 0, \tag{2.13}$$

where

$$J_{\rm CP} = |{\rm Im}(V_{i\alpha} V_{j\beta} V_{i\beta}^* V_{j\alpha}^*)| \quad (i \neq j,\, \alpha \neq \beta)\,. \tag{2.14}$$

The mass factors in (2.13) are related to the fact that the CP-violating phase of the CKM matrix could be eliminated through an appropriate unitary transformation of the quark fields if any two quarks with the same charge had the same mass. Consequently, the origin of CP violation is closely related to the "flavour problem" in elementary particle physics, and cannot be understood in a deeper way, unless we have fundamental insights into the hierarchy of quark masses and the number of fermion generations.

The second element of (2.13), the "Jarlskog parameter" $J_{\rm CP}$ [33], can be interpreted as a measure of the strength of CP violation in the SM. It does not depend on the chosen quark-field parametrization, i.e. it is invariant under (2.8), and the unitarity of the CKM matrix implies that all combinations $|{\rm Im}(V_{i\alpha} V_{j\beta} V_{i\beta}^* V_{j\alpha}^*)|$ are equal to one another. Using the standard parametrization of the CKM matrix introduced in (2.11), we obtain

$$J_{\rm CP} = s_{12} s_{13} s_{23} c_{12} c_{23} c_{13}^2 \sin\delta_{13}. \tag{2.15}$$

Since the current experimental information on the CKM parameters implies a value of $J_{\rm CP}$ at the 10^{-5} level, CP violation is a small effect in the SM. However, new complex couplings are typically present in scenarios for NP [8, 9], thereby yielding additional sources of CP violation.

2.4 Experimental Information on $|V_{\rm CKM}|$

In order to determine the magnitudes $|V_{ij}|$ of the elements of the CKM matrix, we may use the following tree-level processes:

- Nuclear beta decays, neutron decays $\Rightarrow |V_{ud}|$.
- $K \to \pi \ell \bar\nu$ decays $\Rightarrow |V_{us}|$.
- ν production of charm off valence d quarks $\Rightarrow |V_{cd}|$.
- Charm-tagged W decays (as well as ν production and semileptonic D decays) $\Rightarrow |V_{cs}|$.
- Exclusive and inclusive $b \to c \ell \bar\nu$ decays $\Rightarrow |V_{cb}|$.
- Exclusive and inclusive $b \to u \ell \bar\nu$ decays $\Rightarrow |V_{ub}|$.
- $\bar t \to \bar b \ell \bar\nu$ processes $\Rightarrow$ (crude direct determination of) $|V_{tb}|$.

If we use the corresponding experimental information, together with the CKM unitarity condition, and assume that there are only three generations, we arrive at the following 90% C.L. limits for the $|V_{ij}|$ [31]:

$$|\hat V_{\rm CKM}| = \begin{pmatrix} 0.9741\text{–}0.9756 & 0.219\text{–}0.226 & 0.0025\text{–}0.0048 \\ 0.219\text{–}0.226 & 0.9732\text{–}0.9748 & 0.038\text{–}0.044 \\ 0.004\text{–}0.014 & 0.037\text{–}0.044 & 0.9990\text{–}0.9993 \end{pmatrix}. \tag{2.16}$$

In Fig. 2, we have illustrated the resulting hierarchy of the strengths of the charged-current quark-level processes: transitions within the same generation are governed by CKM matrix elements of $\mathcal{O}(1)$, those between the first and the second generation are suppressed by CKM factors of $\mathcal{O}(10^{-1})$, those between the second and the third generation are suppressed by $\mathcal{O}(10^{-2})$, and the transitions between the first and the third generation are even suppressed by CKM factors of $\mathcal{O}(10^{-3})$. In the standard parametrization (2.11), this hierarchy is reflected by

$$s_{12} = 0.22 \gg s_{23} = \mathcal{O}(10^{-2}) \gg s_{13} = \mathcal{O}(10^{-3}). \tag{2.17}$$

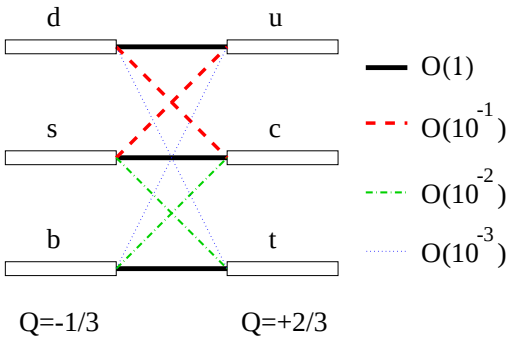

Fig. 2: Hierarchy of the quark transitions mediated through charged-current processes.

2.5 Wolfenstein Parametrization of the CKM Matrix

For phenomenological applications, it would be useful to have a parametrization of the CKM matrix available that makes the hierarchy arising in (2.16) – and illustrated in Fig. 2 – explicit [35]. In order to derive such a parametrization, we introduce a set of new parameters, λ, A, ρ and η, by imposing the following relations [36]:

$$s_{12} \equiv \lambda = 0.22, \quad s_{23} \equiv A\lambda^2, \quad s_{13}e^{-i\delta_{13}} \equiv A\lambda^3(\rho - i\eta). \tag{2.18}$$

If we now go back to the standard parametrization (2.11), we obtain an *exact* parametrization of the CKM matrix as a function of λ (and A, ρ, η), allowing us to expand each CKM element in powers of the small parameter λ. If we neglect terms of $\mathcal{O}(\lambda^4)$, we arrive at the famous "Wolfenstein parametrization" [35]:

$$\hat{V}_{\rm CKM} = \begin{pmatrix} 1 - \frac{1}{2}\lambda^2 & \lambda & A\lambda^3(\rho - i\eta) \\ -\lambda & 1 - \frac{1}{2}\lambda^2 & A\lambda^2 \\ A\lambda^3(1 - \rho - i\eta) & -A\lambda^2 & 1 \end{pmatrix} + \mathcal{O}(\lambda^4), \tag{2.19}$$

which makes the hierarchical structure of the CKM matrix very transparent and is an important tool for phenomenological considerations, as we will see throughout these lectures.

For several applications, next-to-leading order corrections in λ play an important rôle. Using the exact parametrization following from (2.11) and (2.18), they can be calculated straightforwardly by expanding each CKM element to the desired accuracy in λ [36, 37]:

$$\begin{aligned} V_{ud} &= 1 - \frac{1}{2}\lambda^2 - \frac{1}{8}\lambda^4 + \mathcal{O}(\lambda^6), \quad V_{us} = \lambda + \mathcal{O}(\lambda^7), \quad V_{ub} = A\lambda^3(\rho - i\,\eta), \\ V_{cd} &= -\lambda + \frac{1}{2}A^2\lambda^5\left[1 - 2(\rho + i\eta)\right] + \mathcal{O}(\lambda^7), \\ V_{cs} &= 1 - \frac{1}{2}\lambda^2 - \frac{1}{8}\lambda^4(1 + 4A^2) + \mathcal{O}(\lambda^6), \\ V_{cb} &= A\lambda^2 + \mathcal{O}(\lambda^8), \quad V_{td} = A\lambda^3\left[1 - (\rho + i\eta)\left(1 - \frac{1}{2}\lambda^2\right)\right] + \mathcal{O}(\lambda^7), \\ V_{ts} &= -A\lambda^2 + \frac{1}{2}A(1 - 2\rho)\lambda^4 - i\eta A\lambda^4 + \mathcal{O}(\lambda^6), \quad V_{tb} = 1 - \frac{1}{2}A^2\lambda^4 + \mathcal{O}(\lambda^6). \end{aligned} \tag{2.20}$$

It should be noted that

$$V_{ub} \equiv A\lambda^3(\rho - i\eta) \tag{2.21}$$

receives *by definition* no power corrections in λ within this prescription. If we follow [36] and introduce the generalized Wolfenstein parameters

$$\bar{\rho} \equiv \rho\left(1 - \frac{1}{2}\lambda^2\right), \quad \bar{\eta} \equiv \eta\left(1 - \frac{1}{2}\lambda^2\right), \tag{2.22}$$

we may simply write, up to corrections of $\mathcal{O}(\lambda^7)$,

$$V_{td} = A\lambda^3(1 - \bar{\rho} - i\,\bar{\eta}). \tag{2.23}$$

Moreover, we have to an excellent accuracy

$$V_{us} = \lambda \quad \text{and} \quad V_{cb} = A\lambda^2, \tag{2.24}$$

as these quantities receive only corrections at the λ^7 and λ^8 levels, respectively. In comparison with other generalizations of the Wolfenstein parametrization found in the literature, the advantage of (2.20) is the absence of relevant corrections to V_{us} and V_{cb}, and that V_{ub} and V_{td} take forms similar to those in (2.19). As far as the Jarlskog parameter introduced in (2.14) is concerned, we obtain the simple expression

$$J_{\rm CP} = \lambda^6 A^2 \eta, \tag{2.25}$$

which should be compared with (2.15).

2.6 Unitarity Triangles of the CKM Matrix

The unitarity of the CKM matrix, which is described by

$$\hat{V}_{\rm CKM}^{\,\dagger} \cdot \hat{V}_{\rm CKM} = \hat{1} = \hat{V}_{\rm CKM} \cdot \hat{V}_{\rm CKM}^{\,\dagger}, \tag{2.26}$$

leads to a set of 12 equations, consisting of 6 normalization and 6 orthogonality relations. The latter can be represented as 6 triangles in the complex plane [38], all having the same area, $2A_\Delta = J_{\rm CP}$ [39]. Let us now have a closer look at these relations: those describing the orthogonality of different columns of the CKM matrix are given by

$$\underbrace{V_{ud}V_{us}^*}_{\mathcal{O}(\lambda)} + \underbrace{V_{cd}V_{cs}^*}_{\mathcal{O}(\lambda)} + \underbrace{V_{td}V_{ts}^*}_{\mathcal{O}(\lambda^5)} = 0 \tag{2.27}$$

$$\underbrace{V_{us}V_{ub}^*}_{\mathcal{O}(\lambda^4)} + \underbrace{V_{cs}V_{cb}^*}_{\mathcal{O}(\lambda^2)} + \underbrace{V_{ts}V_{tb}^*}_{\mathcal{O}(\lambda^2)} = 0 \tag{2.28}$$

$$\underbrace{V_{ud}V_{ub}^*}_{(\rho+i\eta)A\lambda^3} + \underbrace{V_{cd}V_{cb}^*}_{-A\lambda^3} + \underbrace{V_{td}V_{tb}^*}_{(1-\rho-i\eta)A\lambda^3} = 0, \tag{2.29}$$

whereas those associated with the orthogonality of different rows take the following form:

$$\underbrace{V_{ud}^*V_{cd}}_{\mathcal{O}(\lambda)} + \underbrace{V_{us}^*V_{cs}}_{\mathcal{O}(\lambda)} + \underbrace{V_{ub}^*V_{cb}}_{\mathcal{O}(\lambda^5)} = 0 \tag{2.30}$$

$$\underbrace{V_{cd}^*V_{td}}_{\mathcal{O}(\lambda^4)} + \underbrace{V_{cs}^*V_{ts}}_{\mathcal{O}(\lambda^2)} + \underbrace{V_{cb}^*V_{tb}}_{\mathcal{O}(\lambda^2)} = 0 \tag{2.31}$$

$$\underbrace{V_{ud}^*V_{td}}_{(1-\rho-i\eta)A\lambda^3} + \underbrace{V_{us}^*V_{ts}}_{-A\lambda^3} + \underbrace{V_{ub}^*V_{tb}}_{(\rho+i\eta)A\lambda^3} = 0. \tag{2.32}$$

Here we have also indicated the structures that arise if we apply the Wolfenstein parametrization by keeping just the leading, non-vanishing terms. We observe that only in (2.29) and (2.32), which describe the orthogonality of the first and third columns and of the first and third rows, respectively, all three sides are of comparable magnitude, $\mathcal{O}(\lambda^3)$, while in the remaining relations, one side is suppressed with respect to the others by factors of $\mathcal{O}(\lambda^2)$ or $\mathcal{O}(\lambda^4)$. Consequently, we have to deal with only *two* non-squashed unitarity triangles in the complex plane. However, as we have already indicated in (2.29) and (2.32), the corresponding orthogonality relations agree with each other at the λ^3 level, yielding

$$[(\rho + i\eta) + (-1) + (1 - \rho - i\eta)]\, A\lambda^3 = 0. \tag{2.33}$$

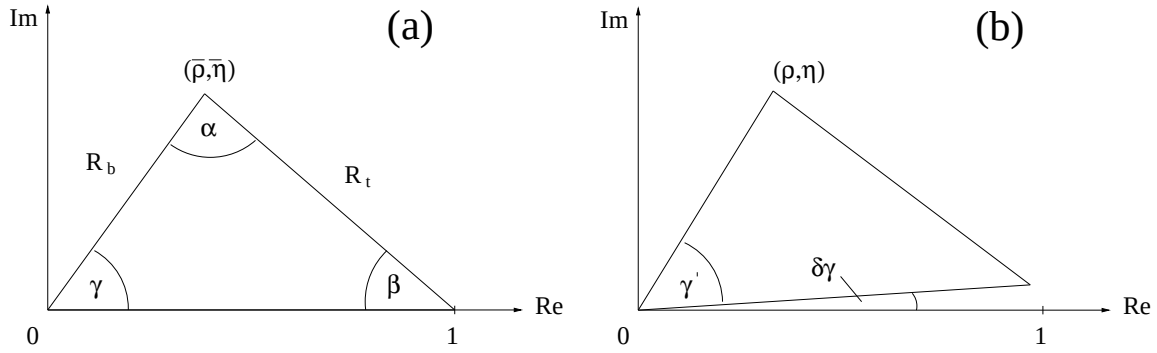

Fig. 3: The two non-squashed unitarity triangles of the CKM matrix, as explained in the text: (a) and (b) correspond to the orthogonality relations (2.29) and (2.32), respectively.

Consequently, they describe the same triangle, which is usually referred to as *the* unitarity triangle of the CKM matrix [39, 40].

In the era of second-generation B-decay experiments of the LHC era, the experimental accuracy will be so tremendous that we will also have to take the next-to-leading order terms of the Wolfenstein expansion into account, and will have to distinguish between the unitarity triangles following from (2.29) and (2.32). Let us first have a closer look at the former relation. Including terms of $\mathcal{O}(\lambda^5)$, we obtain the following generalization of (2.33):

$$\left[(\bar\rho + i\bar\eta) + (-1) + (1 - \bar\rho - i\bar\eta)\right] A\lambda^3 + \mathcal{O}(\lambda^7) = 0, \tag{2.34}$$

where $\bar\rho$ and $\bar\eta$ are as defined in (2.22). If we divide this relation by the overall normalization factor $A\lambda^3$, and introduce

$$R_b \equiv \sqrt{\overline{\rho}^2 + \overline{\eta}^2} = \left(1 - \frac{\lambda^2}{2}\right) \frac{1}{\lambda} \left|\frac{V_{ub}}{V_{cb}}\right| \tag{2.35}$$

$$R_t \equiv \sqrt{(1 - \overline{\rho})^2 + \overline{\eta}^2} = \frac{1}{\lambda} \left|\frac{V_{td}}{V_{cb}}\right|, \tag{2.36}$$

we arrive at the unitarity triangle illustrated in Fig. 3 (a). It is a straightforward generalization of the leading-order case described by (2.33): instead of (ρ, η), the apex is now simply given by $(\bar\rho, \bar\eta)$ [36]. The two sides R_b and R_t, as well as the three angles α, β and γ, will show up at several places throughout these lectures. Moreover, the relations

$$V_{ub} = A\lambda^3 \left(\frac{R_b}{1 - \lambda^2/2}\right) e^{-i\gamma}, \quad V_{td} = A\lambda^3 R_t e^{-i\beta} \tag{2.37}$$

are also useful for phenomenological applications, since they make the dependences of γ and β explicit; they correspond to the phase convention chosen both in the standard parametrization (2.11) and in the generalized Wolfenstein parametrization (2.20). Finally, if we take also (2.18) into account, we obtain

$$\delta_{13} = \gamma. \tag{2.38}$$

Let us now turn to (2.32). Here we arrive at an expression that is more complicated than (2.34):

$$\left[\left\{1 - \frac{\lambda^2}{2} - (1 - \lambda^2)\rho - i(1 - \lambda^2)\eta\right\} + \left\{-1 + \left(\frac{1}{2} - \rho\right)\lambda^2 - i\eta\lambda^2\right\} + \{\rho + i\eta\}\right] A\lambda^3 + \mathcal{O}(\lambda^7) = 0. \tag{2.39}$$

If we divide again by $A\lambda^3$, we obtain the unitarity triangle sketched in Fig. 3 (b), where the apex is given by (ρ, η) and *not* by $(\bar\rho, \bar\eta)$. On the other hand, we encounter a tiny angle

$$\delta\gamma \equiv \lambda^2\eta = \mathcal{O}(1^\circ) \tag{2.40}$$

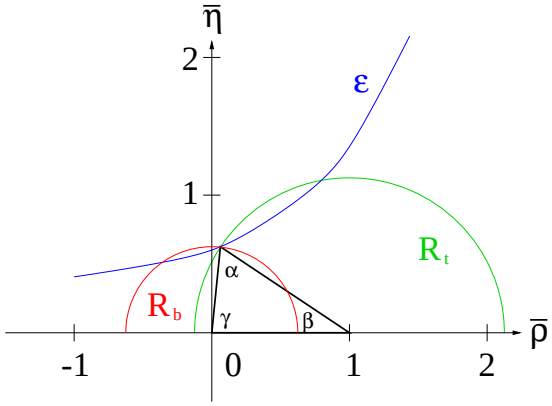

Fig. 4: Contours in the $\bar{\rho}$–$\bar{\eta}$ plane, allowing us to determine the apex of the UT.

between real axis and basis of the triangle, which satisfies

$$\gamma = \gamma' + \delta\gamma, \tag{2.41}$$

where γ coincides with the corresponding angle in Fig. 3 (a).

Whenever we will refer to a "unitarity triangle" (UT) in the following discussion, we mean the one illustrated in Fig. 3 (a), which is the generic generalization of the leading-order case described by (2.33). As we will see below, the UT is the central target of the experimental tests of the SM description of CP violation. Interestingly, also the tiny angle $\delta\gamma$ can be probed directly through certain CP-violating effects that can be explored at hadron colliders, in particular at the LHC.

2.7 Towards an Allowed Region in the $\bar{\rho}$–$\bar{\eta}$ Plane

It is possible to constrain – and even determine – the apex of the UT in the $\bar{\rho}$–$\bar{\eta}$ plane with the help of experimental data. Unfortunately, we do not yet have the theoretical framework available to discuss in detail how this can actually be done (but this will become obvious in the course of these lectures). However, it is nevertheless useful to sketch the corresponding procedure – the "CKM fits" – already now, consisting of the following elements:

- The parameter R_b introduced in (2.35), which involves the ratio $|V_{ub}/V_{cb}|$. It can be determined experimentally through $b \to u\ell\bar{\nu}$ and $b \to c\ell\bar{\nu}$ decay processes. Following these lines, we may fix a circle in the $\bar{\rho}$–$\bar{\eta}$ plane that is centred at the origin $(0,0)$ and has the radius R_b.
- The parameter R_t introduced in (2.36), which involves the ratio $|V_{td}/V_{cb}|$. It can be determined with the help of the mass differences $\Delta M_{d,s}$ of the mass eigenstates of the neutral B_d- and B_s-meson systems. Experimental information on these quantities then allows us to fix another circle in the $\bar{\rho}$–$\bar{\eta}$ plane, which is centred at $(1,0)$ and has the radius R_t.
- Finally, we may convert the measurement of the observable ε, which describes the CP violation in the neutral kaon system that was discovered in 1964, into a hyperbola in the $\bar{\rho}$–$\bar{\eta}$ plane.

In Fig. 4, we have illustrated these contours; their intersection allows us to determine the apex of the UT within the SM. The curves that are implied by ΔM_d and ε depend on the CKM parameter A and the top-quark mass m_t, as well as on certain perturbatively calculable QCD corrections and non-perturbative parameters. Consequently, strong correlations between the theoretical and experimental uncertainties arise in the CKM fits. As discussed in detail in [41], several different approaches can be found in the literature to deal with the corresponding error propagation. The typical (conservative) ranges for the UT angles that follow from the CKM fits read as follows:

$$70^\circ \lesssim \alpha \lesssim 130^\circ, \quad 20^\circ \lesssim \beta \lesssim 30^\circ, \quad 50^\circ \lesssim \gamma \lesssim 70^\circ. \tag{2.42}$$

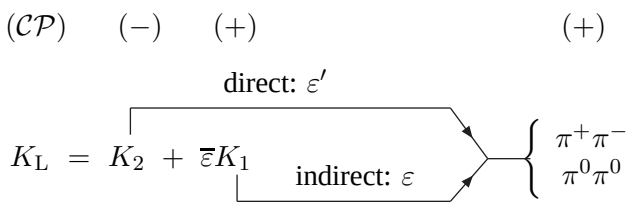

Fig. 5: Illustration of indirect and direct CP violation in $K_{\rm L} \to \pi\pi$ decays.

On the other hand, CP violation in the B-meson system provides various strategies to determine these angles *directly*, thereby offering different ways to fix the apex of the UT in the $\bar{\rho}$–$\bar{\eta}$ plane. Following these lines, a powerful test of the KM mechanism can be performed. This very interesting feature is also reflected by the tremendous efforts to explore CP violation in B decays experimentally in this decade. Before having a closer look at B mesons, their decays, the theoretical tools to deal with them and the general requirements for having non-vanishing CP asymmetries, let us first turn to the kaon system.

3 A FIRST LOOK AT CP VIOLATION AND RARE DECAYS IN THE KAON SYSTEM

3.1 CP Violation: ε and ε'

As we have already noted, in 1964, CP violation was discovered – as a big surprise – in the famous experiment by Christenson et al. [1], who observed $K_{\rm L} \to \pi^+\pi^-$ decays. If the weak interactions *were* invariant under CP transformations, the mass eigenstates $K_{\rm S}$ and $K_{\rm L}$ of the Hamilton operator describing K^0–$\bar{K}^0$ mixing *were* eigenstates of the CP operator, with eigenvalues $+1$ and -1, respectively. Since the $\pi^+\pi^-$ final state of $K_{\rm L} \to \pi^+\pi^-$ is CP-even, the detection of this transition signals indeed the violation of the CP symmetry in weak interaction processes. The discussion in this subsection serves mainly to make a first contact with this phenomenon; for detailed presentations of CP violation in kaon decays, we refer the reader to [21, 22, 37].

In the neutral K-meson system, CP violation is described by two complex quantities, called ε and ε', which are defined by the following ratios of decay amplitudes:

$$\frac{A(K_{\rm L} \to \pi^+\pi^-)}{A(K_{\rm S} \to \pi^+\pi^-)} \approx \varepsilon + \varepsilon', \quad \frac{A(K_{\rm L} \to \pi^0\pi^0)}{A(K_{\rm S} \to \pi^0\pi^0)} \approx \varepsilon - 2\,\varepsilon'. \tag{3.1}$$

These parameters are associated with "indirect" and "direct" CP violation, as we have illustrated in Fig. 5, where K_1 and K_2 denote the CP eigenstates of the neutral kaon system with CP eigenvalues $+1$ and -1, respectively. The terminology of "indirect CP violation" originates from the fact that the mass eigenstate $K_{\rm L}$ of the neutral kaon system is *not* an eigenstate of the CP operator because of the small admixture of the CP-even K_1 state, which may decay – through a CP-conserving transition – into a $\pi\pi$ final state. On the other hand, direct CP violation originates from *direct* transitions of the CP-odd K_2 state into the CP-even $\pi\pi$ final state.

After the discovery of indirect CP violation through $K_{\rm L} \to \pi^+\pi^-$ decays, this phenomenon could also be observed in $K_{\rm L} \to \pi^0\pi^0$, $\pi\ell\bar{\nu}$, $\pi^+\pi^-\gamma$ modes, and recently in $K_{\rm L} \to \pi^+\pi^- e^+e^-$ transitions. All these effects can be described by

$$\varepsilon = (2.280 \pm 0.013) \times e^{i\frac{\pi}{4}} \times 10^{-3}. \tag{3.2}$$

As we noted in Subsection 2.7, the knowledge of the CKM parameter A and the top-quark mass m_t allows us – in combination with the calculation of perturbative QCD corrections and estimates of non-perturbative parameters – to convert the observable ε into a hyperbola in the $\bar{\rho}$–$\bar{\eta}$ plane, as is explicitly shown in [21, 22, 37]. This analysis implies in particular $\bar{\eta} > 0$, i.e. that the appex of the UT lies in the *upper* half of the $\bar{\rho}$–$\bar{\eta}$ plane.

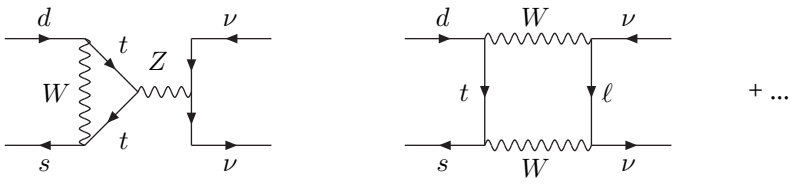

Fig. 6: Decay processes contributing to $K_{\rm L} \to \pi^0 \nu\bar{\nu}$ in the SM.

Direct CP violation in neutral $K \to \pi\pi$ decays can be described through the quantity $\mathrm{Re}(\varepsilon'/\varepsilon)$. In 1999, measurements at CERN (NA48) [2] and FNAL (KTeV) [3] have demonstrated – after tremendous efforts over many years – that this observable is actually *different* from zero, thereby establishing the phenomenon of *direct* CP violation. The experimental status is now given as follows:

$$\mathrm{Re}(\varepsilon'/\varepsilon) = \begin{cases} (14.7 \pm 2.2) \times 10^{-4} & \text{(NA48 [42]),} \\ (20.7 \pm 2.8) \times 10^{-4} & \text{(KTeV [43]).} \end{cases} \tag{3.3}$$

If we take also the previous results of the NA31 and E731 collaborations into account, we obtain the world average

$$\mathrm{Re}(\varepsilon'/\varepsilon) = (16.6 \pm 1.6) \times 10^{-4}. \tag{3.4}$$

Within the SM, calculations of $\mathrm{Re}(\varepsilon'/\varepsilon)$ give the same order of magnitude (for an overview of the current status, see [44]). However, these analyses are affected by large hadronic uncertainties; the situation is particularly unfavourable, since $\mathrm{Re}(\varepsilon'/\varepsilon)$ is governed by the competition between two different decay topologies and suffers from a strong cancellation between them. Consequently, although the measurement of $\mathrm{Re}(\varepsilon'/\varepsilon)$ led to the discovery of a new kind of CP violation, this observable does unfortunately not allow us to perform stringent tests of the KM mechanism of CP violation, unless better techniques to deal with the hadronic uncertainties are available.

3.2 Rare Decays: $K \to \pi\nu\bar{\nu}$

From a theoretical point of view, the decays $K_{\rm L} \to \pi^0 \nu\bar{\nu}$ and $K^+ \to \pi^+ \nu\bar{\nu}$ are very interesting. Since we will have a detailed look at them in Subsection 9.3, let us here just sketch their most interesting features. As can easily be seen, these transitions originate from FCNC processes. Consequently, because of the GIM mechanism, they receive no contributions at the tree level in the SM. However, they may be induced through loop processes of the kind shown in Fig. 6, and are therefore strongly suppressed transitions, which are referred to as "rare" decays. One of the most exciting features of the $K \to \pi\nu\bar{\nu}$ modes is that they are theoretically very clean. Moreover, it can be shown that the measurement of the $K_{\rm L} \to \pi^0 \nu\bar{\nu}$ branching ratio allows us to determine $|\bar{\eta}|$, whereas the one of $K^+ \to \pi^+ \nu\bar{\nu}$ can be converted into an ellipse in the $\bar{\rho}$–$\bar{\eta}$ plane. The intersection of these contours provides an interesting determination of the UT, where in particular $\sin 2\beta$ can be extracted with respectable accuracy [45]. We may hence perform a stringent test of the SM description of CP violation by comparing the UT thus determined with the ones following from the construction illustrated in Fig. 4 and the studies of CP violation in the B-meson system. In particular, as we will see in Subsection 6.1, $B_d \to J/\psi K_{\rm S}$ decays allow also a clean determination of $\sin 2\beta$, so that a violation of the SM relation

$$(\sin 2\beta)_{\pi\nu\bar{\nu}} = (\sin 2\beta)_{\psi K_{\rm S}} \tag{3.5}$$

would indicate sources of CP violation lying beyond the SM. Moreover, also the determination of the angle γ of the UT is interesting for the search of NP with $K \to \pi\nu\bar{\nu}$ decays [46, 47].

Unfortunately, the $K \to \pi\nu\bar{\nu}$ branching ratios are extremely small. A recent update of the corresponding calculations within the SM yields the following results [48]:

$$\mathrm{BR}(K^+ \to \pi^+ \nu\bar{\nu}) = (8.0 \pm 1.1) \times 10^{-11}, \quad \mathrm{BR}(K_{\rm L} \to \pi^0 \nu\bar{\nu}) = (3.2 \pm 0.6) \times 10^{-11}, \tag{3.6}$$

which are in the ballpark of other recent analyses [49, 50]. Interestingly, a third event for the former channel was very recently observed by the E949 experiment at BNL [51], thereby complementing the previous observation of the two events by the E787 collaboration [52]. The three observed $K^+ \to \pi^+\nu\bar{\nu}$ events can be converted into the following branching ratio:

$$\mathrm{BR}(K^+ \to \pi^+\nu\bar{\nu}) = (14.7^{+13.0}_{-8.9}) \times 10^{-11}. \tag{3.7}$$

On the other hand, for the $K_{\rm L} \to \pi^0\nu\bar{\nu}$ channel, only the experimental upper bound

$$\mathrm{BR}(K_{\rm L} \to \pi^0\nu\bar{\nu}) < 5.9 \times 10^{-7} \tag{3.8}$$

is available from the KTeV collaboration [53].

In the presence of NP, the $K \to \pi\nu\bar{\nu}$ branching ratios may differ strongly from the SM expectations given in (3.6). For instance, in a recent NP analysis [48, 54], which is motivated by certain puzzling patterns in the B-factory data and will be discussed in Subsection 9.4, a spectacular enhancement of the $K_{\rm L} \to \pi^0\nu\bar{\nu}$ branching ratio, by one order of magnitude, is found, and the relation in (3.5) would in fact be dramatically violated.

Concerning the experimental aspects of the $K \to \pi\nu\bar{\nu}$ modes, we refer the reader to the recent overview given in [55]. Let us now move on to the central topic of these lectures, the B-meson system.

4 DECAYS OF B MESONS

The B-meson system consists of charged and neutral B mesons, which are characterized by the

$$\begin{array}{ll} B^+ \sim u\,\bar{b}, & \quad B^- \sim \bar{u}\,b \\ B_c^+ \sim c\,\bar{b}, & \quad B_c^+ \sim \bar{c}\,b \end{array}$$

and

$$\begin{array}{ll} B_d^0 \sim d\,\bar{b}, & \quad \bar{B}_d^0 \sim \bar{d}\,b \\ B_s^0 \sim s\,\bar{b}, & \quad \bar{B}_s^0 \sim \bar{s}\,b \end{array}$$

valence-quark contents, respectively. The characteristic feature of the neutral B_q ($q \in \{d, s\}$) mesons is the phenomenon of B_q^0–$\bar{B}_q^0$ mixing (the counterpart of K^0–$\bar{K}^0$ mixing), which will be discussed in Subsection 5.1. As far as the weak decays of B mesons are concerned, we distinguish between leptonic, semileptonic and non-leptonic transitions.

4.1 Leptonic Decays

The simplest B-meson decay class is given by leptonic decays of the kind $B^- \to \ell\bar{\nu}$, as illustrated in Fig. 7. If we evaluate the corresponding Feynman diagram, we arrive at the following transition amplitude:

$$T_{fi} = -\frac{g_2^2}{8} V_{ub} \underbrace{[\bar{u}_\ell \gamma^\alpha (1-\gamma_5) v_\nu]}_{\text{Dirac spinors}} \left[\frac{g_{\alpha\beta}}{k^2 - M_W^2}\right] \underbrace{\langle 0|\bar{u}\gamma^\beta(1-\gamma_5)b|B^-\rangle}_{\text{hadronic ME}}, \tag{4.1}$$

where g_2 is the $SU(2)_{\rm L}$ gauge coupling, V_{ub} the corresponding element of the CKM matrix, α and β are Lorentz indices, and M_W denotes the mass of the W gauge boson. Since the four-momentum k that is carried by the W satisfies $k^2 = M_B^2 \ll M_W^2$, we may write

$$\frac{g_{\alpha\beta}}{k^2 - M_W^2} \quad \longrightarrow \quad -\frac{g_{\alpha\beta}}{M_W^2} \equiv -\left(\frac{8 G_{\rm F}}{\sqrt{2} g_2^2}\right) g_{\alpha\beta}, \tag{4.2}$$

where $G_{\rm F}$ is Fermi's constant. Consequently, we may "integrate out" the W boson in (4.1), which yields

$$T_{fi} = \frac{G_{\rm F}}{\sqrt{2}} V_{ub} \,[\bar{u}_\ell \gamma^\alpha (1-\gamma_5) v_\nu] \,\langle 0|\bar{u}\gamma_\alpha(1-\gamma_5)b|B^-\rangle. \tag{4.3}$$

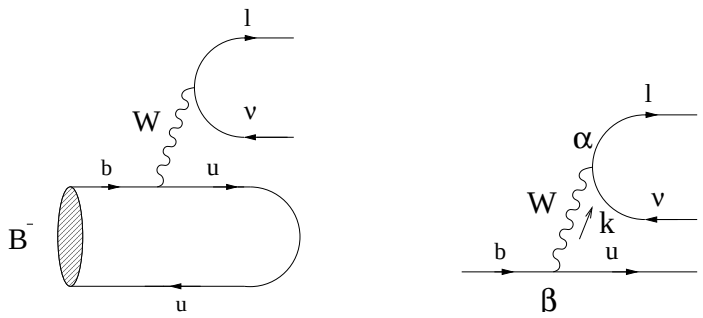

Fig. 7: Feynman diagram contributing to the leptonic decay $B^- \to \ell\bar{\nu}$.

In this simple expression, *all* the hadronic physics is encoded in the *hadronic matrix element*

$$\langle 0|\bar{u}\gamma_\alpha(1-\gamma_5)b|B^-\rangle,$$

i.e. there are no other strong-interaction (QCD) effects. Since the B^- meson is a pseudoscalar particle, we have

$$\langle 0|\overline{u}\gamma_\alpha b|B^-\rangle = 0, \tag{4.4}$$

and may write

$$\langle 0|\bar{u}\gamma_\alpha\gamma_5 b|B^-(q)\rangle = if_B q_\alpha, \tag{4.5}$$

where f_B is the B-meson *decay constant*, which is an important input for phenomenological studies. In order to determine this quantity, which is a very challenging task, non-perturbative techniques, such as lattice [56] or QCD sum-rule analyses [57], are required. If we use (4.3) with (4.4) and (4.5), and perform the corresponding phase-space integrations, we obtain the following decay rate:

$$\Gamma(B^- \to \ell\bar{\nu}) = \frac{G_{\rm F}^2}{8\pi}|V_{ub}|^2 M_B m_\ell^2 \left(1-\frac{m_\ell^2}{M_B^2}\right)^2 f_B^2, \tag{4.6}$$

where M_B and m_ℓ denote the masses of the B^- and ℓ, respectively. Because of the tiny value of $|V_{ub}| \propto \lambda^3$ and a helicity-suppression mechanism, we obtain unfortunately very small branching ratios of $\mathcal{O}(10^{-10})$ and $\mathcal{O}(10^{-7})$ for $\ell = e$ and $\ell = \mu$, respectively [58]. The helicity suppression is not effective for $\ell = \tau$, but – because of the required τ reconstruction – these modes are also very challenging from an experimental point of view. A measurement of leptonic B-meson decays would nevertheless be very interesting, as it would allow an experimental determination of f_B, thereby providing tests of non-perturbative calculations of this important parameter.[1] The CKM element $|V_{ub}|$ can be extracted from semileptonic B decays, our next topic.

4.2 Semileptonic Decays

4.2.1 General Structure

Semileptonic B-meson decays of the kind shown in Fig. 8 have a structure that is more complicated than the one of the leptonic transitions. If we evaluate the corresponding Feynman diagram for the $b \to c$ case, we obtain

$$T_{fi} = -\frac{g_2^2}{8}V_{cb}\underbrace{[\bar{u}_\ell\gamma^\alpha(1-\gamma_5)v_\nu]}_{\text{Dirac spinors}}\left[\frac{g_{\alpha\beta}}{k^2-M_W^2}\right]\underbrace{\langle D^+|\bar{c}\gamma^\beta(1-\gamma_5)b|\bar{B}_d^0\rangle}_{\text{hadronic ME}}. \tag{4.7}$$

[1] Leptonic decays of $D_{(s)}$ mesons allow the extraction of the corresponding decay constants $f_{D_{(s)}}$, which are defined in analogy to (4.5). These measurements are an important element of the CLEO-c research programme [59].

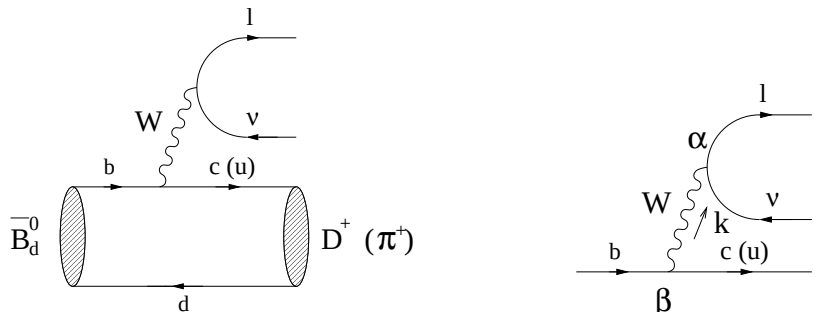

Fig. 8: Feynman diagram contributing to semileptonic $\bar{B}_d^0 \to D^+(\pi^+)\ell\bar{\nu}$ decays.

Because of $k^2 \sim M_B^2 \ll M_W^2$, we may again – as in (4.1) – integrate out the W boson with the help of (4.2), which yields

$$T_{fi} = \frac{G_{\rm F}}{\sqrt{2}} V_{cb} \left[\bar{u}_\ell \gamma^\alpha (1-\gamma_5) v_\nu\right] \langle D^+ | \bar{c} \gamma_\alpha (1-\gamma_5) b | \bar{B}_d^0 \rangle, \tag{4.8}$$

where *all* the hadronic physics is encoded in the hadronic matrix element

$$\langle D^+ | \bar{c} \gamma_\alpha (1-\gamma_5) b | \bar{B}_d^0 \rangle,$$

i.e. there are *no* other strong-interaction (QCD) effects. Since the $\bar{B}_d^0$ and D^+ are pseudoscalar mesons, we have

$$\langle D^+ | \bar{c} \gamma_\alpha \gamma_5 b | \bar{B}_d^0 \rangle = 0, \tag{4.9}$$

and may write

$$\langle D^+(k) | \bar{c} \gamma_\alpha b | \bar{B}_d^0(p) \rangle = F_1(q^2) \left[(p+k)_\alpha - \left(\frac{M_B^2 - M_D^2}{q^2}\right) q_\alpha\right] + F_0(q^2) \left(\frac{M_B^2 - M_D^2}{q^2}\right) q_\alpha, \tag{4.10}$$

where $q \equiv p - k$, and the $F_{1,0}(q^2)$ denote the *form factors* of the $\bar{B} \to D$ transitions. Consequently, in contrast to the simple case of the leptonic transitions, semileptonic decays involve *two* hadronic form factors instead of the decay constant f_B. In order to calculate these parameters, which depend on the momentum transfer q, again non-perturbative techniques (lattice, QCD sum rules, etc.) are required.

4.2.2 Aspects of the Heavy-Quark Effective Theory

If the mass m_Q of a quark Q is much larger than the QCD scale parameter $\Lambda_{\rm QCD} = \mathcal{O}(100\,\text{MeV})$, it is referred to as a "heavy" quark. Since the bottom and charm quarks have masses at the level of $5\,\text{GeV}$ and $1\,\text{GeV}$, respectively, they belong to this important category. As far as the extremely heavy top quark, with $m_t \sim 170\,\text{GeV}$ is concerned, it decays unfortunately through weak interactions before a hadron can be formed. Let us now consider a heavy quark that is bound inside a hadron, i.e. a bottom or a charm quark. The heavy quark then moves almost with the hadron's four velocity v and is almost on-shell, so that

$$p_Q^\mu = m_Q v^\mu + k^\mu, \tag{4.11}$$

where $v^2 = 1$ and $k \ll m_Q$ is the "residual" momentum. Owing to the interactions of the heavy quark with the light degrees of freedom of the hadron, the residual momentum may only change by $\Delta k \sim \Lambda_{\rm QCD}$, and $\Delta v \to 0$ for $\Lambda_{\rm QCD}/m_Q \to 0$.

It is now instructive to have a look at the elastic scattering process $\bar{B}(v) \to \bar{B}(v')$ in the limit of $\Lambda_{\rm QCD}/m_b \to 0$, which is characterized by the following matrix element:

$$\frac{1}{M_B} \langle \bar{B}(v') | \bar{b}_{v'} \gamma_\alpha b_v | \bar{B}(v) \rangle = \xi(v' \cdot v)(v + v')_\alpha. \tag{4.12}$$

Since the contraction of this matrix element with $(v - v')^\alpha$ has to vanish because of $\not{v} b_v = b_v$ and $\overline{b}_v \not{v}' = \overline{b}_{v'}$, no $(v - v')_\alpha$ term arises in the parametrization in (4.12). On the other hand, the $1/M_B$ factor is related to the normalization of states, i.e. the right-hand side of

$$\left(\frac{1}{\sqrt{M_B}}\langle \bar{B}(p')|\right)\left(|\bar{B}(p)\rangle\frac{1}{\sqrt{M_B}}\right) = 2v^0(2\pi)^3\delta^3(\vec{p} - \vec{p}') \tag{4.13}$$

does not depend on M_B. Finally, current conservation implies the following normalization condition:

$$\xi(v' \cdot v = 1) = 1, \tag{4.14}$$

where the "Isgur–Wise" function $\xi(v' \cdot v)$ does *not* depend on the flavour of the heavy quark (heavy-quark symmetry) [60]. Consequently, for $\Lambda_{\rm QCD}/m_{b,c} \to 0$, we may write

$$\frac{1}{\sqrt{M_D M_B}}\langle D(v')|\bar{c}_{v'}\gamma_\alpha b_v|\bar{B}(v)\rangle = \xi(v' \cdot v)(v + v')_\alpha, \tag{4.15}$$

and observe that this transition amplitude is governed – in the heavy-quark limit – by *one* hadronic form factor $\xi(v' \cdot v)$, which satisfies $\xi(1) = 1$. If we now compare (4.15) with (4.10), we obtain

$$F_1(q^2) = \frac{M_D + M_B}{2\sqrt{M_D M_B}}\xi(w) \tag{4.16}$$

$$F_0(q^2) = \frac{2\sqrt{M_D M_B}}{M_D + M_B}\left[\frac{1 + w}{2}\right]\xi(w), \tag{4.17}$$

with

$$w \equiv v_D \cdot v_B = \frac{M_D^2 + M_B^2 - q^2}{2M_D M_B}. \tag{4.18}$$

Similar relations hold also for the $\bar{B} \to D^*$ form factors because of the heavy-quark spin symmetry, since the D^* is related to the D by a rotation of the heavy-quark spin. A detailed discussion of these interesting features and the associated "heavy-quark effective theory" (HQET) is beyond the scope of these lectures. For a detailed overview, we refer the reader to [61], where also a comprehensive list of the original references can be found. For a more phenomenological discussion, also [17] is very useful.

4.2.3 Applications

An important application of the formalism sketched above is the extraction of the CKM element $|V_{cb}|$. To this end, $\bar{B} \to D^* \ell \bar{\nu}$ decays are particularly promising. The corresponding rate can be written as

$$\frac{{\rm d}\Gamma}{{\rm d}w} = G_{\rm F}^2 K(M_B, M_{D^*}, w) F(w)^2 |V_{cb}|^2, \tag{4.19}$$

where $K(M_B, M_{D^*}, w)$ is a known kinematic function, and $F(w)$ agrees with the Isgur–Wise function, up to perturbative QCD corrections and $\Lambda_{\rm QCD}/m_{b,c}$ terms. The form factor $F(w)$ is a non-perturbative quantity. However, it satisfies the following normalization condition:

$$F(1) = \eta_A(\alpha_s)\left[1 + \frac{0}{m_c} + \frac{0}{m_b} + \mathcal{O}(\Lambda_{\rm QCD}^2/m_{b,c}^2)\right], \tag{4.20}$$

where $\eta_A(\alpha_s)$ is a perturbatively calculable short-distance QCD factor, and the $\Lambda_{\rm QCD}/m_{b,c}$ corrections *vanish* [61, 62]. The important latter feature is an implication of Luke's theorem [63]. Consequently, if we extract $F(w)|V_{cb}|$ from a measurement of (4.19) as a function of w and extrapolate to the "zero-recoil point" $w = 1$ (where the rate vanishes), we may determine $|V_{cb}|$. In the case of $\bar{B} \to D\ell\bar{\nu}$ decays, we have $\mathcal{O}(\Lambda_{\rm QCD}/m_{b,c})$ corrections to the corresponding rate ${\rm d}\Gamma/{\rm d}w$ at $w = 1$. In order to determine $|V_{cb}|$, inclusive $B \to X_c \ell \bar{\nu}$ decays offer also very attractive avenues. As becomes obvious from (2.24) and

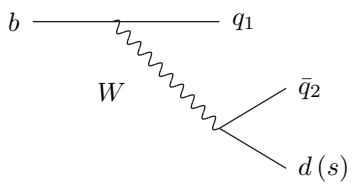

Fig. 9: Tree diagrams ($q_1, q_2 \in \{u, c\}$).

the considerations in Subsection 2.6, $|V_{cb}|$ fixes the normalization of the UT. Moreover, this quantity is an important input parameter for various theoretical calculations. Its current experimental status can be summarized as follows:

$$|V_{cb}| = 0.04 \times [1 \pm 0.05] \quad \Rightarrow \quad A = 0.83 \times [1 \pm 0.05]. \tag{4.21}$$

Let us now turn to $\bar{B} \to \pi\ell\bar{\nu}, \rho\ell\bar{\nu}$ decays, which originate from $b \to u\ell\bar{\nu}$ quark-level processes, as can be seen in Fig. 8, and provide access to $|V_{ub}|$. If we complement this CKM matrix element with $|V_{cb}|$, we may determine the side R_b of the UT with the help of (2.35). The determination of $|V_{ub}|$ is hence a very important aspect of flavour physics. Since the π and ρ are "light" mesons, the HQET symmetry relations cannot be applied to the $\bar{B} \to \pi\ell\bar{\nu}, \rho\ell\bar{\nu}$ modes. Consequently, in order to determine $|V_{ub}|$ from these exclusive channels, the corresponding heavy-to-light form factors have to be described by models. An important alternative is provided by inclusive decays. The corresponding decay rate takes the following form:

$$\Gamma(\bar{B} \to X_u\ell\bar{\nu}) = \frac{G_{\rm F}^2|V_{ub}|^2}{192\pi^3} m_b^5 \left[1 - 2.41\frac{\alpha_s}{\pi} + \frac{\lambda_1 - 9\lambda_2}{2m_b^2} + \ldots\right], \tag{4.22}$$

where λ_1 and λ_2 are non-perturbative parameters, which describe the hadronic matrix elements of certain "kinetic" and "chromomagnetic" operators appearing within the framework of the HQET. Using the heavy-quark expansions

$$M_B = m_b + \bar{\Lambda} - \frac{\lambda_1 + 3\lambda_2}{2m_b} + \ldots, \quad M_{B^*} = m_b + \bar{\Lambda} - \frac{\lambda_1 - \lambda_2}{2m_b} + \ldots \tag{4.23}$$

for the $B^{(*)}$-meson masses, where $\bar{\Lambda} \sim \Lambda_{\rm QCD}$ is another non-perturbative parameter that is related to the light degrees of freedom, the parameter λ_2 can be determined from the measured values of the $M_{B^{(*)}}$. The strong dependence of (4.22) on m_b is a significant source of uncertainty. On the other hand, the $1/m_b^2$ corrections can be better controlled than in the exclusive case (4.20), where we have, moreover, to deal with $1/m_c^2$ corrections. From an experimental point of view, we have to struggle with large backgrounds, which originate from $b \to c\ell\bar{\nu}$ processes and require also a model-dependent treatment. The determination of $|V_{ub}|$ from exclusive and inclusive B-meson decays caused by $b \to u\ell\bar{\nu}$ quark-level processes is therefore a very challenging issue; a summary of the current status is given by

$$|V_{ub}| = 0.0037 \times [1 \pm 0.15]. \tag{4.24}$$

If we now insert (4.24) and (4.21) into (2.35) and use $\lambda = 0.22$, we obtain

$$R_b = 0.41 \pm 0.07. \tag{4.25}$$

For a much more detailed discussion of the determinations of $|V_{cb}|$ and $|V_{ub}|$, addressing also the various interesting recent developments and the future prospects, we refer the reader to [41], where also the references to the vast original literature can be found. Another excellent presentation is given in [17].

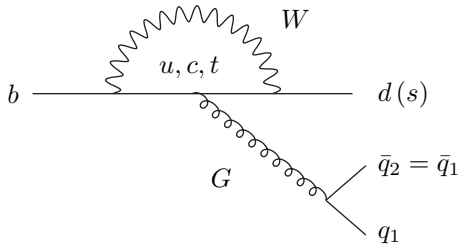

Fig. 10: QCD penguin diagrams ($q_1 = q_2 \in \{u, d, c, s\}$).

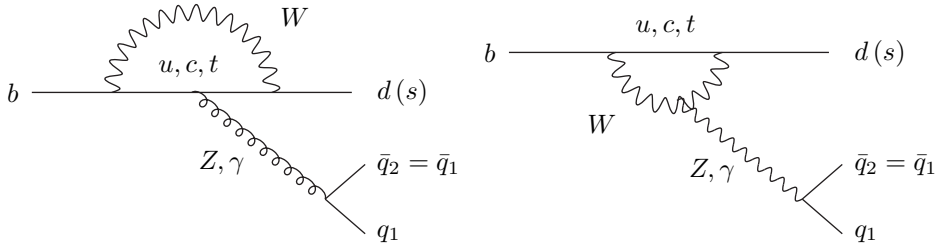

Fig. 11: Electroweak penguin diagrams ($q_1 = q_2 \in \{u, d, c, s\}$).

4.3 Non-Leptonic Decays

4.3.1 Classification

The most complicated B decays are the non-leptonic transitions, which are mediated by $b \to q_1\,\bar{q}_2\,d\,(s)$ quark-level processes, with $q_1, q_2 \in \{u, d, c, s\}$. There are two kinds of topologies contributing to such decays: tree-diagram-like and "penguin" topologies. The latter consist of gluonic (QCD) and electroweak (EW) penguins. In Figs. 9–11, the corresponding leading-order Feynman diagrams are shown. Depending on the flavour content of their final states, we may classify $b \to q_1\,\bar{q}_2\,d\,(s)$ decays as follows:

- $q_1 \neq q_2 \in \{u, c\}$: *only* tree diagrams contribute.
- $q_1 = q_2 \in \{u, c\}$: tree *and* penguin diagrams contribute.
- $q_1 = q_2 \in \{d, s\}$: *only* penguin diagrams contribute.

4.3.2 Low-Energy Effective Hamiltonians

In order to analyse non-leptonic B decays theoretically, one uses low-energy effective Hamiltonians, which are calculated by making use of the "operator product expansion", yielding transition matrix elements of the following structure:

$$\langle f|\mathcal{H}_{\text{eff}}|i\rangle = \frac{G_{\text{F}}}{\sqrt{2}}\lambda_{\text{CKM}}\sum_k C_k(\mu)\langle f|Q_k(\mu)|i\rangle\,. \tag{4.26}$$

The technique of the operator product expansion allows us to separate the short-distance contributions to this transition amplitude from the long-distance ones, which are described by perturbative quantities $C_k(\mu)$ ("Wilson coefficient functions") and non-perturbative quantities $\langle f|Q_k(\mu)|i\rangle$ ("hadronic matrix elements"), respectively. As before, G_{F} is the Fermi constant, whereas λ_{CKM} is a CKM factor and μ denotes an appropriate renormalization scale. The Q_k are local operators, which are generated by electroweak interactions and QCD, and govern "effectively" the decay in question. The Wilson coefficients $C_k(\mu)$ can be considered as scale-dependent couplings related to the vertices described by the Q_k.

In order to illustrate this rather abstract formalism, let us consider the decay $\bar{B}^0_d \to D^+ K^-$, which allows a transparent discussion of the evaluation of the corresponding low-energy effective Hamiltonian. Since this transition originates from a $b \to c\bar{u}s$ quark-level process, it is – as we have seen in our classification in Subsection 4.3.1 – a pure "tree" decay, i.e. we do not have to deal with penguin topologies, which simplifies the analysis considerably. The leading-order Feynman diagram contributing to $\bar{B}^0_d \to D^+ K^-$ can straightforwardly be obtained from Fig. 8 by substituting ℓ and ν by s and u, respectively. Consequently, the lepton current is simply replaced by a quark current, which will have important implications shown below. Evaluating the corresponding Feynman diagram yields

$$-\frac{g_2^2}{8} V_{us}^* V_{cb} \left[\bar{s}\gamma^\nu (1-\gamma_5) u\right] \left[\frac{g_{\nu\mu}}{k^2 - M_W^2}\right] \left[\bar{c}\gamma^\mu (1-\gamma_5) b\right]. \tag{4.27}$$

Because of $k^2 \sim m_b^2 \ll M_W^2$, we may – as in (4.7) – "integrate out" the W boson with the help of (4.2), and arrive at

$$\begin{aligned} \mathcal{H}_{\text{eff}} &= \frac{G_{\text{F}}}{\sqrt{2}} V_{us}^* V_{cb} \left[\bar{s}_\alpha \gamma_\mu (1-\gamma_5) u_\alpha\right] \left[\bar{c}_\beta \gamma^\mu (1-\gamma_5) b_\beta\right] \\ &= \frac{G_{\text{F}}}{\sqrt{2}} V_{us}^* V_{cb} (\bar{s}_\alpha u_\alpha)_{\text{V–A}} (\bar{c}_\beta b_\beta)_{\text{V–A}} \equiv \frac{G_{\text{F}}}{\sqrt{2}} V_{us}^* V_{cb} O_2 \,, \end{aligned} \tag{4.28}$$

where α and β denote the colour indices of the $SU(3)_{\text{C}}$ gauge group of QCD. Effectively, our $b \to c\bar{u}s$ decay process is now described by the "current–current" operator O_2.

If we take QCD corrections into account, operator mixing induces a second "current–current" operator, which is given by

$$O_1 \equiv \left[\bar{s}_\alpha \gamma_\mu (1-\gamma_5) u_\beta\right] \left[\bar{c}_\beta \gamma^\mu (1-\gamma_5) b_\alpha\right]. \tag{4.29}$$

Consequently, we obtain a low-energy effective Hamiltonian of the following structure:

$$\mathcal{H}_{\text{eff}} = \frac{G_{\text{F}}}{\sqrt{2}} V_{us}^* V_{cb} \left[C_1(\mu) O_1 + C_2(\mu) O_2\right], \tag{4.30}$$

where $C_1(\mu) \neq 0$ and $C_2(\mu) \neq 1$ are due to QCD renormalization effects [64]. In order to evaluate these coefficients, we must first calculate the QCD corrections to the decay processes both in the full theory, i.e. with W exchange, and in the effective theory, where the W is integrated out, and have then to express the QCD-corrected transition amplitude in terms of QCD-corrected matrix elements and Wilson coefficients as in (4.26). This procedure is called "matching" between the full and the effective theory. The results for the $C_k(\mu)$ thus obtained contain terms of $\log(\mu/M_W)$, which become large for $\mu = \mathcal{O}(m_b)$, the scale governing the hadronic matrix elements of the O_k. Making use of the renormalization group, which exploits the fact that the transition amplitude (4.26) cannot depend on the chosen renormalization scale μ, we may sum up the following terms of the Wilson coefficients:

$$\alpha_s^n \left[\log\left(\frac{\mu}{M_W}\right)\right]^n \text{ (LO)}, \quad \alpha_s^n \left[\log\left(\frac{\mu}{M_W}\right)\right]^{n-1} \text{ (NLO)}, \quad \ldots \quad ; \tag{4.31}$$

detailed discussions of these rather technical aspects can be found in [22, 65].

For the exploration of CP violation, the class of non-leptonic B decays that receives contributions both from tree and from penguin topologies plays a key rôle. In this important case, the operator basis is much larger than in our example (4.30), where we considered a pure "tree" decay. If we apply the relation

$$V_{ur}^* V_{ub} + V_{cr}^* V_{cb} + V_{tr}^* V_{tb} = 0 \quad (r \in \{d, s\}), \tag{4.32}$$

which follows from the unitarity of the CKM matrix, and "integrate out" the top quark (which enters through the penguin loop processes) and the W boson, we may write

$$\mathcal{H}_{\text{eff}} = \frac{G_{\text{F}}}{\sqrt{2}} \left[\sum_{j=u,c} V_{jr}^* V_{jb} \left\{ \sum_{k=1}^{2} C_k(\mu)\, Q_k^{jr} + \sum_{k=3}^{10} C_k(\mu)\, Q_k^{r} \right\} \right]. \tag{4.33}$$

Here we have introduced another quark-flavour label $j \in \{u, c\}$, and the Q_k^{jr} can be divided as follows:

- Current–current operators:

$$\begin{array}{rcl} Q_1^{jr} & = & (\bar{r}_\alpha j_\beta)_{\text{V–A}} (\bar{j}_\beta b_\alpha)_{\text{V–A}} \\ Q_2^{jr} & = & (\bar{r}_\alpha j_\alpha)_{\text{V–A}} (\bar{j}_\beta b_\beta)_{\text{V–A}}. \end{array} \tag{4.34}$$

- QCD penguin operators:

$$\begin{array}{rcl} Q_3^{r} & = & (\bar{r}_\alpha b_\alpha)_{\text{V–A}} \sum_{q'} (\bar{q}'_\beta q'_\beta)_{\text{V–A}} \\ Q_4^{r} & = & (\bar{r}_\alpha b_\beta)_{\text{V–A}} \sum_{q'} (\bar{q}'_\beta q'_\alpha)_{\text{V–A}} \\ Q_5^{r} & = & (\bar{r}_\alpha b_\alpha)_{\text{V–A}} \sum_{q'} (\bar{q}'_\beta q'_\beta)_{\text{V+A}} \\ Q_6^{r} & = & (\bar{r}_\alpha b_\beta)_{\text{V–A}} \sum_{q'} (\bar{q}'_\beta q'_\alpha)_{\text{V+A}}. \end{array} \tag{4.35}$$

- EW penguin operators (the $e_{q'}$ denote the electrical quark charges):

$$\begin{array}{rcl} Q_7^{r} & = & \frac{3}{2} (\bar{r}_\alpha b_\alpha)_{\text{V–A}} \sum_{q'} e_{q'} (\bar{q}'_\beta q'_\beta)_{\text{V+A}} \\ Q_8^{r} & = & \frac{3}{2} (\bar{r}_\alpha b_\beta)_{\text{V–A}} \sum_{q'} e_{q'} (\bar{q}'_\beta q'_\alpha)_{\text{V+A}} \\ Q_9^{r} & = & \frac{3}{2} (\bar{r}_\alpha b_\alpha)_{\text{V–A}} \sum_{q'} e_{q'} (\bar{q}'_\beta q'_\beta)_{\text{V–A}} \\ Q_{10}^{r} & = & \frac{3}{2} (\bar{r}_\alpha b_\beta)_{\text{V–A}} \sum_{q'} e_{q'} (\bar{q}'_\beta q'_\alpha)_{\text{V–A}}. \end{array} \tag{4.36}$$

The current–current, QCD and EW penguin operators are related to the tree, QCD and EW penguin processes shown in Figs. 9–11. At a renormalization scale $\mu = \mathcal{O}(m_b)$, the Wilson coefficients of the current–current operators are $C_1(\mu) = \mathcal{O}(10^{-1})$ and $C_2(\mu) = \mathcal{O}(1)$, whereas those of the penguin operators are $\mathcal{O}(10^{-2})$ [22, 65]. Note that penguin topologies with internal charm- and up-quark exchanges [66] are described in this framework by penguin-like matrix elements of the corresponding current–current operators [67], and may also have important phenomenological consequences [68, 69].

Since the ratio $\alpha/\alpha_s = \mathcal{O}(10^{-2})$ of the QED and QCD couplings is very small, we would expect naïvely that EW penguins should play a minor rôle in comparison with QCD penguins. This would actually be the case if the top quark was not "heavy". However, since the Wilson coefficient C_9 increases strongly with m_t, we obtain interesting EW penguin effects in several B decays: $B \to K\phi$ modes are affected significantly by EW penguins, whereas $B \to \pi\phi$ and $B_s \to \pi^0\phi$ transitions are even *dominated* by such topologies [70, 71]. EW penguins also have an important impact on the $B \to \pi K$ system [72], as we will see in Subsection 7.2.

The low-energy effective Hamiltonians discussed above apply to all B decays that are caused by the same quark-level transition, i.e. they are "universal". Consequently, the differences between the various exclusive modes of a given decay class arise within this formalism only through the hadronic matrix elements of the relevant four-quark operators. Unfortunately, the evaluation of such matrix elements is associated with large uncertainties and is a very challenging task. In this context, "factorization" is a widely used concept, which is our next topic.

4.3.3 Factorization of Hadronic Matrix Elements

In order to discuss "factorization", let us consider once more the decay $\bar{B}_d^0 \to D^+ K^-$. Evaluating the corresponding transition amplitude, we encounter the hadronic matrix elements of the $O_{1,2}$ operators between the $\langle K^- D^+|$ final and the $|\bar{B}_d^0\rangle$ initial states. If we use the well-known $SU(N_{\text{C}})$ colour-algebra relation

$$T^a_{\alpha\beta} T^a_{\gamma\delta} = \frac{1}{2} \left(\delta_{\alpha\delta}\delta_{\beta\gamma} - \frac{1}{N_{\text{C}}} \delta_{\alpha\beta}\delta_{\gamma\delta} \right) \tag{4.37}$$

to rewrite the operator O_1, we obtain

$$\langle K^- D^+|\mathcal{H}_{\rm eff}|\bar{B}^0_d\rangle = \frac{G_{\rm F}}{\sqrt{2}} V^*_{us} V_{cb}\Big[a_1 \langle K^- D^+|(\bar{s}_\alpha u_\alpha)_{\rm V\text{–}A}(\bar{c}_\beta b_\beta)_{\rm V\text{–}A}|\bar{B}^0_d\rangle + 2\, C_1 \langle K^- D^+|(\bar{s}_\alpha\, T^a_{\alpha\beta}\, u_\beta)_{\rm V\text{–}A}(\bar{c}_\gamma\, T^a_{\gamma\delta}\, b_\delta)_{\rm V\text{–}A}|\bar{B}^0_d\rangle\Big], \tag{4.38}$$

with

$$a_1 = C_1/N_{\rm C} + C_2 \sim 1. \tag{4.39}$$

It is now straightforward to "factorize" the hadronic matrix elements in (4.38):

$$\begin{aligned}
&\langle K^- D^+|(\bar{s}_\alpha u_\alpha)_{\rm V\text{–}A}(\bar{c}_\beta b_\beta)_{\rm V\text{–}A}|\bar{B}^0_d\rangle\Big|_{\rm fact} \\
&\quad = \langle K^-|\,[\bar{s}_\alpha \gamma_\mu(1-\gamma_5)u_\alpha]\,|0\rangle \langle D^+|\,[\bar{c}_\beta\gamma^\mu(1-\gamma_5)b_\beta]\,|\bar{B}^0_d\rangle \\
&\quad = \underbrace{i f_K}_{\text{decay constant}} \times \underbrace{F_0^{(BD)}(M_K^2)}_{B\to D\text{ form factor}} \times \underbrace{(M_B^2 - M_D^2)}_{\text{kinematical factor}},
\end{aligned} \tag{4.40}$$

$$\langle K^- D^+|(\bar{s}_\alpha\, T^a_{\alpha\beta}\, u_\beta)_{\rm V\text{–}A}(\bar{c}_\gamma\, T^a_{\gamma\delta}\, b_\delta)_{\rm V\text{–}A}|\bar{B}^0_d\rangle\Big|_{\rm fact} = 0. \tag{4.41}$$

The quantity a_1 is a phenomenological "colour factor", which governs "colour-allowed" decays; the decay $\bar{B}^0_d \to D^+ K^-$ belongs to this category, since the colour indices of the K^- meson and the $\bar{B}^0_d$–D^+ system run independently from each other in the corresponding leading-order diagram. On the other hand, in the case of "colour-suppressed" modes, for instance $\bar{B}^0_d \to \pi^0 D^0$, where only one colour index runs through the whole diagram, we have to deal with the combination

$$a_2 = C_1 + C_2/N_{\rm C} \sim 0.25. \tag{4.42}$$

The concept of factorizing the hadronic matrix elements of four-quark operators into the product of hadronic matrix elements of quark currents has a long history [73], and can be justified, for example, in the large-$N_{\rm C}$ limit [74]. Interesting recent developments are the following:

- "QCD factorization" [75], which is in accordance with the old picture that factorization should hold for certain decays in the limit of $m_b \gg \Lambda_{\rm QCD}$ [76], provides a formalism to calculate the relevant amplitudes at the leading order of a $\Lambda_{\rm QCD}/m_b$ expansion. The resulting expression for the transition amplitudes incorporates elements both of the naïve factorization approach sketched above and of the hard-scattering picture. Let us consider a decay $\bar{B} \to M_1 M_2$, where M_1 picks up the spectator quark. If M_1 is either a heavy (D) or a light (π, K) meson, and M_2 a light (π, K) meson, QCD factorization gives a transition amplitude of the following structure:

  $$A(\bar{B} \to M_1 M_2) = [\text{"naïve factorization"}] \times [1 + \mathcal{O}(\alpha_s) + \mathcal{O}(\Lambda_{\rm QCD}/m_b)]\,. \tag{4.43}$$

  While the $\mathcal{O}(\alpha_s)$ terms, i.e. the radiative non-factorizable corrections, can be calculated systematically, the main limitation of the theoretical accuracy originates from the $\mathcal{O}(\Lambda_{\rm QCD}/m_b)$ terms.
- Another QCD approach to deal with non-leptonic B-meson decays – the "perturbative hard-scattering approach " (PQCD) – was developed independently in [77], and differs from the QCD factorization formalism in some technical aspects.
- A very useful technique for "factorization proofs" is provided by the framework of the "soft collinear effective theory" (SCET) [78].
- Non-leptonic B decays can also be studied within QCD light-cone sum-rule approaches [79].

A detailed presentation of these topics would be very technical and is beyond the scope of these lectures. However, for the discussion of the CP-violating effects in the B-meson system, we must only be familiar with the general structure of the non-leptonic B decay amplitudes and not enter the details of the techniques to deal with the corresponding hadronic matrix elements. Let us finally note that the B-factory data will eventually decide how well factorization and the new concepts sketched above are actually working. For example, recent data on the $B \to \pi\pi$ system point towards large non-factorizable corrections [48, 54], to which we shall return in Subsection 6.2.2.

4.4 Towards Studies of CP Violation

As we have seen above, leptonic and semileptonic B-meson decays involve only a single weak (CKM) amplitude. On the other hand, the structure of non-leptonic transitions is considerably more complicated. However, because of the unitarity of the CKM matrix, which implies the relation in (4.32), we may write the amplitude of *any* non-leptonic B-meson decay within the SM in such a manner that we encounter at most two contributions with different CKM factors (we will encounter explicit examples below):

$$A(\bar{B} \to \bar{f}) = e^{+i\varphi_1}|A_1|e^{i\delta_1} + e^{+i\varphi_2}|A_2|e^{i\delta_2} \tag{4.44}$$

$$A(B \to f) = e^{-i\varphi_1}|A_1|e^{i\delta_1} + e^{-i\varphi_2}|A_2|e^{i\delta_2}. \tag{4.45}$$

Here the $\varphi_{1,2}$ denote CP-violating weak phases, which are introduced by the elements of the CKM matrix, whereas the $|A_{1,2}|e^{i\delta_{1,2}}$ are CP-conserving "strong" amplitudes, which contain the whole hadron dynamics of the decay at hand:

$$|A|e^{i\delta} \sim \sum_k \underbrace{C_k(\mu)}_{\text{pert. QCD}} \times \underbrace{\langle \bar{f}|Q_k(\mu)|\bar{B}\rangle}_{\text{non-pert. QCD}}. \tag{4.46}$$

If we use (4.44) and (4.45), it is an easy exercise to calculate the following CP-violating rate asymmetry:

$$\begin{aligned} \mathcal{A}_{\rm CP} &\equiv \frac{\Gamma(B \to f) - \Gamma(\bar{B} \to \bar{f})}{\Gamma(B \to f) + \Gamma(\bar{B} \to \bar{f})} = \frac{|A(B \to f)|^2 - |A(\bar{B} \to \bar{f})|^2}{|A(B \to f)|^2 + |A(\bar{B} \to \bar{f})|^2} \\ &= \frac{2|A_1||A_2|\sin(\delta_1 - \delta_2)\sin(\varphi_1 - \varphi_2)}{|A_1|^2 + 2|A_1||A_2|\cos(\delta_1 - \delta_2)\cos(\varphi_1 - \varphi_2) + |A_2|^2}. \end{aligned} \tag{4.47}$$

Consequently, a non-vanishing CP asymmetry $\mathcal{A}_{\rm CP}$ arises from the interference effects between the two weak amplitudes, and requires both a non-trivial weak phase difference $\varphi_1 - \varphi_2$ and a non-trivial strong phase difference $\delta_1 - \delta_2$. This kind of CP violation is referred to as "direct" CP violation, as it originates directly at the amplitude level of the considered decay. It is the B-meson counterpart of the effects that are probed through $\mathrm{Re}(\varepsilon'/\varepsilon)$ in the neutral kaon system.[2] Since $\varphi_1 - \varphi_2$ is in general given by one of the angles of the UT – usually γ – the goal is to determine this quantity from the measured value of $\mathcal{A}_{\rm CP}$. Unfortunately, the extraction of $\varphi_1 - \varphi_2$ from $\mathcal{A}_{\rm CP}$ is affected by hadronic uncertainties, which are related to the poorly known hadronic matrix elements entering the expression (4.46) for the strong amplitudes $|A_{1,2}|e^{i\delta_{1,2}}$. In order to deal with this problem, we may, in principle, proceed along one of the following three main avenues:

i) The most obvious one – but also the most challenging – is to try to *calculate* the relevant hadronic matrix elements $\langle \bar{f}|Q_k(\mu)|\bar{B}\rangle$. As we have noted above, interesting progress has recently been made in this direction through the development of the QCD factorization, PQCD, SCET and QCD light-cone sum-rule approaches.

ii) We may search for fortunate cases, where relations between various decay amplitudes allow us to *eliminate* the poorly known hadronic matrix elements. As we shall see, this avenue offers in particular determinations of the UT angle γ: we distinguish between exact relations, which are provided by pure "tree" decays of the kind $B \to KD$ or $B_c \to D_s D$, and relations, which follow from the flavour symmetries of strong interactions, involving $B_{(s)} \to \pi\pi, \pi K, KK$ transitions.

iii) Finally, we may exploit the fact that in decays of neutral B_q mesons ($q \in \{d, s\}$) interference effects between B_q^0–$\bar{B}_q^0$ mixing and decay processes may yield another kind of CP violation, "mixing-induced CP violation". In certain cases, the hadronic matrix elements *cancel* in such CP asymmeties.

[2] In order to calculate this quantity, an approriate low-energy effective Hamiltonian having the same structure as (4.33) is used. The large theoretical uncertainties mentioned in Subsection 3.1 originate from a strong cancellation between the contributions of the QCD and EW penguins (caused by the large top-quark mass) and the associated hadronic matrix elements.

In the remainder of these lectures, we will not consider (i) further. For the exploration of CP violation and the testing of the KM mechanism, the theoretical input related to strong-interaction physics should obviously be reduced as much as possible. In contrast to (i), this feature is present in (ii) and (iii), which provide – as a by-product – also important insights into hadron dynamics. In particular, we may extract various hadronic parameters from the data that can be calculated with the help of the theoretical frameworks listed in (i), thereby allowing us to test them through a confrontation with nature. Since neutral B_q mesons are a key element in this programme, offering also attractive connections between (ii) and (iii), let us next have a closer look at their most important features.

5 FEATURES OF NEUTRAL $B_{d,s}$ MESONS

5.1 $B^0_{d,s}$–$\bar{B}^0_{d,s}$ Mixing

Within the SM, B^0_q–$\bar{B}^0_q$ mixing ($q \in \{d, s\}$) arises from the box diagrams shown in Fig. 12. Because of this phenomenon, an initially, i.e. at time $t = 0$, present B^0_q-meson state evolves into a time-dependent linear combination of B^0_q and $\bar{B}^0_q$ states:

$$|B_q(t)\rangle = a(t)|B^0_q\rangle + b(t)|\bar{B}^0_q\rangle, \tag{5.1}$$

where $a(t)$ and $b(t)$ are governed by a Schrödinger equation of the following form:

$$i\,\frac{\mathrm{d}}{\mathrm{d}t}\begin{pmatrix} a(t) \\ b(t)\end{pmatrix} = H\cdot\begin{pmatrix} a(t) \\ b(t)\end{pmatrix} \equiv \underbrace{\left[\begin{pmatrix} M^{(q)}_0 & M^{(q)}_{12} \\ M^{(q)*}_{12} & M^{(q)}_0\end{pmatrix}\right.}_{\text{mass matrix}} \underbrace{\left. -\frac{i}{2}\begin{pmatrix} \Gamma^{(q)}_0 & \Gamma^{(q)}_{12} \\ \Gamma^{(q)*}_{12} & \Gamma^{(q)}_0\end{pmatrix}\right]}_{\text{decay matrix}}\cdot\begin{pmatrix} a(t) \\ b(t)\end{pmatrix}. \tag{5.2}$$

The special form $H_{11} = H_{22}$ of the Hamiltonian H is an implication of the CPT theorem, i.e. of the invariance under combined CP and time-reversal (T) transformations.

5.1.1 Solution of the Schrödinger Equation

It is straightforward to calculate the eigenstates $|B^{(q)}_\pm\rangle$ and eigenvalues $\lambda^{(q)}_\pm$ of (5.2):

$$|B^{(q)}_\pm\rangle = \frac{1}{\sqrt{1+|\alpha_q|^2}}\left(|B^0_q\rangle \pm \alpha_q|\bar{B}^0_q\rangle\right) \tag{5.3}$$

$$\lambda^{(q)}_\pm = \left(M^{(q)}_0 - \frac{i}{2}\Gamma^{(q)}_0\right) \pm \left(M^{(q)}_{12} - \frac{i}{2}\Gamma^{(q)}_{12}\right)\alpha_q, \tag{5.4}$$

where

$$\alpha_q e^{+i\left(\Theta^{(q)}_{\Gamma_{12}}+n'\pi\right)} = \sqrt{\frac{4|M^{(q)}_{12}|^2 e^{-i2\delta\Theta^{(q)}_{M/\Gamma}} + |\Gamma^{(q)}_{12}|^2}{4|M^{(q)}_{12}|^2 + |\Gamma^{(q)}_{12}|^2 - 4|M^{(q)}_{12}||\Gamma^{(q)}_{12}|\sin\delta\Theta^{(q)}_{M/\Gamma}}}. \tag{5.5}$$

Here we have written

$$M^{(q)}_{12} \equiv e^{i\Theta^{(q)}_{M_{12}}}|M^{(q)}_{12}|, \quad \Gamma^{(q)}_{12} \equiv e^{i\Theta^{(q)}_{\Gamma_{12}}}|\Gamma^{(q)}_{12}|, \quad \delta\Theta^{(q)}_{M/\Gamma} \equiv \Theta^{(q)}_{M_{12}} - \Theta^{(q)}_{\Gamma_{12}}, \tag{5.6}$$

and have introduced the quantity $n' \in \{0, 1\}$ to parametrize the sign of the square root in (5.5).

Evaluating the dispersive parts of the box diagrams shown in Fig 12, which are dominated by internal top-quark exchanges, yields (for a more detailed discussion, see [21]):

$$M^{(q)}_{12} = \frac{G^2_{\mathrm{F}}M^2_W}{12\pi^2}\eta_B M_{B_q}\hat{B}_{B_q}f^2_{B_q}\left(V^*_{tq}V_{tb}\right)^2 S_0(x_t)e^{i(\pi-\phi_{\mathrm{CP}}(B_q))}, \tag{5.7}$$

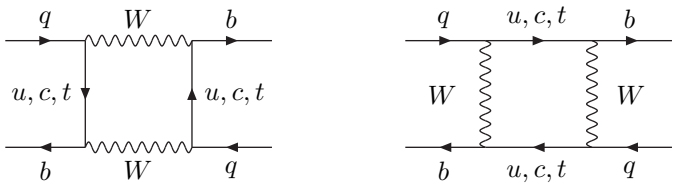

Fig. 12: Box diagrams contributing to B_q^0–$\bar{B}_q^0$ mixing in the SM ($q \in \{d, s\}$).

where $\eta_B = 0.55 \pm 0.01$ is a perturbative QCD correction [80],[3] the non-perturbative "bag" parameter $\hat{B}_{B_q}$ is related to the hadronic matrix element $\langle \bar{B}_q^0 | (\bar{b}q)_{\mathrm{V-A}} (\bar{b}q)_{\mathrm{V-A}} | B_q^0 \rangle$, and $S_0(x_t \equiv m_t^2/M_W^2)$ is one of the "Inami–Lim" functions [81], describing the dependence on the top-quark mass m_t. In the SM, we may write – to a good approximation – the following expression [82]:

$$S_0(x_t) = 2.40 \times \left[\frac{m_t}{167\,\mathrm{GeV}} \right]^{1.52}. \tag{5.8}$$

Finally, $\phi_{\mathrm{CP}}(B_q)$ is a convention-dependent phase, which is introduced through the CP transformation

$$(\mathcal{CP}) |B_q^0\rangle = e^{i\phi_{\mathrm{CP}}(B_q)} |\bar{B}_q^0\rangle. \tag{5.9}$$

If we calculate also the absorptive parts of the box diagrams in Fig 12, we obtain

$$\frac{\Gamma_{12}^{(q)}}{M_{12}^{(q)}} \approx -\frac{3\pi}{2 S_0(x_t)} \left(\frac{m_b^2}{M_W^2} \right) = \mathcal{O}(m_b^2/m_t^2) \ll 1. \tag{5.10}$$

Consequently, we may expand (5.5) in $\Gamma_{12}^{(q)}/M_{12}^{(q)}$. Neglecting second-order terms, we arrive at

$$\alpha_q = \left[1 + \frac{1}{2} \left| \frac{\Gamma_{12}^{(q)}}{M_{12}^{(q)}} \right| \sin \delta\Theta_{M/\Gamma}^{(q)} \right] e^{-i\left(\Theta_{M_{12}}^{(q)} + n'\pi\right)}. \tag{5.11}$$

The deviation of $|\alpha_q|$ from 1 measures CP violation in B_q^0–$\bar{B}_q^0$ oscillations, and can be probed through the following "wrong-charge" lepton asymmetries:

$$\mathcal{A}_{\mathrm{SL}}^{(q)} \equiv \frac{\Gamma(B_q^0(t) \to \ell^- \bar{\nu} X) - \Gamma(\bar{B}_q^0(t) \to \ell^+ \nu X)}{\Gamma(B_q^0(t) \to \ell^- \bar{\nu} X) + \Gamma(\bar{B}_q^0(t) \to \ell^+ \nu X)} = \frac{|\alpha_q|^4 - 1}{|\alpha_q|^4 + 1} \approx \left| \frac{\Gamma_{12}^{(q)}}{M_{12}^{(q)}} \right| \sin \delta\Theta_{M/\Gamma}^{(q)}. \tag{5.12}$$

Because of $|\Gamma_{12}^{(q)}|/|M_{12}^{(q)}| \propto m_b^2/m_t^2$ and $\sin \delta\Theta_{M/\Gamma}^{(q)} \propto m_c^2/m_b^2$, the asymmetry $\mathcal{A}_{\mathrm{SL}}^{(q)}$ is suppressed by a factor of $m_c^2/m_t^2 = \mathcal{O}(10^{-4})$ and is hence tiny in the SM. However, this observable may be enhanced through NP effects, thereby representing an interesing probe for physics beyond the SM [83, 84]. The current experimental constraints for $\mathcal{A}_{\mathrm{SL}}^{(q)}$ are at the 10^{-2} level.

5.1.2 Mixing Parameters

Let us denote the masses of the eigenstates of (5.2) by $M_{\mathrm{H}}^{(q)}$ ("heavy") and $M_{\mathrm{L}}^{(q)}$ ("light"). It is then useful to introduce

$$M_q \equiv \frac{M_{\mathrm{H}}^{(q)} + M_{\mathrm{L}}^{(q)}}{2} = M_0^{(q)}, \tag{5.13}$$

as well as the mass difference

$$\Delta M_q \equiv M_{\mathrm{H}}^{(q)} - M_{\mathrm{L}}^{(q)} = 2|M_{12}^{(q)}| > 0, \tag{5.14}$$

[3] Note that the short-distance parameter η_B does *not* depend on $q \in \{d, s\}$, i.e. is the same for B_d and B_s mesons.

which is by definition *positive*. Using (2.36) and (5.7), we find that we may convert the mass difference ΔM_d of the B_d-meson system into the side R_t of the UT with the help of the following expression:

$$R_t = \frac{1.10}{A\sqrt{|S_0(x_t)|}} \sqrt{\frac{\Delta M_d}{0.50\,\mathrm{ps}^{-1}}} \left[\frac{230\,\mathrm{MeV}}{\sqrt{\hat{B}_{B_d}} f_{B_d}}\right] \sqrt{\frac{0.55}{\eta_B}}, \tag{5.15}$$

where A is the usual Wolfenstein parameter. We shall return to this important issue in Subsection 8.1.2.

On the other hand, the decay widths $\Gamma_{\mathrm{H}}^{(q)}$ and $\Gamma_{\mathrm{L}}^{(q)}$ of the mass eigenstates, which correspond to $M_{\mathrm{H}}^{(q)}$ and $M_{\mathrm{L}}^{(q)}$, respectively, satisfy

$$\Delta\Gamma_q \equiv \Gamma_{\mathrm{H}}^{(q)} - \Gamma_{\mathrm{L}}^{(q)} = \frac{4\,\mathrm{Re}\left[M_{12}^{(q)}\Gamma_{12}^{(q)*}\right]}{\Delta M_q}, \tag{5.16}$$

whereas

$$\Gamma_q \equiv \frac{\Gamma_{\mathrm{H}}^{(q)} + \Gamma_{\mathrm{L}}^{(q)}}{2} = \Gamma_0^{(q)}. \tag{5.17}$$

There is the following interesting relation:

$$\frac{\Delta\Gamma_q}{\Gamma_q} \approx -\frac{3\pi}{2S_0(x_t)} \left(\frac{m_b^2}{M_W^2}\right) x_q = -\mathcal{O}(10^{-2}) \times x_q, \tag{5.18}$$

where

$$x_q \equiv \frac{\Delta M_q}{\Gamma_q} = \begin{cases} 0.771 \pm 0.012 & (q = d) \\ \mathcal{O}(20) & (q = s) \end{cases} \tag{5.19}$$

denotes the B_q^0–$\bar{B}_q^0$ "mixing parameter".[4] Consequently, we observe that $\Delta\Gamma_d/\Gamma_d \sim 10^{-2}$ is negligibly small, while $\Delta\Gamma_s/\Gamma_s \sim 10^{-1}$ may be sizeable. For a discussion of the experimental status of the B_q mixing parameters, the reader is referred to [85, 86].

5.1.3 Time-Dependent Decay Rates

The time evolution of initially, i.e. at $t = 0$, pure B_q^0- and $\bar{B}_q^0$-meson states is given by

$$|B_q^0(t)\rangle = f_+^{(q)}(t)|B_q^0\rangle + \alpha_q f_-^{(q)}(t)|\bar{B}_q^0\rangle \tag{5.20}$$

and

$$|\bar{B}_q^0(t)\rangle = \frac{1}{\alpha_q} f_-^{(q)}(t)|B_q^0\rangle + f_+^{(q)}(t)|\bar{B}_q^0\rangle, \tag{5.21}$$

respectively, with

$$f_\pm^{(q)}(t) = \frac{1}{2}\left[e^{-i\lambda_+^{(q)}t} \pm e^{-i\lambda_-^{(q)}t}\right]. \tag{5.22}$$

These time-dependent state vectors allow the calculation of the corresponding transition rates. To this end, it is useful to introduce

$$|g_\pm^{(q)}(t)|^2 = \frac{1}{4}\left[e^{-\Gamma_{\mathrm{L}}^{(q)}t} + e^{-\Gamma_{\mathrm{H}}^{(q)}t} \pm 2\,e^{-\Gamma_q t}\cos(\Delta M_q t)\right] \tag{5.23}$$

$$g_-^{(q)}(t)\,g_+^{(q)}(t)^* = \frac{1}{4}\left[e^{-\Gamma_{\mathrm{L}}^{(q)}t} - e^{-\Gamma_{\mathrm{H}}^{(q)}t} + 2\,i\,e^{-\Gamma_q t}\sin(\Delta M_q t)\right], \tag{5.24}$$

[4] Note that $\Delta\Gamma_q/\Gamma_q$ is negative in the SM because of the minus sign in (5.18).

as well as

$$\xi_f^{(q)} = e^{-i\Theta_{M_{12}}^{(q)}} \frac{A(\bar{B}_q^0 \to f)}{A(B_q^0 \to f)}, \quad \xi_{\bar{f}}^{(q)} = e^{-i\Theta_{M_{12}}^{(q)}} \frac{A(\bar{B}_q^0 \to \bar{f})}{A(B_q^0 \to \bar{f})}. \tag{5.25}$$

Looking at (5.7), we find

$$\Theta_{M_{12}}^{(q)} = \pi + 2\text{arg}(V_{tq}^* V_{tb}) - \phi_{\text{CP}}(B_q), \tag{5.26}$$

and observe that this phase depends on the chosen CKM and CP phase conventions specified in (2.8) and (5.9), respectively. However, these dependences are cancelled through the amplitude ratios in (5.25), so that $\xi_f^{(q)}$ and $\xi_{\bar{f}}^{(q)}$ are *convention-independent* observables. Whereas n' enters the functions in (5.22) through (5.4), the dependence on this parameter is cancelled in (5.23) and (5.24) through the introduction of the *positive* mass difference ΔM_q (see (5.14)). Combining the formulae listed above, we eventually arrive at the following transition rates for decays of initially, i.e. at $t = 0$, present B_q^0 or $\bar{B}_q^0$ mesons:

$$\Gamma(\overset{(-)}{B}{}_q^0\,(t) \to f) = \left[|g_{\mp}^{(q)}(t)|^2 + |\xi_f^{(q)}|^2 |g_{\pm}^{(q)}(t)|^2 - 2\,\text{Re}\left\{\xi_f^{(q)} g_{\pm}^{(q)}(t) g_{\mp}^{(q)}(t)^*\right\}\right] \tilde{\Gamma}_f, \tag{5.27}$$

where the time-independent rate $\tilde{\Gamma}_f$ corresponds to the "unevolved" decay amplitude $A(B_q^0 \to f)$, and can be calculated by performing the usual phase-space integrations. The rates into the CP-conjugate final state $\bar{f}$ can straightforwardly be obtained from (5.27) by making the substitutions

$$\tilde{\Gamma}_f \;\to\; \tilde{\Gamma}_{\bar{f}}, \quad \xi_f^{(q)} \;\to\; \xi_{\bar{f}}^{(q)}. \tag{5.28}$$

5.2 CP Asymmetries

A particularly simple – but also very interesting – situation arises if we restrict ourselves to decays of neutral B_q mesons into final states f that are eigenstates of the CP operator, i.e. satisfy the relation

$$(\mathcal{CP})|f\rangle = \pm|f\rangle. \tag{5.29}$$

Consequently, we have $\xi_f^{(q)} = \xi_{\bar{f}}^{(q)}$ in this case, as can be seen in (5.25). Using the decay rates in (5.27), we find that the corresponding time-dependent CP asymmetry is given by

$$\begin{aligned} \mathcal{A}_{\text{CP}}(t) &\equiv \frac{\Gamma(B_q^0(t) \to f) - \Gamma(\bar{B}_q^0(t) \to f)}{\Gamma(B_q^0(t) \to f) + \Gamma(\bar{B}_q^0(t) \to f)} \\ &= \left[\frac{\mathcal{A}_{\text{CP}}^{\text{dir}}(B_q \to f)\,\cos(\Delta M_q t) + \mathcal{A}_{\text{CP}}^{\text{mix}}(B_q \to f)\,\sin(\Delta M_q t)}{\cosh(\Delta\Gamma_q t/2) - \mathcal{A}_{\Delta\Gamma}(B_q \to f)\,\sinh(\Delta\Gamma_q t/2)}\right], \end{aligned} \tag{5.30}$$

with

$$\mathcal{A}_{\text{CP}}^{\text{dir}}(B_q \to f) \equiv \frac{1 - |\xi_f^{(q)}|^2}{1 + |\xi_f^{(q)}|^2}, \qquad \mathcal{A}_{\text{CP}}^{\text{mix}}(B_q \to f) \equiv \frac{2\,\text{Im}\,\xi_f^{(q)}}{1 + |\xi_f^{(q)}|^2}. \tag{5.31}$$

Because of the relation

$$\mathcal{A}_{\text{CP}}^{\text{dir}}(B_q \to f) = \frac{|A(B_q^0 \to f)|^2 - |A(\bar{B}_q^0 \to \bar{f})|^2}{|A(B_q^0 \to f)|^2 + |A(\bar{B}_q^0 \to \bar{f})|^2}, \tag{5.32}$$

this observable measures the direct CP violation in the decay $B_q \to f$, which originates from the interference between different weak amplitudes, as we have seen in (4.47). On the other hand, the interesting *new* aspect of (5.30) is due to $\mathcal{A}_{\text{CP}}^{\text{mix}}(B_q \to f)$, which originates from interference effects between B_q^0–$\bar{B}_q^0$ mixing and decay processes, and describes "mixing-induced" CP violation. Finally, the width difference $\Delta\Gamma_q$, which may be sizeable in the B_s-meson system, provides another observable,

$$\mathcal{A}_{\Delta\Gamma}(B_q \to f) \equiv \frac{2\,\text{Re}\,\xi_f^{(q)}}{1 + |\xi_f^{(q)}|^2}, \tag{5.33}$$

which is, however, not independent from $\mathcal{A}_{\rm CP}^{\rm dir}(B_q \to f)$ and $\mathcal{A}_{\rm CP}^{\rm mix}(B_q \to f)$, satisfying

$$\left[\mathcal{A}_{\rm CP}^{\rm dir}(B_q \to f)\right]^2 + \left[\mathcal{A}_{\rm CP}^{\rm mix}(B_q \to f)\right]^2 + \left[\mathcal{A}_{\Delta\Gamma}(B_q \to f)\right]^2 = 1. \tag{5.34}$$

In order to calculate the quantity $\xi_f^{(q)}$, which contains essentially all the information that is required for the evaluation of the observables provided by the time-dependent CP asymmetry introduced in (5.30), we employ the low-energy effective Hamiltonian (4.33):

$$\begin{aligned} A(\bar{B}_q^0 \to f) &= \langle f|\mathcal{H}_{\rm eff}|\bar{B}_q^0\rangle \\ &= \frac{G_{\rm F}}{\sqrt{2}}\left[\sum_{j=u,c} V_{jr}^* V_{jb}\left\{\sum_{k=1}^{2} C_k(\mu)\langle f|Q_k^{jr}(\mu)|\bar{B}_q^0\rangle + \sum_{k=3}^{10} C_k(\mu)\langle f|Q_k^{r}(\mu)|\bar{B}_q^0\rangle\right\}\right]. \end{aligned} \tag{5.35}$$

On the other hand, we also have

$$\begin{aligned} A(B_q^0 \to f) &= \langle f|\mathcal{H}_{\rm eff}^\dagger|B_q^0\rangle \\ &= \frac{G_{\rm F}}{\sqrt{2}}\left[\sum_{j=u,c} V_{jr} V_{jb}^*\left\{\sum_{k=1}^{2} C_k(\mu)\langle f|Q_k^{jr\dagger}(\mu)|B_q^0\rangle + \sum_{k=3}^{10} C_k(\mu)\langle f|Q_k^{r\dagger}(\mu)|B_q^0\rangle\right\}\right]. \end{aligned} \tag{5.36}$$

If we now insert the operator $(\mathcal{CP})^\dagger(\mathcal{CP}) = \hat{1}$ both after the $\langle f|$ and in front of the $|B_q^0\rangle$, we obtain

$$\begin{aligned} A(B_q^0 \to f) &= \pm e^{i\phi_{\rm CP}(B_q)} \\ &\times \frac{G_{\rm F}}{\sqrt{2}}\left[\sum_{j=u,c} V_{jr} V_{jb}^*\left\{\sum_{k=1}^{2} C_k(\mu)\langle f|Q_k^{jr}(\mu)|\bar{B}_q^0\rangle + \sum_{k=3}^{10} C_k(\mu)\langle f|Q_k^{r}(\mu)|\bar{B}_q^0\rangle\right\}\right], \end{aligned} \tag{5.37}$$

where we have also applied the relation $(\mathcal{CP})Q_k^{jr\dagger}(\mathcal{CP})^\dagger = Q_k^{jr}$, and have furthermore taken (5.9) into account. Using then (5.25) and (5.26), we observe that the phase-convention-dependent quantity $\phi_{\rm CP}(B_q)$ cancels, and finally arrive at

$$\xi_f^{(q)} = \mp\, e^{-i\phi_q}\left[\frac{\sum\limits_{j=u,c} V_{jr}^* V_{jb}\langle f|\mathcal{Q}^{jr}|\bar{B}_q^0\rangle}{\sum\limits_{j=u,c} V_{jr} V_{jb}^*\langle f|\mathcal{Q}^{jr}|\bar{B}_q^0\rangle}\right]. \tag{5.38}$$

Here we have introduced the abbreviation

$$\mathcal{Q}^{jr} \equiv \sum_{k=1}^{2} C_k(\mu)\, Q_k^{jr} + \sum_{k=3}^{10} C_k(\mu)\, Q_k^{r}, \tag{5.39}$$

and

$$\phi_q \equiv 2\arg(V_{tq}^* V_{tb}) = \begin{cases} +2\beta & (q = d) \\ -2\delta\gamma & (q = s) \end{cases} \tag{5.40}$$

(where β and $\delta\gamma$ are the angles in the unitarity triangles illustrated in Fig. 3) is the CP-violating weak phase introduced by B_q^0–$\bar{B}_q^0$ mixing within the SM.

Using the notation of (4.44) and (4.45), we may rewrite (5.38) as follows:

$$\xi_f^{(q)} = \mp\, e^{-i\phi_q}\left[\frac{e^{+i\varphi_1}|A_1|e^{i\delta_1} + e^{+i\varphi_2}|A_2|e^{i\delta_2}}{e^{-i\varphi_1}|A_1|e^{i\delta_1} + e^{-i\varphi_2}|A_2|e^{i\delta_2}}\right]. \tag{5.41}$$

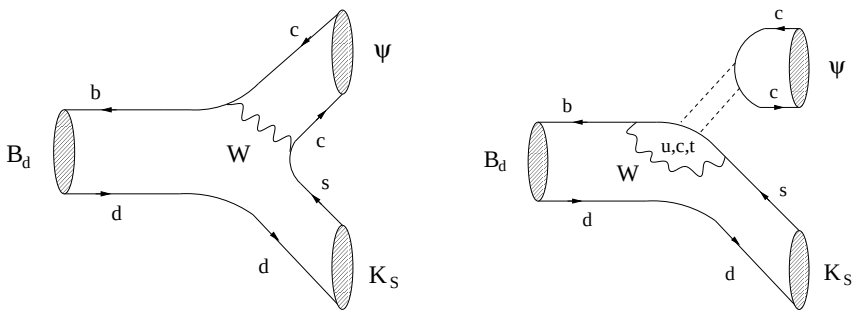

Fig. 13: Feynman diagrams contributing to $B_d^0 \to J/\psi K_{\rm S}$. The dashed lines in the penguin topology represent a colour-singlet exchange.

In analogy to the discussion of direct CP violation in Subsection 4.4, the calculation of $\xi_f^{(q)}$ suffers – in general – from large hadronic uncertainties. However, if one CKM amplitude plays the *dominant* rôle in the transition $B_q \to f$, we obtain

$$\xi_f^{(q)} = \mp\, e^{-i\phi_q} \left[\frac{e^{+i\phi_f/2}|M_f|e^{i\delta_f}}{e^{-i\phi_f/2}|M_f|e^{i\delta_f}}\right] = \mp\, e^{-i(\phi_q-\phi_f)}, \tag{5.42}$$

and observe that the hadronic matrix element $|M_f|e^{i\delta_f}$ *cancels* in this expression. Since the requirements for direct CP violation discussed in the context of (4.47) are no longer satisfied, we have vanishing direct CP violation in this important special case, i.e. $\mathcal{A}_{\rm CP}^{\rm dir}(B_q \to f) = 0$, which is also obvious from (5.31) and (5.42). On the other hand, we still have mixing-induced CP violation. In particular,

$$\mathcal{A}_{\rm CP}^{\rm mix}(B_q \to f) = \pm \sin\phi \tag{5.43}$$

is now governed by the CP-violating weak phase difference $\phi \equiv \phi_q - \phi_f$ and is *not* affected by hadronic uncertainties. The corresponding time-dependent CP asymmetry then takes the simple form

$$\left.\frac{\Gamma(B_q^0(t) \to f) - \Gamma(\bar{B}_q^0(t) \to \bar{f})}{\Gamma(B_q^0(t) \to f) + \Gamma(\bar{B}_q^0(t) \to \bar{f})}\right|_{\Delta\Gamma_q=0} = \pm \sin\phi\, \sin(\Delta M_q t), \tag{5.44}$$

and allows an elegant determination of $\sin\phi$.

Let us next apply the formalism developed above to discuss decays of (neutral) B mesons that are particularly important for the physics programme of the B factories.

6 BENCHMARK MODES FOR THE B FACTORIES

6.1 Exploring CP Violation through $B \to J/\psi K$

6.1.1 Amplitude Structure and CP Asymmetries

One of the most prominent B decays is given by $B_d \to J/\psi K_{\rm S}$. If we take the CP parities of the J/ψ and $K_{\rm S}$ into account,[5] and note that these mesons are produced in a P wave with angular momentum $L = 1$, we find that the final state of this transition is an eigenstate of the CP operator, with eigenvalue

$$\underbrace{(+1)}_{J/\psi} \times \underbrace{(+1)}_{K_{\rm S}} \times \underbrace{(-1)^1}_{L=1} = -1.$$

As can be seen in Fig. 13, $B_d^0 \to J/\psi K_{\rm S}$ originates from $\bar{b} \to \bar{c}c\bar{s}$ quark-level decays, and receives contributions from tree and penguin topologies (see the classification in Subsection 4.3.1). Consequently,

[5] Here we neglect the tiny indirect CP violation in the neutral kaon system.

we may write the decay amplitude as follows [87]:

$$A(B_d^0 \to J/\psi K_{\rm S}) = \lambda_c^{(s)} \left(A_{\rm T}^{c'} + A_{\rm P}^{c'}\right) + \lambda_u^{(s)} A_{\rm P}^{u'} + \lambda_t^{(s)} A_{\rm P}^{t'}, \tag{6.1}$$

where $A_{\rm T}^{c'}$ corresponds to the tree process in Fig. 13, and the strong amplitudes $A_{\rm P}^{q'}$ describe the penguin topologies with internal q-quark exchanges ($q \in \{u, c, t\}$), including QCD and EW penguins; the primes remind us that we are dealing with a $\bar{b} \to \bar{s}$ transition. Finally, the

$$\lambda_q^{(s)} \equiv V_{qs} V_{qb}^* \tag{6.2}$$

are CKM factors. If we eliminate now $\lambda_t^{(s)}$ through (4.32) and apply the Wolfenstein parametrization, we straightforwardly arrive at

$$A(B_d^0 \to J/\psi K_{\rm S}) \propto \left[1 + \lambda^2 a e^{i\theta} e^{i\gamma}\right], \tag{6.3}$$

where

$$a e^{i\vartheta} \equiv \left(\frac{R_b}{1-\lambda^2}\right) \left[\frac{A_{\rm P}^{u'} - A_{\rm P}^{t'}}{A_{\rm T}^{c'} + A_{\rm P}^{c'} - A_{\rm P}^{t'}}\right] \tag{6.4}$$

is a hadronic parameter that is a measure for the ratio of the $B_d^0 \to J/\psi K_{\rm S}$ penguin to tree contributions. Using the results derived in Subsection 5.2, we obtain

$$\xi_{\psi K_{\rm S}}^{(d)} = +e^{-i\phi_d} \left[\frac{1 + \lambda^2 a e^{i\vartheta} e^{-i\gamma}}{1 + \lambda^2 a e^{i\vartheta} e^{+i\gamma}}\right]. \tag{6.5}$$

Unfortunately, the parameter $a e^{i\vartheta}$ can only be estimated with large hadronic uncertainties. However, since it enters (6.5) in a doubly Cabibbo-suppressed way, its impact on the CP-violating observables is practically negligible. We can put this statement on a more quantitative basis by making the plausible assumption that $a = \mathcal{O}(\bar{\lambda}) = \mathcal{O}(0.2) = \mathcal{O}(\lambda)$, where $\bar{\lambda}$ is a "generic" expansion parameter. Applying now (5.31) yields

$$\mathcal{A}_{\rm CP}^{\rm dir}(B_d \to J/\psi K_{\rm S}) = 0 + \mathcal{O}(\overline{\lambda}^3) \tag{6.6}$$

$$\mathcal{A}_{\rm CP}^{\rm mix}(B_d \to J/\psi K_{\rm S}) = -\sin\phi_d + \mathcal{O}(\overline{\lambda}^3) \stackrel{\rm SM}{=} -\sin 2\beta + \mathcal{O}(\overline{\lambda}^3). \tag{6.7}$$

These expressions are one of the most important applications of the general features that we discussed in the context of (5.42)–(5.44).

6.1.2 Experimental Status and Theoretical Uncertainties

Looking at (6.7), we observe that the mixing-induced CP violation in $B_d \to J/\psi K_{\rm S}$ allows us to determine $\sin 2\beta$ in an essentially *clean* manner [88]. Because of this feature, this transition is referred to as the "golden" mode to measure the angle β of the UT. After important first steps by the OPAL, CDF and ALEPH collaborations, the $B_d \to J/\psi K_{\rm S}$ mode (and similar decays) eventually led, in 2001, to the observation of CP violation in the B system [4, 5]. The current status of $\sin 2\beta$ is given as follows:

$$\sin 2\beta = \begin{cases} 0.741 \pm 0.067 \pm 0.033 & \text{(BaBar [89])} \\ 0.733 \pm 0.057 \pm 0.028 & \text{(Belle [90])}, \end{cases} \tag{6.8}$$

yielding the world average

$$\sin 2\beta = 0.736 \pm 0.049. \tag{6.9}$$

On the other hand, the CKM fits of the UT described in Subsection 2.7 imply the ranges in (2.42), where the one for β can be converted into

$$0.6 \lesssim \sin 2\beta \lesssim 0.9, \tag{6.10}$$

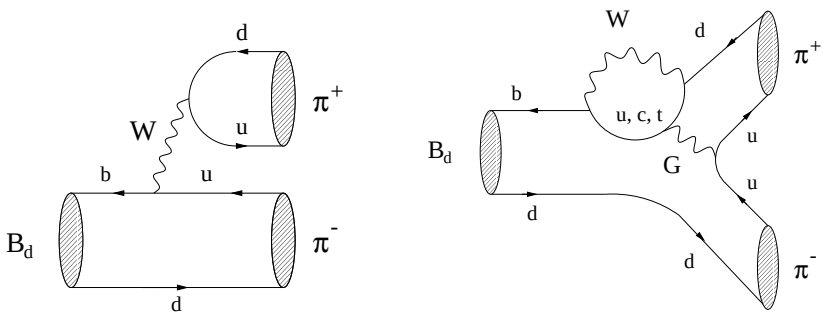

Fig. 14: Feynman diagrams contributing to $B_d^0 \to \pi^+\pi^-$.

which agrees well with the *direct* determination summarized in (6.9).

As far as the theoretical accuracy of (6.6) and (6.7) is concerned, the corrections, which originate from the penguin contributions and are at most of $\mathcal{O}(1\%)$,[6] are not yet an issue. However, in the era of the LHC [19], the experimental accuracy will be so tremendous that we have to start to deal with these terms. A possibility to control them is provided by the $B_s \to J/\psi K_{\rm S}$ channel, which can be combined with $B_d \to J/\psi K_{\rm S}$ through flavour-symmetry relations [87]. Moreover, also the direct CP violation in the $B \to J/\psi K$ system allows us to probe such penguin effects [71], where a combined analysis of the neutral $B_d \to J/\psi K_{\rm S}$ and charged $B^\pm \to J/\psi K^\pm$ modes provides the whole picture [91]; the current B-factory data for the corresponding direct CP asymmetries are consistent with zero. In a very recent analysis [92], this issue was also addressed from a more theoretical point of view. The corresponding estimates lead to tiny corrections at the 10^{-3} level, in accordance with the picture developed in [91].

Although the agreement between (6.9) and the results of the CKM fits is striking, it should not be forgotten that NP may – in principle – nevertheless hide in $\mathcal{A}_{\rm CP}^{\rm mix}(B_d \to J/\psi K_{\rm S})$. The point is that the key quantity is actually ϕ_d, which is fixed through $\sin\phi_d = 0.736 \pm 0.049$ up to a twofold ambiguity,

$$\phi_d = (47 \pm 4)^\circ \ \vee \ (133 \pm 4)^\circ. \tag{6.11}$$

Here the former solution would be in perfect agreement with CKM fits, implying $40^\circ \lessapprox 2\beta \stackrel{\rm SM}{=} \phi_d \lessapprox 60^\circ$, whereas the latter would correspond to NP. The two solutions can be distinguished through a measurement of the sign of $\cos\phi_d$: in the case of $\cos\phi_d = +0.7 > 0$, we would conclude $\phi_d = 47^\circ$, whereas $\cos\phi_d = -0.7 < 0$ would point towards $\phi_d = 133^\circ$, i.e. to NP. There are several strategies on the market to resolve the twofold ambiguity in the extraction of ϕ_d [93]. Unfortunately, they are rather challenging from a practical point of view. For instance, in the $B \to J/\psi K$ system, $\cos\phi_d$ can be extracted from the time-dependent angular distribution of the decay products of $B_d \to J/\psi[\to \ell^+\ell^-]K^*[\to \pi^0 K_{\rm S}]$, if the sign of a hadronic parameter $\cos\delta$ involving a strong phase δ is fixed through factorization [94, 95].

6.2 Exploring CP Violation through $B \to \pi\pi$

6.2.1 Amplitude Structure and CP Asymmetries

Another benchmark mode for the B factories is the decay $B_d^0 \to \pi^+\pi^-$, which is a transition into a CP eigenstate with eigenvalue $+1$, and originates from $\bar b \to \bar u u \bar d$ quark-level processes, as can be seen in Fig. 14. In analogy to (6.1), the decay amplitude can be written in the following form [96]:

$$A(B_d^0 \to \pi^+\pi^-) = \lambda_u^{(d)}\,(A_{\rm T}^u + A_{\rm P}^u) + \lambda_c^{(d)} A_{\rm P}^c + \lambda_t^{(d)} A_{\rm P}^t. \tag{6.12}$$

If we use again (4.32) to eliminate the CKM factor $\lambda_t^{(d)} = V_{td}V_{tb}^*$ and apply once more the Wolfenstein parametrization, we obtain

$$A(B_d^0 \to \pi^+\pi^-) \propto \left[e^{i\gamma} - d e^{i\theta}\right], \tag{6.13}$$

[6] In this case, the penguin topologies would *not* be suppressed with respect to the tree contributions, i.e. $a = \mathcal{O}(1)$.

where the hadronic parameter

$$de^{i\theta} \equiv \frac{1}{R_b}\left[\frac{A_{\rm P}^{\rm c} - A_{\rm P}^{t}}{A_{\rm T}^{u} + A_{\rm P}^{u} - A_{\rm P}^{t}}\right] \tag{6.14}$$

is a measure for the ratio of the $B_d \to \pi^+\pi^-$ penguin to tree amplitudes. The formalism discussed in Subsection 5.2 then implies

$$\xi_{\pi^+\pi^-}^{(d)} = -e^{-i\phi_d}\left[\frac{e^{-i\gamma} - de^{i\theta}}{e^{+i\gamma} - de^{i\theta}}\right]. \tag{6.15}$$

In contrast to the expression for the $B_d^0 \to J/\psi K_{\rm S}$ counterpart given in (6.5), the hadronic parameter $de^{i\theta}$, which suffers from large theoretical uncertainties, does *not* enter in (6.15) in a doubly Cabibbo-suppressed way. This feature is at the basis of the famous "penguin problem" in $B_d \to \pi^+\pi^-$, which was addressed in many papers over the recent years (see, for instance, [97]–[102]). If we had negligible penguin contributions in this channel, i.e. $d = 0$, the corresponding CP-violating observables were simply given as follows:

$$\mathcal{A}_{\rm CP}^{\rm dir}(B_d \to \pi^+\pi^-) = 0 \tag{6.16}$$

$$\mathcal{A}_{\rm CP}^{\rm mix}(B_d \to \pi^+\pi^-) = \sin(\phi_d + 2\gamma) \stackrel{\rm SM}{=} \sin(\underbrace{2\beta + 2\gamma}_{2\pi - 2\alpha}) = -\sin 2\alpha. \tag{6.17}$$

Consequently, $\mathcal{A}_{\rm CP}^{\rm mix}(B_d \to \pi^+\pi^-)$ would allow us to determine α. However, in the general case of $d \neq 0$, we obtain formulae with the help of (5.31) and (6.15), which are considerably more complicated:

$$\mathcal{A}_{\rm CP}^{\rm dir}(B_d \to \pi^+\pi^-) = -\left[\frac{2d\sin\theta\sin\gamma}{1 - 2d\cos\theta\cos\gamma + d^2}\right] \tag{6.18}$$

$$\mathcal{A}_{\rm CP}^{\rm mix}(B_d \to \pi^+\pi^-) = \frac{\sin(\phi_d + 2\gamma) - 2d\cos\theta\sin(\phi_d + \gamma) + d^2\sin\phi_d}{1 - 2d\cos\theta\cos\gamma + d^2}. \tag{6.19}$$

We observe that actually the phases ϕ_d and γ enter directly in the $B_d \to \pi^+\pi^-$ observables, and not α. Consequently, since ϕ_d can be fixed straightforwardly through the mixing-induced CP violation in the "golden" mode $B_d \to J/\psi K_{\rm S}$, as we have seen in (6.7), we may use $B_d \to \pi^+\pi^-$ to probe γ. This is advantageous to deal with penguins and possible NP effects.

6.2.2 Experimental Status and the "$B \to \pi\pi$ Puzzle"

Measurements of the $B_d \to \pi^+\pi^-$ CP asymmetries are already available:

$$\mathcal{A}_{\rm CP}^{\rm dir}(B_d \to \pi^+\pi^-) = \begin{cases} -0.19 \pm 0.19 \pm 0.05 & \text{(BaBar [103])} \\ -0.77 \pm 0.27 \pm 0.08 & \text{(Belle [104])} \end{cases} \tag{6.20}$$

$$\mathcal{A}_{\rm CP}^{\rm mix}(B_d \to \pi^+\pi^-) = \begin{cases} +0.40 \pm 0.22 \pm 0.03 & \text{(BaBar [103])} \\ +1.23 \pm 0.41^{+0.07}_{-0.08} & \text{(Belle [104]).} \end{cases} \tag{6.21}$$

Unfortunately, the BaBar and Belle results are not fully consistent with each other, although both experiments point towards the same signs, and the last BaBar update of $\mathcal{A}_{\rm CP}^{\rm mix}(B_d \to \pi^+\pi^-)$ has moved towards Belle. In [86], the Heavy Flavour Averaging Group (HFAG) gave the following averages:

$$\mathcal{A}_{\rm CP}^{\rm dir}(B_d \to \pi^+\pi^-) = -0.38 \pm 0.16 \tag{6.22}$$

$$\mathcal{A}_{\rm CP}^{\rm mix}(B_d \to \pi^+\pi^-) = +0.58 \pm 0.20. \tag{6.23}$$

Direct CP violation at this level would require large penguin contributions with large CP-conserving strong phases, as is evident from (6.18). As we will see in Subsection 8.3.3, the CP asymmetries in

(6.22) and (6.23) can be converted into the angle γ of the UT, with a result around 65°, in remarkable accordance with the SM picture [48, 105].

In addition to the decays $B_d \to \pi^+\pi^-$ and $B^\pm \to \pi^\pm\pi^0$, the B factories have recently reported the observation of the $B_d \to \pi^0\pi^0$ channel, with the following CP-averaged branching ratios:

$$\mathrm{BR}(B_d \to \pi^0\pi^0) = \begin{cases} (2.1 \pm 0.6 \pm 0.3) \times 10^{-6} & \text{(BaBar [106])} \\ (1.7 \pm 0.6 \pm 0.2) \times 10^{-6} & \text{(Belle [107]);} \end{cases} \tag{6.24}$$

CP-averaged branching ratios of this kind are generally defined through

$$\mathrm{BR} \equiv \frac{1}{2}\left[\mathrm{BR}(B \to f) + \mathrm{BR}(\bar{B} \to \bar{f})\right]. \tag{6.25}$$

These measurements represent quite a challenge for theory. For example, in a recent state-of-the-art calculation within QCD factorization [108], a $B_d \to \pi^0\pi^0$ branching ratio that is about six times smaller is favoured, whereas the calculation of $B_d \to \pi^+\pi^-$ points towards a branching ratio about two times larger than the current experimental average. On the other hand, the calculation of $B^\pm \to \pi^\pm\pi^0$ reproduces the data rather well. This "$B \to \pi\pi$ puzzle" is reflected by the following quantities [48, 54]:

$$R_{+-}^{\pi\pi} \equiv 2\left[\frac{\mathrm{BR}(B^\pm \to \pi^\pm\pi^0)}{\mathrm{BR}(B_d \to \pi^+\pi^-)}\right]\frac{\tau_{B_d^0}}{\tau_{B^+}} = 2.12 \pm 0.37 \tag{6.26}$$

$$R_{00}^{\pi\pi} \equiv 2\left[\frac{\mathrm{BR}(B_d \to \pi^0\pi^0)}{\mathrm{BR}(B_d \to \pi^+\pi^-)}\right] = 0.83 \pm 0.23; \tag{6.27}$$

the central values calculated within QCD factorization give $R_{+-}^{\pi\pi} = 1.24$ and $R_{00}^{\pi\pi} = 0.07$ [108] . As was discussed in detail in [48, 54], the $B \to \pi\pi$ puzzle can straightforwardly be accommodated within the SM through non-factorizable hadronic interference effects.[7] If we use

$$\phi_d = (47 \pm 4)^\circ, \quad \gamma = (65 \pm 7)^\circ, \tag{6.28}$$

as in the SM [41], this analysis allows us to convert the $B \to \pi\pi$ data into certain hadronic parameters. In particular, we obtain

$$d = 0.48^{+0.35}_{-0.22}, \quad \theta = +(138^{+19}_{-23})^\circ, \tag{6.29}$$

whereas QCD factorization favours $d \sim 0.3$ and $\theta \sim 180^\circ$. Moreover, the CP-violating observables of $B_d \to \pi^0\pi^0$ can be predicted, with the result

$$\mathcal{A}_{\mathrm{CP}}^{\mathrm{dir}}(B_d \to \pi^0\pi^0) = -0.41^{+0.35}_{-0.17}, \quad \mathcal{A}_{\mathrm{CP}}^{\mathrm{mix}}(B_d \to \pi^0\pi^0) = -0.55^{+0.43}_{-0.45}. \tag{6.30}$$

We shall return to $B_d \to \pi^+\pi^-$ in Subsection 8.3, in the context of $B_s \to K^+K^-$ [96].

6.3 Exploring CP Violation through $B \to \phi K$

6.3.1 Amplitude Structure and CP Asymmetries

Another important mode for the testing of the KM mechanism of CP violation is provided by $B_d \to \phi K_{\mathrm{S}}$, which is – in analogy to $B_d \to J/\psi K_{\mathrm{S}}$ – a decay into a CP-odd final state. As can be seen in Fig. 15, $B_d^0 \to \phi K_{\mathrm{S}}$ originates from $\bar{b} \to \bar{s}s\bar{s}$ quark-level processes, i.e. is a pure penguin mode. Consequently, $B_d^0 \to \phi K_{\mathrm{S}}$ and its charged counterpart $B^+ \to \phi K^+$ are governed by QCD penguin topologies [112], but also EW penguins have a sizeable impact because of the large top-quark mass [70, 113]. Using the same notation as above, we may write the $B_d^0 \to \phi K_{\mathrm{S}}$ decay amplitude within the SM as follows:

$$A(B_d^0 \to \phi K_{\mathrm{S}}) = \lambda_u^{(s)}\tilde{A}_{\mathrm{P}}^{u'} + \lambda_c^{(s)}\tilde{A}_{\mathrm{P}}^{c'} + \lambda_t^{(s)}\tilde{A}_{\mathrm{P}}^{t'}. \tag{6.31}$$

[7] Similar conclusions were also drawn very recently in [109, 110]. In [109], also the phenomenological implications of bounds on the UT that can be derived from the CP-violating $B_d \to \pi^+\pi^-$ observables, as pointed out in [111], were discussed.

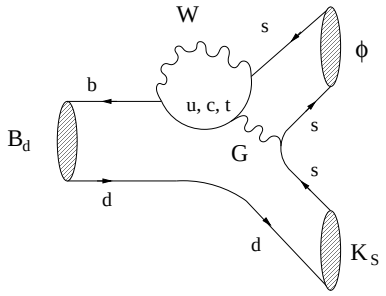

Fig. 15: Feynman diagrams contributing to $B_d \to \phi K_{\rm S}$.

Applying now once more (4.32) to eliminate the CKM factor $\lambda_t^{(s)}$, we obtain

$$A(B_d^0 \to \phi K_{\rm S}) \propto \left[1 + \lambda^2 b e^{i\Theta} e^{i\gamma}\right], \tag{6.32}$$

so that

$$\xi_{\phi K_{\rm S}}^{(d)} = +e^{-i\phi_d}\left[\frac{1 + \lambda^2 b e^{i\Theta} e^{-i\gamma}}{1 + \lambda^2 b e^{i\Theta} e^{+i\gamma}}\right], \tag{6.33}$$

with

$$b e^{i\Theta} = \left(\frac{R_b}{1-\lambda^2}\right)\left[\frac{\tilde{A}_{\rm P}^{u'} - \tilde{A}_{\rm P}^{t'}}{\tilde{A}_{\rm P}^{c'} - \tilde{A}_{\rm P}^{t'}}\right]. \tag{6.34}$$

The theoretical estimates of the hadronic parameter $be^{i\Theta}$ suffer from large uncertainties. However, since this parameter enters (6.33) in a doubly Cabibbo-suppressed way, we obtain the simple expressions

$$\mathcal{A}_{\rm CP}^{\rm dir}(B_d \to \phi K_{\rm S}) = 0 + \mathcal{O}(\lambda^2) \tag{6.35}$$

$$\mathcal{A}_{\rm CP}^{\rm mix}(B_d \to \phi K_{\rm S}) = -\sin\phi_d + \mathcal{O}(\lambda^2), \tag{6.36}$$

where we made the plausible assumption that $b = \mathcal{O}(1)$. On the other hand, the mixing-induced CP asymmetry of the "golden" mode $B_d \to J/\psi K_{\rm S}$ measures also $-\sin\phi_d$ (see (6.7)). Consequently, we arrive at the following relation [71, 114, 115, 116]:

$$\mathcal{A}_{\rm CP}^{\rm mix}(B_d \to \phi K_{\rm S}) = \mathcal{A}_{\rm CP}^{\rm mix}(B_d \to J/\psi K_{\rm S}) + \mathcal{O}(\lambda^2), \tag{6.37}$$

which offers a very interesting test of the SM description of CP violation. In order to obtain the whole picture and to search for NP systematically, it is useful to perform a combined analysis of the neutral $B_d \to \phi K_{\rm S}$ and the charged $B^\pm \to \phi K^\pm$ modes [116] (for a recent update, see [48]).

6.3.2 Experimental Status

The experimental status of the CP-violating $B_d \to \phi K_{\rm S}$ observables is given as follows [117]:[8]

$$\mathcal{A}_{\rm CP}^{\rm dir}(B_d \to \phi K_{\rm S}) = \begin{cases} +0.01 \pm 0.33 \pm 0.10 & \text{(BaBar [118])} \\ +0.15 \pm 0.29 \pm 0.07 & \text{(Belle [119])} \end{cases} \tag{6.38}$$

$$\mathcal{A}_{\rm CP}^{\rm mix}(B_d \to \phi K_{\rm S}) = \begin{cases} -0.47 \pm 0.34^{+0.06}_{-0.08} & \text{(BaBar [118])} \\ +0.96 \pm 0.50^{+0.11}_{-0.09} & \text{(Belle [119]),} \end{cases} \tag{6.39}$$

Since we have, on the other hand, $\mathcal{A}_{\rm CP}^{\rm mix}(B_d \to J/\psi K_{\rm S}) = -0.736 \pm 0.049$, we arrive at a puzzling situation, which has already stimulated many speculations about NP effects in the decay $B_d \to \phi K_{\rm S}$ (see, for instance, [120]). However, because of the very unsatisfactory current experimental picture, it seems too early to get too excited by the possibility of having a violation of the SM relation (6.37). It will be very interesting to observe how the B-factory data will evolve, and to keep also an eye on $B_d \to \eta' K_{\rm S}$ and other related modes.

[8] Note that the very recent BaBar update in [118] uses also $B_d \to \phi K_{\rm L}$ to extract the CP asymmetries of $B_d^0 \to \phi K^0$.

6.4 Manifestations of New Physics

6.4.1 New-Physics Effects in B^0_d–$\bar{B}^0_d$ Mixing

As we have seen in Subsection 5.1, B^0_d–$\bar{B}^0_d$ mixing originates in the SM from box diagrams, which are characterized by the Inami–Lim function $S_0(x_t)$. Concerning the impact of NP, it may enter B^0_d–$\bar{B}^0_d$ mixing through new-particle exchanges in the loop diagrams shown in Fig. 12, or through new FCNC processes arising at the tree level. The impact on the mixing parameters is twofold:

- The mass difference of the mass eigenstates is generalized as

$$\Delta M_d = \Delta M_d^{\rm SM} + \Delta M_d^{\rm NP}, \tag{6.40}$$

  so that the NP contribution would affect the determination of the UT side R_t through (5.15).

- The CP-violating weak mixing phase is generalized as

$$\phi_d = \phi_d^{\rm SM} + \phi_d^{\rm NP} = 2\beta + \phi_d^{\rm NP}, \tag{6.41}$$

  so that NP may enter the mixing-induced CP asymmetries through $\phi_d^{\rm NP}$.

On the basis of dimensional arguments borrowed from effective field theory (see, for instance, [47, 91]), and in specific NP scenarios, the following pattern may – in principle – be possible:

$$\Delta M_d^{\rm NP}/\Delta M_d^{\rm SM} \sim 1, \quad \phi_d^{\rm NP}/\phi_d^{\rm SM} \sim 1. \tag{6.42}$$

The same is true for the case of B^0_s–$\bar{B}^0_s$ mixing, which may be significantly affected by NP as well.[9]

6.4.2 New-Physics Effects in Decay Amplitudes

Another way for NP to manifest itself is through contributions to decay amplitudes. If the decay does *not* arise at the tree level in the SM, we may have potentially large NP effects. In particular, NP may enter through new particles running in the loops, or through new FCNC processes arising at the tree level. An important example for such decays is given by the $B \to \phi K$ system, which is governed by $\bar{b} \to \bar{s}s\bar{s}$ penguin processes, as we have seen above. On the basis of general dimensional arguments [116], and in specific NP scenarios [120], significant effects may in fact arise in the $B \to \phi K$ amplitudes. The B-factory data may already indicate the presence of such a kind of NP, although it is too early to draw definite conclusions on this exciting possibility.

On the other hand, if a transition is dominated by a SM tree contribution, the impact of NP on the decay amplitude is generally small. An important example of this feature is given by the decay $B^0_d \to J/\psi K_{\rm S}$, which is governed by the $\bar{b} \to \bar{c}c\bar{s}$ process, arising at the tree level in the SM. Generic dimensional arguments then indicate that we may have NP effects at the $B \to J/\psi K$ amplitude level of at most $\mathcal{O}(10\%)$ for a NP scale in the TeV regime. In order to search systematically for such effects, it is useful to perform a combined analysis of the neutral and charged $B \to J/\psi K$ modes, and to introduce appropriate observable combinations [91]; the current B-factory data do not indicate any anomaly (for a recent update, see [48]). Since the determination of ϕ_d from the mixing-induced CP violation in $B_d \to J/\psi K_{\rm S}$ is very robust under NP, we may use the corresponding experimental result as an input for other studies of CP violation, as we have noted above.

6.4.3 Back to the Status of the B^0_d–$\bar{B}^0_d$ Mixing Phase ϕ_d

Let us now briefly come back to the two solutions for ϕ_d in (6.11). In this context, it is interesting to note that an upper bound on ϕ_d is implied by an upper bound on $R_b \propto |V_{ub}/V_{cb}|$, as can straightforwardly be seen in Fig. 4. To be specific, we have

$$\sin\beta_{\rm max} = R_b^{\rm max}, \tag{6.43}$$

[9] Let us note that also D^0–$\bar{D}^0$ mixing offers an interesting probe to search for NP. Within the SM, this phenomenon is tiny, but it may be enhanced by the presence of NP. A similar comment applies to the CP-violating effects in D-meson decays. For a recent overview, we refer the reader to [121], and the references therein.

which yields $(\phi_d)^{\rm SM}_{\rm max} \sim 57^\circ$ for $R_b^{\rm max} \sim 0.48$. Since the determination of R_b from the semileptonic (tree-level) decays discussed in Subsection 4.2 is not expected to be sensitive to NP, $\phi_d \sim 133^\circ$ would require CP-violating NP contributions to B^0_d–$\bar{B}^0_d$ mixing. An interesting connection between the two solutions for ϕ_d and the UT angle γ is provided by the CP asymmetries of $B_d \to \pi^+\pi^-$ [47, 105]. We shall return to this feature in Section 8.

6.4.4 Models with Minimal Flavour Violation

An interesting scenario for NP is provided by the simplest class of extensions of the SM. It is represented by models with "minimal flavour violation" (MFV), which we may characterize as follows [122, 123] (for alternative definitions, see [124, 125]):

- All flavour-changing transitions are still governed by the CKM matrix, in particular no new phases.
- The only relevant operators are those already present in the SM.

Important examples are the Two-Higgs-Doublet Model II, the constrained MSSM (if $\tan\overline{\beta} = v_2/v_1$ is not too large), and models with universal extra dimensions [122]. As was pointed out in [123], a "universal unitarity triangle" can be constructed for such MFV models with the help of those quantities that are not affected by the corresponding NP contributions. Following these lines, the "true" values of $\bar{\rho}$ and $\bar{\eta}$ can still be determined in a transparent manner, despite the presence of NP.

Because of the items listed above, all SM expressions for decay amplitudes, as well as for particle–antiparticle mixing, can be generalized to the MFV models through a straightforward replacement of the initial Wilson coefficients for the renormalization-group evolution from $\mu = \mathcal{O}(M_W)$ down to appropriate "low-energy" scales μ through characteristic NP coefficients. If we consider, for example, B^0_d–$\bar{B}^0_d$ mixing, we just have to make the following substitution for the Inami–Lim function $S_0(x_t)$:

$$S_0(x_t) \to S(v), \tag{6.44}$$

where v, which equals $x_t = m_t^2/M_W^2$ in the SM, denotes collectively the parameters of a given MFV model. Note that the *same* short-distance function governs also B^0_s–$\bar{B}^0_s$ mixing, as well as K^0–$\bar{K}^0$ mixing, so that it also enters the expression for the CP-violating observable ε.

Since no new phases appear in MFV models, one may think that the B^0_d–$\bar{B}^0_d$ mixing phase introduced in (5.40) would not be affected in such scenarios. However, because of a subtlety, this is actually not the case [126]. If we look at (5.7), we observe that the sign of $S_0(x_t)$ enters implicitly ϕ_d; in (5.26) and (5.40), we have actually used the fact that $S_0(x_t)$ is *positive*. However, since $S_0(x_t)$ is now replaced by $S(v)$, which needs no longer be positive, the expression for ϕ_d in (5.40) is generalized as follows:

$$\phi_d = 2\beta + \arg(S(v)), \tag{6.45}$$

so that $\phi_d^{\rm NP}$ in (6.41) is either 0° or 180° for $S(v) > 0$ or $S(v) < 0$, respectively. Consequently, in the most general MFV case, the mixing-induced CP asymmetry of $B_d \to J/\psi K_{\rm S}$ is given by

$$-\mathcal{A}_{\rm CP}^{\rm mix}(B_d \to J/\psi K_{\rm S}) \equiv a_{\psi K_{\rm S}} = {\rm sgn}(S(v)) \sin 2\beta. \tag{6.46}$$

On the other hand, $\Delta M_d^{\rm NP}$ in (6.40) may have a significant impact on ΔM_d. Similarly, also ε may be affected. However, since the NP effects enter ΔM_d and ε through the same generalized Inami–Lim function $S(v)$, we obtain correlations between these observables. In fact, the interplay between B^0_d–$\bar{B}^0_d$ mixing and ε in the CKM fits implies bounds on $\sin 2\beta$ [127]. Using (6.46), we may cancel the sign ambiguity due to ${\rm sgn}(S(v))$, and obtain the following lower bounds for $a_{\psi K_{\rm S}}$:

$$(a_{\psi K_{\rm S}})_{\rm min} = \begin{cases} 0.42 & (S(v) > 0 \text{ [127]}) \\ 0.69 & (S(v) < 0 \text{ [126]}). \end{cases} \tag{6.47}$$

Although these bounds were very exciting immediately after the first B-factory data for $a_{\psi K_{\rm S}}$ were announced, which favoured rather small values, they are now not effective because of the world average given in (6.9). We shall come back to NP scenarios with MFV in Subsections 9.1–9.3. For a very comprehensive discussion, we refer the reader to [122].

7 AMPLITUDE RELATIONS

As we have noted in Subsection 4.4, amplitude relations offer another important tool to explore CP violation. Let us now have a closer look at the corresponding strategies, where we distinguish between the use of theoretically clean and flavour-symmetry relations.

7.1 Theoretically Clean Relations

7.1.1 $B^\pm \to K^\pm D$

The prototype of the strategies using theoretically clean amplitude relations is provided by $B^\pm \to K^\pm D$ decays [128]. Looking at Fig. 16, we observe that $B^+ \to K^+\bar{D}^0$ and $B^+ \to K^+D^0$ are pure "tree" decays. If we consider, in addition, the transition $B^+ \to D_+^0 K^+$, where D_+^0 denotes the CP eigenstate of the neutral D-meson system with eigenvalue $+1$,

$$|D_+^0\rangle = \frac{1}{\sqrt{2}}\left[|D^0\rangle + |\bar{D}^0\rangle\right], \tag{7.1}$$

we obtain interference effects, which are described by

$$\sqrt{2}A(B^+ \to K^+ D_+^0) = A(B^+ \to K^+ D^0) + A(B^+ \to K^+\bar{D}^0) \tag{7.2}$$

$$\sqrt{2}A(B^- \to K^- D_+^0) = A(B^- \to K^-\bar{D}^0) + A(B^- \to K^- D^0). \tag{7.3}$$

These relations can be represented as two triangles in the complex plane. Since we have only to deal with tree-diagram-like topologies, we have moreover

$$A(B^+ \to K^+\bar{D}^0) = A(B^- \to K^- D^0) \tag{7.4}$$

$$A(B^+ \to K^+ D^0) = A(B^- \to K^-\bar{D}^0) \times e^{2i\gamma}, \tag{7.5}$$

allowing a *theoretically clean* extraction of γ, as shown in Fig. 17. Unfortunately, these triangles are very squashed, since $B^+ \to K^+D^0$ is colour-suppressed with respect to $B^+ \to K^+\bar{D}^0$:

$$\left|\frac{A(B^+ \to K^+ D^0)}{A(B^+ \to K^+\bar{D}^0}\right| = \left|\frac{A(B^- \to K^-\bar{D}^0)}{A(B^- \to K^- D^0}\right| \approx \frac{1}{\lambda}\frac{|V_{ub}|}{|V_{cb}|} \times \frac{a_2}{a_1} \approx 0.4 \times 0.3 = \mathcal{O}(0.1), \tag{7.6}$$

where the phenomenological "colour" factors were introduced in Subsection 4.3.3.

Another – more subtle – problem is related to the measurement of BR$(B^+ \to K^+D^0)$. From the theoretical point of view, $D^0 \to K^-\ell^+\nu$ would be ideal to measure this tiny branching ratio. However, because of the huge background from semileptonic B decays, we must rely on Cabibbo-allowed hadronic $D^0 \to f_{\rm NE}$ decays, such as $f_{\rm NE} = \pi^+K^-$, ρ^+K^-, ..., i.e. have to measure

$$B^+ \to K^+ D^0\,[\to f_{\rm NE}]. \tag{7.7}$$

Unfortunately, we then encounter another decay path into the *same* final state $K^+ f_{\rm NE}$ through

$$B^+ \to K^+\bar{D}^0\,[\to f_{\rm NE}], \tag{7.8}$$

where BR$(B^+ \to K^+\bar{D}^0)$ is *larger* than BR$(B^+ \to K^+D^0)$ by a factor of $\mathcal{O}(10^2)$, while $\bar{D}^0 \to f_{\rm NE}$ is doubly Cabibbo-suppressed, i.e. the corresponding branching ratio is suppressed with respect to the one of $D^0 \to f_{\rm NE}$ by a factor of $\mathcal{O}(10^{-2})$. Consequently, we obtain interference effects of $\mathcal{O}(1)$ between the decay chains in (7.7) and (7.8). If two different final states $f_{\rm NE}$ are considered, γ could – in principle – be extracted [129], although this determination would then be more involved than the original triangle approach presented in [128].

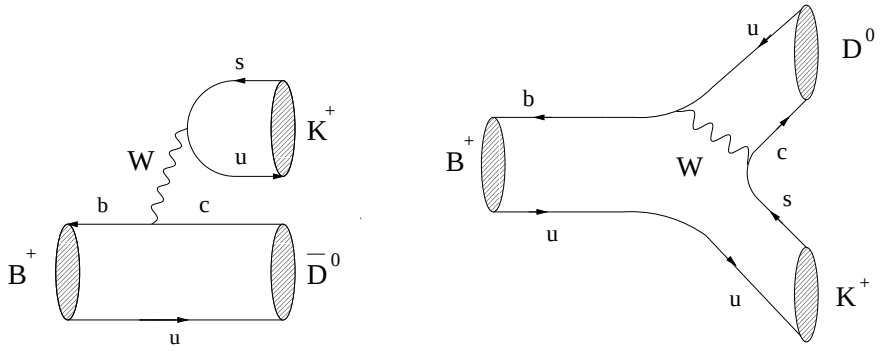

Fig. 16: Feynman diagrams contributing to $B^+ \to K^+\bar{D}^0$ and $B^+ \to K^+D^0$.

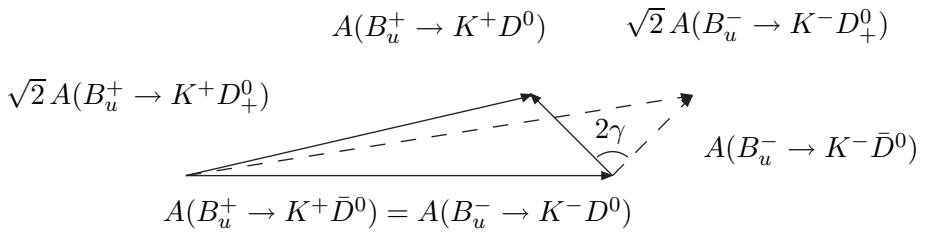

Fig. 17: The extraction of γ from $B^\pm \to K^\pm\{D^0, \bar{D}^0, D_+^0\}$ decays.

7.1.2 $B_c^\pm \to D_s^\pm D$

In addition to the "conventional" $B_u^\pm$ mesons, there is yet another species of charged B mesons, the B_c-meson system, which consists of $B_c^+ \sim c\overline{b}$ and $B_c^- \sim b\overline{c}$. These mesons were observed by the CDF collaboration through their decay $B_c^+ \to J/\psi\ell^+\nu$, with the following mass and lifetime [130]:

$$M_{B_c} = (6.40 \pm 0.39 \pm 0.13)\,\text{GeV}, \quad \tau_{B_c} = (0.46^{+0.18}_{-0.16} \pm 0.03)\,\text{ps}. \tag{7.9}$$

Since a huge number of B_c mesons ($\sim 10^{10}$/year) will be produced at LHCb [19], the natural question of whether also the charged B_c-meson system provides a triangle approach to determine γ arises. Such a determination is actually offered by the decays $B_c^\pm \to D_s^\pm D$, which are the B_c-meson counterparts of the $B_u^\pm \to K^\pm D$ modes (see Fig. 18), and satisfy the following amplitude relations [131]:

$$\sqrt{2}A(B_c^+ \to D_s^+ D_+^0) = A(B_c^+ \to D_s^+ D^0) + A(B_c^+ \to D_s^+ \bar{D}^0) \tag{7.10}$$
$$\sqrt{2}A(B_c^- \to D_s^- D_+^0) = A(B_c^- \to D_s^- \bar{D}^0) + A(B_c^- \to D_s^- D^0), \tag{7.11}$$

with

$$A(B_c^+ \to D_s^+ \bar{D}^0) = A(B_c^- \to D_s^- D^0) \tag{7.12}$$
$$A(B_c^+ \to D_s^+ D^0) = A(B_c^- \to D_s^- \bar{D}^0) \times e^{2i\gamma}. \tag{7.13}$$

At first sight, everything is completely analogous to the $B_u^\pm \to K^\pm D$ case. However, there is an important difference [132], which becomes obvious by comparing the Feynman diagrams shown in Figs. 16 and 18: in the $B_c^\pm \to D_s^\pm D$ system, the amplitude with the rather small CKM matrix element V_{ub} is not colour-suppressed, while the larger element V_{cb} comes with a colour-suppression factor. Therefore, we obtain

$$\left|\frac{A(B_c^+ \to D_s^+ D^0)}{A(B_c^+ \to D_s^+ \bar{D}^0)}\right| = \left|\frac{A(B_c^- \to D_s^- \bar{D}^0)}{A(B_c^- \to D_s^- D^0)}\right| \approx \frac{1}{\lambda}\frac{|V_{ub}|}{|V_{cb}|} \times \frac{a_1}{a_2} \approx 0.4 \times 3 = \mathcal{O}(1), \tag{7.14}$$

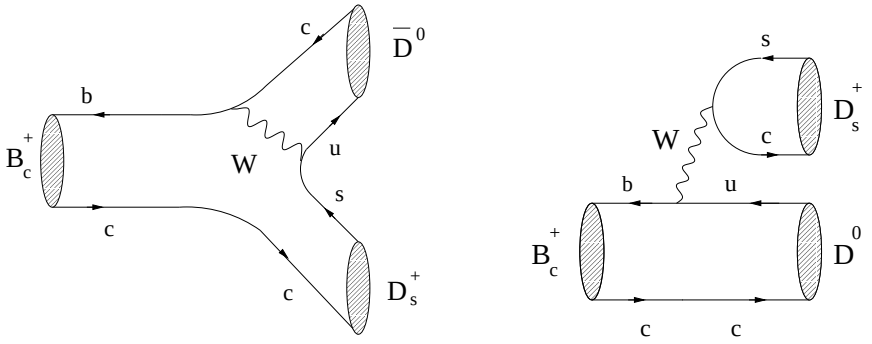

Fig. 18: Feynman diagrams contributing to $B_c^+ \to D_s^+ \bar{D}^0$ and $B^+ \to D_s^+ D^0$.

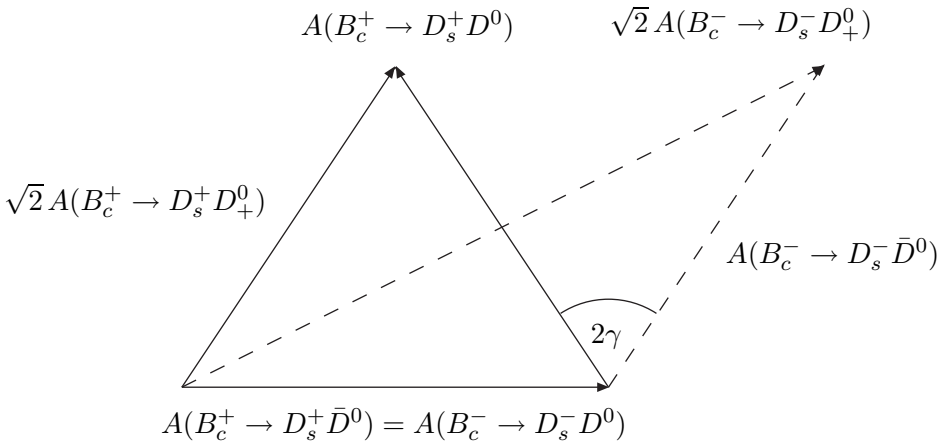

Fig. 19: The extraction of γ from $B_c^\pm \to D_s^\pm \{D^0, \bar{D}^0, D_+^0\}$ decays.

and conclude that the two amplitudes are similar in size. In contrast to this favourable situation, in the decays $B_u^\pm \to K^\pm D$, the matrix element V_{ub} comes with the colour-suppression factor, resulting in a very stretched triangle. The extraction of γ from the $B_c^\pm \to D_s^\pm D$ triangles is illustrated in Fig. 19, which should be compared with the squashed $B_u^\pm \to K^\pm D$ triangles shown in Fig. 17. Another important advantage is that the interference effects arising from $D^0, \bar{D}^0 \to \pi^+ K^-$ are practically unimportant for the measurement of BR$(B_c^+ \to D_s^+ D^0)$ and BR$(B_c^+ \to D_s^+ \bar{D}^0)$ since the B_c-decay amplitudes are of the same order of magnitude. Consequently, the $B_c^\pm \to D_s^\pm D$ decays provide – from the theoretical point of view – the ideal realization of the "triangle" approach to determine γ. On the other hand, the practical implementation still appears to be challenging, although detailed experimental feasibility studies for LHCb are strongly encouraged. The corresponding branching ratios were recently estimated in [133], with a pattern in accordance with (7.14).

7.2 Flavour-Symmetry Relations: $B \to \pi K$

Let us now turn to amplitude relations that follow from the flavour symmetries of the strong interactions, which are – in contrast to the relations discussed in Subsection 7.1 – not theoretically clean, but are nevertheless very useful to explore CP violation and to obtain insights into hadron dynamics. Here the prototype is provided by $B \to \pi K$ decays, which received a lot of attention in the B-physics community. Since a detailed discussion of the corresponding strategies is beyond the scope of these lectures, we address only their most important features and refer the interested reader to [26], where also a comprehensive list of references can be found.

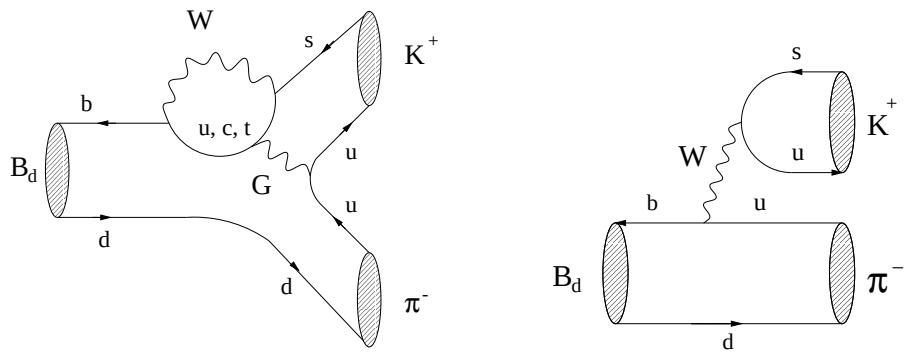

Fig. 20: Feynman diagrams contributing to $B^0_d \to \pi^- K^+$.

7.2.1 General Features

In order to get more familiar with the $B \to \pi K$ modes, let us consider the decay $B^0_d \to \pi^- K^+$. As can be seen in Fig. 20, this channel receives contributions from penguin and tree topologies. Consequently, $B^0_d \to \pi^- K^+$ exhibits interference effects between the penguin and tree amplitudes, where the latter brings the angle γ of the UT into the game. Because of the small ratio $|V_{us}V^*_{ub}/(V_{ts}V^*_{tb})| \approx 0.02$, the QCD penguin topologies play the dominant rôle in this decay, despite their loop suppression. The ratio of the tree to the penguin amplitudes is generically expected at the 20% level. Interestingly, all $B \to \pi K$ modes are governed by their QCD penguin contributions. Because of the large top-quark mass, we have also to care about EW penguins:

- In the case of $B^0_d \to \pi^- K^+$ and $B^+ \to \pi^+ K^0$, these topologies contribute only in colour-suppressed form and are hence expected to play a minor rôle, thereby leading to contributions to the decay amplitudes of $\mathcal{O}(1\%)$.
- On the other hand, EW penguins may also contribute to $B^+ \to \pi^0 K^+$ and $B^0_d \to \pi^0 K^0$ in colour-allowed form, and may here even compete with the tree-diagram-like topologies, thereby leading to contributions to the decay amplitudes of $\mathcal{O}(20\%)$.

It can be shown that the isospin flavour symmetry of strong interactions implies the relation

$$\begin{aligned}\sqrt{2}A(B^+ \to \pi^0 K^+) + A(B^+ \to \pi^+ K^0) &= \sqrt{2}A(B^0_d \to \pi^0 K^0) + A(B^0_d \to \pi^- K^+) \\ &= -\Big[\underbrace{|T+C|e^{i\delta_{T+C}}e^{i\gamma}}_{\text{tree topologies}} + \underbrace{(P_{\text{ew}} + P^{\text{C}}_{\text{ew}})}_{\text{EW penguins}}\Big] \propto \left[e^{i\gamma} - q\right], \end{aligned} \tag{7.15}$$

where the T (P_{ew}) and C (P^{C}_{ew}) denote the amplitudes of the colour-allowed and colour-suppressed tree (EW penguin) topologies, respectively, δ_{T+C} is a CP-conserving strong phase, and the factors of $\sqrt{2}$ originate from the wave functions of the neutral pions. Note that the QCD penguin contributions cancel in this expression. A relation with an analogous phase structure can also be derived for the $B^+ \to \pi^+ K^0$, $B^0_d \to \pi^- K^+$ system.

7.2.2 Extraction of γ and Strong Phases

The $B \to \pi K$ observables allow us to determine the angle γ of the UT. Because of the isospin relation in (7.15), we may separately consider the following decay combinations to this end:

- The "mixed" system of the charged $B^\pm \to \pi^\pm K$ and neutral $B_d \to \pi^\mp K^\pm$ modes [134]–[137].
- The system of the charged $B^\pm \to \pi^\pm K$, $B^\pm \to \pi^0 K^\pm$ modes [138]–[140].
- The system of the neutral $B_d \to \pi^0 K$, $B_d \to \pi^\mp K^\pm$ modes [140, 141].

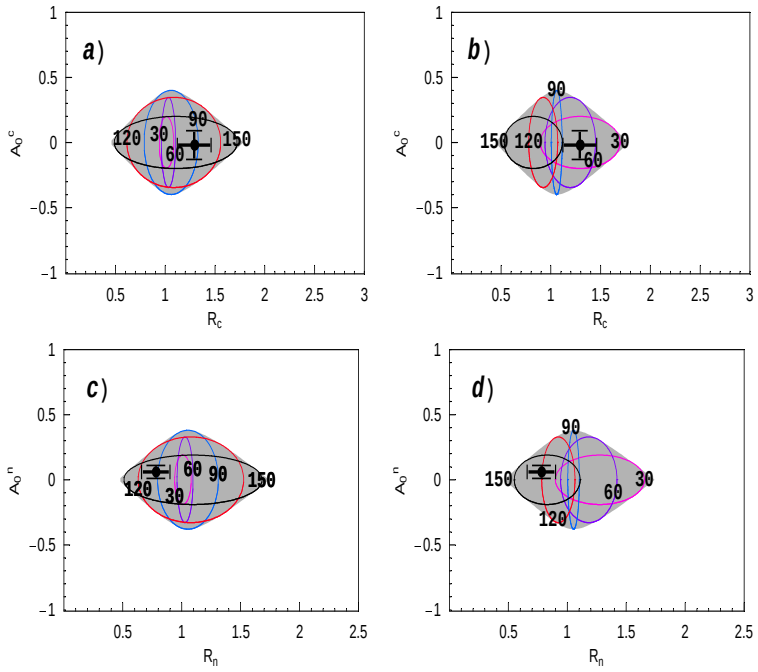

Fig. 21: The allowed regions in observable space of the charged ($r_{\rm c} = 0.20$; (a), (b)) and neutral ($r_{\rm n} = 0.19$; (c), (d)) $B \to \pi K$ systems for $q = 0.69$: in (a) and (c), we show also the contours for fixed values of γ, whereas we give the curves arising for fixed values of $|\delta_{\rm c}|$ and $|\delta_{\rm n}|$ in (b) and (d), respectively.

Correspondingly, we introduce the following sets of observables [140]:

$$\left\{ \begin{array}{c} R \\ A_0 \end{array} \right\} \equiv \left[\frac{\mathrm{BR}(B_d^0 \to \pi^- K^+) \pm \mathrm{BR}(\bar{B}_d^0 \to \pi^+ K^-)}{\mathrm{BR}(B^+ \to \pi^+ K^0) + \mathrm{BR}(B^- \to \pi^- \bar{K}^0)} \right] \frac{\tau_{B^+}}{\tau_{B_d^0}} \tag{7.16}$$

$$\left\{ \begin{array}{c} R_{\rm c} \\ A_0^{\rm c} \end{array} \right\} \equiv 2 \left[\frac{\mathrm{BR}(B^+ \to \pi^0 K^+) \pm \mathrm{BR}(B^- \to \pi^0 K^-)}{\mathrm{BR}(B^+ \to \pi^+ K^0) + \mathrm{BR}(B^- \to \pi^- \bar{K}^0)} \right] \tag{7.17}$$

$$\left\{ \begin{array}{c} R_{\rm n} \\ A_0^{\rm n} \end{array} \right\} \equiv \frac{1}{2} \left[\frac{\mathrm{BR}(B_d^0 \to \pi^- K^+) \pm \mathrm{BR}(\bar{B}_d^0 \to \pi^+ K^-)}{\mathrm{BR}(B_d^0 \to \pi^0 K^0) + \mathrm{BR}(\bar{B}_d^0 \to \pi^0 \bar{K}^0)} \right], \tag{7.18}$$

where the $R_{\rm (c,n)}$ and $A_0^{\rm (c,n)}$ refer to the plus and minus signs, respectively; the factors of 2 and $1/2$ are due to the wave functions of the neutral pions. In contrast to the observables in (7.16), those in (7.17) and (7.18) are significantly affected by EW penguins. We will return to this important feature below.

As noted in [140], all three $B \to \pi K$ systems can be described by the same set of formulae, just making straightforward replacements of variables. Let us first focus on the charged and neutral $B \to \pi K$ systems. For the parametrization of their observables, we employ the isospin relation mentioned above, and assume that certain rescattering effects are small; large rescattering processes would be indicated by large direct CP violation in $B^\pm \to \pi^\pm K$, which is not supported by the current B-factory average [86]:

$$\mathcal{A}_{\rm CP}^{\rm dir}(B^\pm \to \pi^\pm K) = -0.02 \pm 0.06, \tag{7.19}$$

and by an enhancement of the $B \to KK$ branching ratios, which are already strongly constrained by the B-factory data as well (for detailed discussions, see [26, 48]). Following these lines, we may write

$$R_{\rm c,n} = \text{function}(q, r_{\rm c,n}, \delta_{\rm c,n}, \gamma), \quad A_0^{\rm c,n} = \text{function}(r_{\rm c,n}, \delta_{\rm c,n}, \gamma), \tag{7.20}$$

where the parameters q, $r_{\rm c,n}$ and $\delta_{\rm c,n}$ have the following meaning:

- q describes the ratio of the EW penguin to tree contributions (see (7.15)), which can be determined with the help of $SU(3)$ flavour-symmetry arguments, yielding the following SM result [48, 138]:

$$q|_{\rm SM} = 0.69 \times \left[\frac{0.086}{|V_{ub}/V_{cb}|}\right]. \tag{7.21}$$

- The parameters $r_{\rm c,n}$ measure the ratios of the tree to QCD penguin topologies, and can be fixed through $SU(3)$ arguments and the data for BR$(B^\pm \to \pi^\pm\pi^0)$ [142], yielding $r_{\rm c,n} \sim 0.2$.
- The $\delta_{\rm c,n}$ are the CP-conserving strong phases between the tree and QCD penguin amplitudes.

Let us now consider either the charged or the neutral $B \to \pi K$ system. Since we may fix q and the corresponding $r_{\rm c,n}$ with the help of $SU(3)$ flavour-symmetry relations, the observables $R_{\rm c,n}$ and $A_0^{\rm c,n}$ depend only on the two "unknown" parameters $\delta_{\rm c,n}$ and γ. If we vary them within their allowed ranges, i.e. $-180^\circ \leq \delta_{\rm c,n} \leq +180^\circ$ and $0^\circ \leq \gamma \leq 180^\circ$, we obtain an allowed region in the $R_{\rm c,n}$–$A_0^{\rm c,n}$ plane [105, 143]. Should the measured values of $R_{\rm c,n}$ and $A_0^{\rm c,n}$ fall outside this region, we would have an immediate signal for NP. On the other hand, should the measurements lie inside the allowed range, γ and $\delta_{\rm c,n}$ could be extracted. The value of γ thus obtained could then be compared with the results of other strategies, whereas the strong phase $\delta_{\rm c,n}$ would offer interesting insights into hadron dynamics.

In Fig. 21, we show the allowed regions in the $R_{\rm c,n}$–$A_0^{\rm c,n}$ planes following [105], where the crosses represent the averages of the B-factory data. As can be read off from the contours in these figures, both the charged and the neutral $B \to \pi K$ data favour $\gamma \gtrsim 90^\circ$, which would be in conflict with the results of the usual CKM fits, as summarized in (2.42). Moreover, we observe that the charged modes point towards $|\delta_{\rm c}| \lesssim 90^\circ$ (QCD factorization predicts $\delta_{\rm c}$ to be close to 0° [75, 108]), whereas the neutral decays prefer $|\delta_{\rm n}| \gtrsim 90^\circ$. Since we do not expect $\delta_{\rm c}$ to differ significantly from $\delta_{\rm n}$, we arrive at a "puzzling" picture of the kind that was already pointed out in the year 2000 [141], and was recently reconsidered in [48, 54, 108, 144, 145, 146]. In the experimental values

$$R_{\rm c} = 1.17 \pm 0.12, \quad R_{\rm n} = 0.76 \pm 0.10, \tag{7.22}$$

this puzzle is reflected in particular by $R_{\rm n} < 1$, while $R_{\rm c} > 1$, as is now consistently favoured by the separate BaBar, Belle and CLEO data [86]. Concerning the mixed $B \to \pi K$ system, the data fall well into the SM region in observable space and do not indicate any "anomalous" behaviour [105].

7.2.3 The "$B \to \pi K$ Puzzle" and Recent Developments

Since $R_{\rm c}$ and $R_{\rm n}$ are affected significantly by colour-allowed EW penguins, whereas such topologies may only contribute to R in colour-suppressed form, the experimental pattern for these observables discussed above may be a manifestation of NP in the EW penguin sector [108, 141, 144, 145, 146], offering an attractive avenue for physics beyond the SM to enter the $B \to \pi K$ system [147, 148]. In order to deal with these effects quantitatively, we have to replace the parameter in (7.21), which characterizes the EW penguins in the SM, through a generalized parameter q, which may, in particular, also be associated with a CP-violating NP phase ϕ.

A detailed analysis of the $B \to \pi K$ puzzle was recently performed in [48, 54]. The starting point is the $B \to \pi\pi$ puzzle addressed in Subsection 6.2.2, which indicates that another hadronic parameter of the neutral $B \to \pi K$ system, $\rho_{\rm n} e^{i\theta_{\rm n}}$, is not as small as naïvely expected. However, using the $SU(3)$ flavour symmetry and plausible dynamical assumptions, it can be shown that we may fix all relevant hadronic $B \to \pi K$ parameters – including CP-conserving strong phases – through their $B \to \pi\pi$ counterparts, i.e. with the help of the B-factory data. Moreover, if we complement $B_d \to \pi^+\pi^-$ with $B_d \to \pi^\mp K^\pm$, we may also extract γ (see Subsection 8.3.3), with a result in excellent accordance with the range for γ in (6.28). Since EW penguins play a very minor rôle in $B \to \pi\pi$ and $B_d \to \pi^\mp K^\pm$ decays, these modes – and the parameters extracted from their observables – are essentially unaffected by NP in the EW penguin sector. Having all $B \to \pi K$ parameters at hand, we may then analyse the $B \to \pi K$ system in the SM.

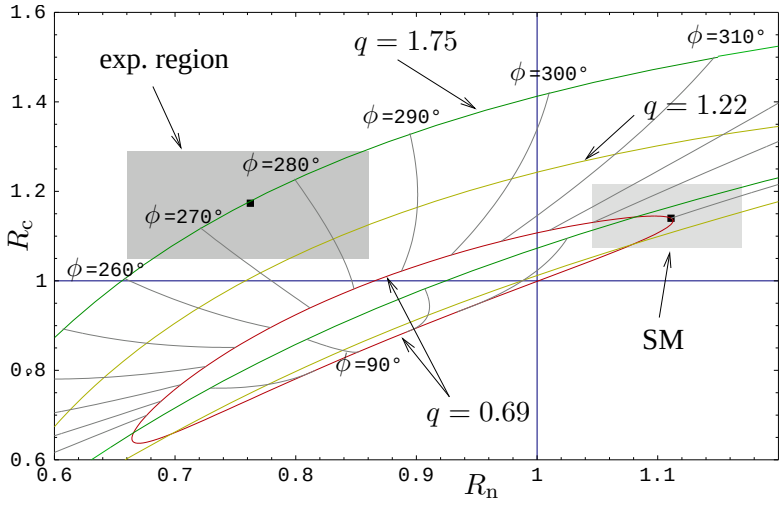

Fig. 22: The situation in the R_n–R_c plane, where the current experimental and SM ranges are indicated in grey. We show also contours for the EW penguin parameters $q = 0.69$, $q = 1.22$ and $q = 1.75$, with a NP phase $\phi \in [0^\circ, 360^\circ]$.

As far as the "mixed" $B \to \pi K$ system is concerned, we obtain

$$R|_{\rm SM} = 0.943^{+0.033}_{-0.026}, \tag{7.23}$$

which agrees well with the experimental result $R = 0.91 \pm 0.07$ following from the averages compiled in [86]. Additional information is provided by direct CP violation. Whereas the direct CP asymmetry of $B^\pm \to \pi^\pm K$ vanishes within our working assumptions, in accordance with the experimental value in (7.19), we find

$$\mathcal{A}_{\rm CP}^{\rm dir}(B_d \to \pi^\mp K^\pm)\Big|_{\rm SM} = 0.140^{+0.139}_{-0.087}, \tag{7.24}$$

which is in agreement with the current B-factory average $\mathcal{A}_{\rm CP}^{\rm dir}(B_d \to \pi^\mp K^\pm) = +0.095 \pm 0.028$.

In order to discuss the observables R_n and R_c, it is convenient to consider the R_n–R_c plane. Since all hadronic parameters are fixed through the $B \to \pi\pi$ data, these observables now depend only on the EW penguin parameters q and ϕ, where the SM is described by (7.21), corresponding to $\phi = 0^\circ$. As can nicely be seen in Fig. 22, the pattern of the SM predictions

$$R_c|_{\rm SM} = 1.14^{+0.08}_{-0.07}, \quad R_n|_{\rm SM} = 1.11^{+0.06}_{-0.07} \tag{7.25}$$

is *not* in accordance with the current experimental picture (7.22), so that we are actually back at the $B \to \pi K$ puzzle described above. In this figure, we have also included various contours corresponding to different fixed values of q, where each point is parametrized through the value of $\phi \in [0^\circ, 360^\circ]$. We observe that we may in fact move to the experimental region for an enhanced value of $q \sim 1.8$ and $\phi \sim -90^\circ$, where in particular the large CP-violating phase is in stark contrast to the SM. In order to put these observations on a more quantitative level, we may convert the experimental values of R_c and R_n into values of q and ϕ, with the following result:

$$q = 1.75^{+1.27}_{-0.99}, \quad \phi = -(85^{+11}_{-14})^\circ. \tag{7.26}$$

Because of the large, non-vanishing value of ϕ, this scenario of NP would require new sources for CP violation, i.e. would *not* belong to the simple class of MFV models specified in Subsection 6.4.4. As far as direct CP violation in $B^\pm \to \pi^0 K^\pm$ is concerned, we obtain

$$\mathcal{A}_{\rm CP}^{\rm dir}(B^\pm \to \pi^0 K^\pm) = 0.04^{+0.37}_{-0.28} \tag{7.27}$$

in our NP scenario, in accordance with the experimental number $\mathcal{A}_{\rm CP}^{\rm dir}(B^\pm \to \pi^0 K^\pm) = 0.00 \pm 0.07$. As was pointed out in [134], also the CP asymmetries of $B_d \to \pi^0 K_{\rm S}$ are an important tool to explore the KM mechanism of CP violation, where the SM corresponds (for $\rho_{\rm n} = 0$) to the relations

$$\mathcal{A}_{\rm CP}^{\rm dir}(B_d \to \pi^0 K_{\rm S}) = 0, \quad \mathcal{A}_{\rm CP}^{\rm mix}(B_d \to \pi^0 K_{\rm S}) = -\sin\phi_d = \mathcal{A}_{\rm CP}^{\rm mix}(B_d \to J/\psi K_{\rm S}), \tag{7.28}$$

in analogy to (6.37). Recently, the BaBar collaboration reported the following results [149]:

$$\mathcal{A}_{\rm CP}^{\rm dir}(B_d \to \pi^0 K_{\rm S}) = 0.40^{+0.27}_{-0.28} \pm 0.09, \quad \mathcal{A}_{\rm CP}^{\rm mix}(B_d \to \pi^0 K_{\rm S}) = -0.48^{-0.38}_{+0.47} \pm 0.06. \tag{7.29}$$

Moreover, also a measurement of the direct CP asymmetry of the $B_d^0 \to \pi^0 K^0$ channel is available [86]:

$$\mathcal{A}_{\rm CP}^{\rm dir}(B_d^0 \to \pi^0 K^0) = -0.03 \pm 0.36 \pm 0.09, \tag{7.30}$$

which is supposed to agree with the direct CP asymmetry in (7.29). Consequently, these experimental numbers are expected to change significantly in the future. On the other hand, the $B \to \pi\pi, \pi K$ analysis described above yields the predictions

$$\mathcal{A}_{\rm CP}^{\rm dir}(B_d \to \pi^0 K_{\rm S}) = +0.05^{+0.24}_{-0.29}, \quad \mathcal{A}_{\rm CP}^{\rm mix}(B_d \to \pi^0 K_{\rm S}) = -0.99^{+0.04}_{-0.01}. \tag{7.31}$$

The measurement of these CP asymmetries will allow an interesting test of the NP scenario of enhanced EW penguins with a large CP-violating phase that is suggested by the $B \to \pi K$ puzzle. In this respect, it is important to consider also rare B and K decays, which offer particularly sensitive probes for the exploration of this kind of NP. We shall return to the corresponding NP effects in Subsection 9.4, where we will also briefly address the impact on ${\rm Re}(\varepsilon'/\varepsilon)$, $B_d \to J/\psi K_{\rm S}$ and $B_d \to \phi K_{\rm S}$.

8 THE B_s-MESON SYSTEM

8.1 General Features

8.1.1 Comparison of the B_d and B_s Systems

At the e^+e^- B factories operating at the $\Upsilon(4S)$ resonance (BaBar and Belle), the B_s-meson system is not accessible since $\Upsilon(4S)$ states decay only into $B_{u,d}$ but not into B_s mesons.[10] On the other hand, plenty of B_s mesons will be produced at hadron colliders. Consequently, these particles are the "El Dorado" for B-decay studies at run II of the Tevatron [18], and later on at the LHC [19]. There are important differences between the B_d and B_s systems:

- The B_s^0–$\bar{B}_s^0$ mixing phase is negligibly small in the SM,

$$\phi_s \equiv 2\arg(V_{ts}^* V_{tb}) = -2\delta\gamma = -2\lambda^2\eta = \mathcal{O}(-2^\circ), \tag{8.1}$$

  whereas $\phi_d \equiv 2\arg(V_{td}^* V_{tb}) = 2\beta = \mathcal{O}(50^\circ)$.

- A large mixing parameter x_s is expected in the SM,

$$x_s \equiv \frac{\Delta M_s}{\Gamma_s} = \mathcal{O}(20), \tag{8.2}$$

  whereas $x_d = 0.771 \pm 0.012$. Consequently, we have to deal with rapid B_s^0–$\bar{B}_s^0$ oscillations. The current experimental lower bound for the mass difference of the B_s mass eigenstates is given by $\Delta M_s > 14.5\,{\rm ps}^{-1}$, corresponding to $x_s > 20.8$ (95% C.L.) [85, 86].

- There may be a sizeable difference between the decay widths of the B_s mass eigenstates,

$$\frac{\Delta\Gamma_s}{\Gamma_s} = \mathcal{O}(-10\%), \tag{8.3}$$

  whereas $\Delta\Gamma_d/\Gamma_d$ is negligibly small, as we have seen in Subsection 5.1.2. The current CDF and LEP average is given by $\Delta\Gamma_s/\Gamma_s = -0.16^{+0.16}_{-0.15}$, $|\Delta\Gamma_s|/\Gamma_s < 0.54$ (95% C.L.) [85, 86].

[10] Operating these machines on the $\Upsilon(5S)$ resonance would also allow the production of B_s mesons.

8.1.2 *Impact of ΔM_s on the Unitarity Triangle*

As we discussed in Subsection 5.1, the mass differences of the B_q mass eigenstates satisfy

$$\Delta M_q \propto M_{B_q} \hat{B}_{B_q} f_{B_q}^2 |V_{tq}^* V_{tb}|^2. \tag{8.4}$$

In the B_d-meson case, this particular structure leads to (5.15), allowing us to determine the side R_t of the UT. To this end, in addition to the CKM parameter A (see (4.21)), also the non-perturbative quantity

$$\sqrt{\hat{B}_{B_d}} f_{B_d} = (235 \pm 33^{+0}_{-24})\,\text{MeV} \tag{8.5}$$

has to be known, where the numerical value follows from lattice QCD studies [41]; QCD sum rules give a similar picture [150]. On the other hand, if we apply the expressions for V_{cb} and V_{ts} in (2.20), we obtain

$$R_t \equiv \frac{1}{\lambda}\left|\frac{V_{td}}{V_{cb}}\right| = \frac{1}{\lambda}\left|\frac{V_{td}}{V_{ts}}\right|\left[1 + \mathcal{O}(\lambda^2)\right]. \tag{8.6}$$

Consequently, we may – up to corrections entering at the λ^2 level – determine R_t through the ratio $|V_{td}/V_{ts}|$. Using now (8.4) yields the following expression [82]:

$$R_t = 0.90\left[\frac{\xi}{1.24}\right]\sqrt{\frac{18.4\,\text{ps}^{-1}}{\Delta M_s}}\sqrt{\frac{\Delta M_d}{0.5\,\text{ps}^{-1}}}, \tag{8.7}$$

where

$$\xi \equiv \frac{\sqrt{\hat{B}_s} f_{B_s}}{\sqrt{\hat{B}_d} f_{B_d}} \tag{8.8}$$

is an $SU(3)$-breaking parameter; lattice QCD studies give

$$\xi = 1.18 \pm 0.04^{+0.12}_{-0}, \tag{8.9}$$

where $\xi = 1.24 \pm 0.08$ should be used for analyses of the UT, as discussed in [41]. In comparison with the quantity in (8.5) entering (5.15), the ratio in (8.8) is more favourable and represents an important aspect of current non-perturbative research [41]. Another advantage of (8.7) is that A, the Inami–Lim function $S_0(x_t)$, and the short-distance QCD correction factor η_B cancel in this expression. Interestingly, it allows us also to convert the lower experimental bound $\Delta M_s > 14.5\,\text{ps}^{-1}$ into the upper bound $R_t < 1.0 \times [\xi/1.24]$, which implies $\gamma \lesssim 90^\circ$, thereby excluding a large fraction of the $\bar{\rho}$–$\bar{\eta}$ plane.

8.1.3 $\Delta\Gamma_s$ *and "Untagged" B_s Rates*

The width difference of the B_s-meson system may provide interesting studies of CP violation through "untagged" B_s rates [151]–[153], which are defined as

$$\langle \Gamma(B_s(t) \to f)\rangle \equiv \Gamma(B_s^0(t) \to f) + \Gamma(\bar{B}_s^0(t) \to f), \tag{8.10}$$

and are characterized by the feature that we do not distinguish between initially, i.e. at time $t = 0$, present B_s^0 or $\bar{B}_s^0$ mesons. If we consider a final state f to which both a B_s^0 and a $\bar{B}_s^0$ may decay, and use the expressions in (5.27), we find

$$\langle \Gamma(B_s(t) \to f)\rangle \propto [\cosh(\Delta\Gamma_s t/2) - \mathcal{A}_{\Delta\Gamma}(B_s \to f)\sinh(\Delta\Gamma_s t/2)]\, e^{-\Gamma_s t}, \tag{8.11}$$

where $\mathcal{A}_{\Delta\Gamma}(B_s \to f) \propto \text{Re}\,\xi_f$ was introduced in (5.33). We observe that the rapidly oscillating $\Delta M_s t$ terms cancel, and that we may obtain information on the phase structure of the observable ξ_f, thereby providing valuable insights into CP violation. For instance, the untagged observables offered by the angular distribution of the $B_s \to K^{*+}K^{*-}, K^{*0}\bar{K}^{*0}$ decay products allow the determination of the UT angle γ, provided $\Delta\Gamma_s$ is actually sizeable [152]. Although B-decay experiments at hadron colliders should be able to resolve the B_s^0–$\bar{B}_s^0$ oscillations, untagged B_s rates are interesting in terms of efficiency, acceptance and purity.

8.2 $B_s \to J/\psi\phi$

This particularly promising channel is the B_s-meson counterpart of the "golden" mode $B_d \to J/\psi K_{\rm S}$, as can be seen from the diagrams shown in Fig. 13, where we just have to replace the down spectator quark by a stange quark in order to obtain the $B_s \to J/\psi\phi$ diagrams. Consequently, this decay is described by a transition amplitude with a structure that is completely analogous to that of (6.3). On the other hand, in contrast to $B_d \to J/\psi K_{\rm S}$, the final state of $B_s \to J/\psi\phi$ is an admixture of different CP eigenstates, which can, however, be disentangled through an angular analysis of the $J/\psi[\to \ell^+\ell^-]\phi[\to \ K^+K^-]$ decay products [154, 155]. Their angular distribution exhibits tiny direct CP violation, whereas mixing-induced CP-violating effects allow the extraction of

$$\sin\phi_s + \mathcal{O}(\overline{\lambda}^3) = \sin\phi_s + \mathcal{O}(10^{-3}). \tag{8.12}$$

Since we have $\phi_s = -2\lambda^2\eta = \mathcal{O}(10^{-2})$ in the SM, the determination of this phase from (8.12) is affected by generic hadronic uncertainties of $\mathcal{O}(10\%)$, which may become an important issue for the LHC era. These uncertainties can be controlled with the help of flavour-symmetry arguments through the decay $B_d \to J/\psi\rho^0$ [156]. Needless to note, the big hope is that experiments will find a *sizeable* value of $\sin\phi_s$, which would immediately signal the presence of NP contributions to B_s^0–$\bar{B}_s^0$ mixing.

Other interesting aspects of the $B_s \to J/\psi\phi$ angular distribution are the determination of the width difference $\Delta\Gamma_s$ from untagged data samples [155] (for recent LHC feasibility studies, see [157]), and the extraction of $\cos\delta_f\cos\phi_s$ terms, where the δ_f are CP-conserving strong phases. If we fix the signs of $\cos\delta_f$ through factorization, we may extract the sign of $\cos\phi_s$, allowing an *unambiguous* determination of ϕ_s [95]. In this context, $B_s \to D_\pm\eta^{(\prime)}$, $D_\pm\phi$, ... decays offer also interesting methods [158, 159].

8.3 $B_s \to K^+K^-$

As can be seen from Fig. 14, the decay $B_d \to \pi^+\pi^-$ is related to the $B_s \to K^+K^-$ channel through an interchange of *all* down and strange quarks. Because of this feature, the U-spin flavour symmetry of strong interactions, which connects the down and strange quarks through $SU(2)$ transformations in the same manner as the ordinary isospin symmetry connects the down and up quarks, allows us to relate the hadronic $B_d \to \pi^+\pi^-$ parameters to their $B_s \to K^+K^-$ counterparts. It can then be shown that these quantities – and the angle γ of the UT – can be extracted from the measured CP asymmetries of the $B_d \to \pi^+\pi^-$, $B_s \to K^+K^-$ system [96]. Also other U-spin strategies were developed, using $B_{s(d)} \to J/\psi K_{\rm S}$ or $B_{d(s)} \to D^+_{d(s)}D^-_{d(s)}$ [87], $B_{d(s)} \to K^{0(*)}\bar{K}^{0(*)}$ [26, 156], $B_{(s)} \to \pi K$ [160], or $B_{s(d)} \to J/\psi\eta$ modes [161]. Since the $B_s \to K^+K^-$, $B_d \to \pi^+\pi^-$ system is particularly promising from an experimental point of view, thereby providing an interesting playground for CDF-II [18] and LHCb [19, 162], let us now have a closer look at the corresponding strategy [96].

8.3.1 Amplitude Structure and CP Asymmetries

If we follow Subsection 6.2, we may write the $B_d \to \pi^+\pi^-$, $B_s \to K^+K^-$ amplitudes as

$$A(B_d^0 \to \pi^+\pi^-) = \mathcal{C}\left[e^{i\gamma} - de^{i\theta}\right] \tag{8.13}$$

$$A(B_s^0 \to K^+K^-) = \left(\frac{\lambda}{1-\lambda^2/2}\right)\mathcal{C}'\left[e^{i\gamma} + \left(\frac{1-\lambda^2}{\lambda^2}\right)d'e^{i\theta'}\right], \tag{8.14}$$

where $de^{i\theta}$ was introduced in (6.14), $d'e^{i\theta'}$ is the $B_s \to K^+K^-$ counterpart of this quantity, and the overall normalization factors $\mathcal{C}$ and $\mathcal{C}'$ are CP-conserving strong amplitudes. Using these general parametrizations, we may write the corresponding CP-violating observables in the following generic form:

$$\mathcal{A}_{\rm CP}^{\rm dir}(B_d \to \pi^+\pi^-) = {\rm fct}(d,\theta,\gamma), \qquad \mathcal{A}_{\rm CP}^{\rm mix}(B_d \to \pi^+\pi^-) = {\rm fct}(d,\theta,\gamma,\phi_d) \tag{8.15}$$

$$\mathcal{A}_{\rm CP}^{\rm dir}(B_s \to K^+K^-) = {\rm fct}(d',\theta',\gamma), \quad \mathcal{A}_{\rm CP}^{\rm mix}(B_s \to K^+K^-) = {\rm fct}(d',\theta',\gamma,\phi_s). \tag{8.16}$$

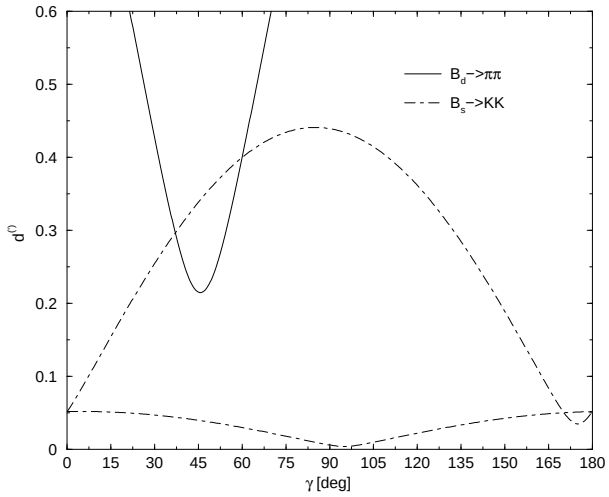

Fig. 23: The contours in the γ–$d^{(\prime)}$ plane for a specific example with $d = d' = 0.4$, $\theta = \theta' = 140^\circ$, $\phi_d = 47^\circ$, $\phi_s = 0^\circ$, $\gamma = 60^\circ$, corresponding to $\mathcal{A}_{\rm CP}^{\rm dir}(B_d \to \pi^+\pi^-) = -0.30$, $\mathcal{A}_{\rm CP}^{\rm mix}(B_d \to \pi^+\pi^-) = +0.63$, $\mathcal{A}_{\rm CP}^{\rm dir}(B_s \to K^+K^-) = +0.16$ and $\mathcal{A}_{\rm CP}^{\rm mix}(B_s \to K^+K^-) = -0.17$.

The explicit expressions for the direct and mixing-induced CP asymmetries of $B_d \to \pi^+\pi^-$ are given in (6.18) and (6.19), respectively, whereas those for their $B_s \to K^+K^-$ counterparts can be found in [96]. Fortunately, these rather complicated expressions are not required for the following discussion.

8.3.2 Extraction of γ and Hadronic Parameters

As we saw in Subsection 6.1, ϕ_d can be extracted through the "golden" mode $B_d \to J/\psi K_{\rm S}$, with the result in (6.11). On the other hand, ϕ_s can be assumed to be negligibly small in the SM, or can be fixed through $B_s \to J/\psi\phi$, as we discussed above. These experimental determinations work also in the presence of NP contributions to B_q^0–$\bar{B}_q^0$ mixing, as is obvious from the discussion in Subsection 6.4.

Looking at (8.15), we observe that a measurement of $\mathcal{A}_{\rm CP}^{\rm dir}(B_d \to \pi^+\pi^-)$ and $\mathcal{A}_{\rm CP}^{\rm mix}(B_d \to \pi^+\pi^-)$ allows us to eliminate the strong phase θ, thereby yielding d as a function of γ in a *theoretically clean* way. In complete analogy, we may use the general parametrizations of the form in (8.16) to eliminate θ', and to determine d' in a *theoretically clean* manner as a function of γ from the measured values of $\mathcal{A}_{\rm CP}^{\rm dir}(B_s \to K^+K^-)$ and $\mathcal{A}_{\rm CP}^{\rm mix}(B_s \to K^+K^-)$. Since $B_d \to \pi^+\pi^-$ and $B_s \to K^+K^-$ are related to each other by interchanging all down and strange quarks, the U-spin flavour symmetry of strong interactions implies the following relations:

$$d' = d, \quad \theta' = \theta. \tag{8.17}$$

Applying the former, we may extract γ and d from the theoretically clean γ–d and γ–d' contours, which we have illustrated for a specific example in Fig. 23. As discussed in [96], it is also possible to resolve the twofold ambiguity for (γ, d) arising from the intersections of the solid and dot-dashed curves in Fig. 23. Moreover, we may determine θ and θ', thereby allowing an interesting internal consistency check of the second U-spin relation in (8.17).[11]

This strategy is very promising from an experimental point of view: at run II of the Tevatron and at the LHC, experimental accuracies for γ of $\mathcal{O}(10^\circ)$ and $\mathcal{O}(1^\circ)$, respectively, are expected [18, 162]. As far as the U-spin-breaking corrections to $d' = d$ are concerned, they enter the determination of γ through a relative shift of the γ–d and γ–d' contours; their impact on the extracted value of γ therefore depends on the form of these curves, which is fixed through the measured observables. In the examples discussed

[11] Alternatively, we may eliminate d and d', and may then extract these parameters and γ through the relation $\theta' = \theta$.

in [26, 96], as well as in the one shown in Fig. 23, the extracted value of γ would be very stable under such corrections. Let us also note that the U-spin relations in (8.17) appear to be quite robust, since the relevant form factors and decay constants cancel within factorization, so that they do not receive U-spin-breaking corrections in this approach [96]. On the other hand, the ratio $|\mathcal{C}'/\mathcal{C}|$, which equals 1 in the strict U-spin limit and enters the U-spin relation

$$\frac{\mathcal{A}_{\rm CP}^{\rm mix}(B_s \to K^+K^-)}{\mathcal{A}_{\rm CP}^{\rm dir}(B_d \to \pi^+\pi^-)} = -\left|\frac{\mathcal{C}'}{\mathcal{C}}\right|^2 \left[\frac{\rm BR(B_d \to \pi^+\pi^-)}{\rm BR(B_s \to K^+K^-)}\right] \frac{\tau_{B_s}}{\tau_{B_d}}, \tag{8.18}$$

is affected by U-spin-breaking effects within factorization. An estimate of the corresponding form factors was recently performed in [163], and certain non-factorizable effects were addressed in [164].

8.3.3 Replacing $B_s \to K^+K^-$ by $B_d \to \pi^\mp K^\pm$

Since $B_s \to K^+K^-$ is not accessible at the e^+e^- B factories operating at the $\Upsilon(4S)$ resonance, we may not yet implement the strategy discussed above. However, as can easily be seen by looking at the corresponding Feynman diagrams, $B_s \to K^+K^-$ is related to $B_d \to \pi^\mp K^\pm$ through an interchange of spectator quarks. Consequently, we may approximately replace $B_s \to K^+K^-$ through $B_d \to \pi^\mp K^\pm$ in order to deal with the penguin problem in $B_d \to \pi^+\pi^-$ [165]. The utility of $B_d \to \pi^\mp K^\pm$ decays to control the penguin effects in $B_d \to \pi^+\pi^-$ was also emphasized in [98]. In order to explore the implications of the B-factory data, the following quantity plays a key rôle:

$$H = \frac{1}{\epsilon}\left(\frac{f_K}{f_\pi}\right)^2 \left[\frac{\rm BR(B_d \to \pi^+\pi^-)}{\rm BR(B_d \to \pi^\mp K^\pm)}\right] = 7.17 \pm 0.75. \tag{8.19}$$

Here $\epsilon \equiv \lambda^2/(1-\lambda^2)$, the ratio $f_K/f_\pi = 160/131$ describes factorizable $SU(3)$-breaking corrections, and the numerical value refers to the averages compiled in [86]. Applying (8.17), we obtain

$$H = \frac{1 - 2d\cos\theta\cos\gamma + d^2}{\epsilon^2 + 2\epsilon d\cos\theta\cos\gamma + d^2}. \tag{8.20}$$

If we now combine the CP asymmetries $\mathcal{A}_{\rm CP}^{\rm dir}(B_d \to \pi^+\pi^-)$ and $\mathcal{A}_{\rm CP}^{\rm mix}(B_d \to \pi^+\pi^-)$ with H, we have sufficient information available to determine γ, as well as d and θ [96, 165]. In practice, this can be done with the help of the expressions in (6.18), (6.19) and (8.20). A detailed discussion of this strategy was given in [47, 105], where also the impact of NP contributions to B^0_d–$\bar{B}^0_d$ mixing was explored. Using additional information from the $B \to \pi K$ analysis discussed in Subsection 7.2.3, the corresponding determination of γ was recently refined in [48], where in particular a twofold ambiguity for γ could be resolved, yielding

$$\gamma = (64.7^{+6.3}_{-6.9})^\circ, \tag{8.21}$$

which is in excellent agreement with the SM picture summarized in (6.28). If we complement this result with the experimental range for R_b and apply the simple relations

$$\bar{\rho} = R_b\cos\gamma, \quad \bar{\eta} = R_b\sin\gamma, \tag{8.22}$$

which follow straightforwardly from Fig. 4, we may also determine α and β:

$$\alpha = (93.6^{+10.3}_{-9.1})^\circ, \quad \beta = (21.7^{+2.5}_{-2.6})^\circ. \tag{8.23}$$

In Fig. 24, we compare these results with the allowed region for the apex of the UT that follows from the CKM fits, as implemented in [166].[12] Here the solid window corresponds to the range for γ in (8.21), whereas the dashed window indicates how the results change when the recently reported new Belle data [167] are used. Needless to note, the consistency of the overall picture is very remarkable.

[12] The small and large ellipses in Fig. 24 refer to the analyses of the SM and NP scenarios with MFV, respectively, as obtained in a recent update [82] of [166].

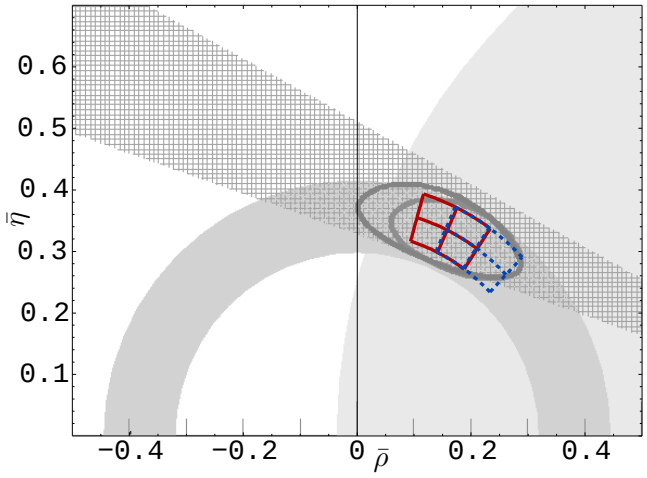

Fig. 24: Comparison of the determination of γ from the $B \to \pi\pi, \pi K$ data with the CKM fits, as discussed in the text.

In the analysis leading to (8.21) and (8.23), it has been assumed that $\phi_d \sim 47^\circ$, as in the SM. However, as discussed in [47, 105], it is interesting to consider also the second, unconventional solution of $\phi_d \sim 133^\circ$ in (6.11). There are simple relations to go from one solution to the other. In particular, if ϕ_d, γ, d and θ are solutions of (6.18), (6.19) and (8.20), then

$$\pi - \phi_d, \quad \pi - \gamma, \quad d, \quad \pi - \theta \tag{8.24}$$

are solutions as well. Consequently, (8.24) allows us to go easily from the $\phi_d \sim 47^\circ$ to the $\phi_d \sim 133^\circ$ case. Interestingly, for the value of θ in (6.29), we obtain $\cos\theta \sim -0.7 < 0$, having the same sign as in factorization, where $\cos\theta|_{\rm fact} = -1$. On the other hand, the value of θ corresponding to $\phi_d \sim 133^\circ$ yields $\cos\theta \sim +0.7 > 0$, i.e. the opposite sign, thereby disfavouring the $\phi_d \sim 133^\circ$ solution [48].

Let us finally note that the results for d and θ in (6.29) following from the $B \to \pi\pi$ analysis discussed in Subsection 6.2.2 allow us also to obtain SM predictions for the CP-violating $B_s \to K^+K^-$ observables with the help of (8.17) [48]:

$$\mathcal{A}_{\rm CP}^{\rm dir}(B_s \to K^+K^-)\Big|_{\rm SM} = 0.14^{+0.14}_{-0.09}, \quad \mathcal{A}_{\rm CP}^{\rm mix}(B_s \to K^+K^-)\Big|_{\rm SM} = -0.18^{+0.08}_{-0.07}. \tag{8.25}$$

On the other hand, the prediction of BR$(B_s \to K^+K^-)$ requires information on the $SU(3)$-breaking form-factor ratios entering $|\mathcal{C}'/\mathcal{C}|$, where the estimates of [163] correspond to a branching ratio at the 3.5×10^{-5} level. It will be very interesting to see the first data for the $B_s \to K^+K^-$ channel from run II of the Tevatron, and to fully expoit its physics potential at LHCb and BTeV. The decay $B_s \to \pi^\pm K^\mp$ offers also various ways to complement the $B \to \pi\pi, \pi K$ strategy discussed in Subsection 7.2.3.

8.4 $B_s \to D_s^{(*)\pm} K^\mp$

Decays of the kind $B_s \to D_s^{(*)\pm} K^\mp, \ldots$ and their counterparts $B_d \to D^{(*)\pm}\pi^\mp, \ldots$ provide another important tool to explore CP violation [168, 169]. Since these transitions can be described on the same theoretical basis, we will consider them simultaneously in this subsection, following [170].

8.4.1 Basic Features

It is convenient to write $B_s \to D_s^{(*)\pm} K^\mp, \ldots$ and $B_d \to D^{(*)\pm}\pi^\mp, \ldots$ decays generically as $B_q^0 \to D_q \bar{u}_q$, so that we may easily distinguish between the following cases:

- $q = s$: $D_s \in \{D_s^+, D_s^{*+}, \ldots\}$, $u_s \in \{K^+, K^{*+}, \ldots\}$.
- $q = d$: $D_d \in \{D^+, D^{*+}, \ldots\}$, $u_d \in \{\pi^+, \rho^+, \ldots\}$.

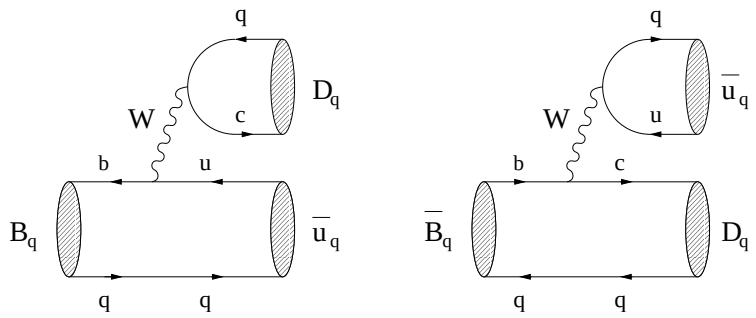

Fig. 25: Feynman diagrams contributing to $B_q^0 \to D_q \bar{u}_q$ and $\bar{B}_q^0 \to D_q \bar{u}_q$.

In the discussion given below, we shall only consider those $B_q^0 \to D_q \bar{u}_q$ decays where at least one of the D_q, $\bar{u}_q$ states is a pseudoscalar meson. In the opposite case, for example $B_s^0 \to D_s^{*+} K^{*-}$, the extraction of weak phases would require a complicated angular analysis. If we look at Fig. 25, we observe that $B_q^0 \to D_q \bar{u}_q$ originates from colour-allowed tree topologies, and that also a $\bar{B}_q^0$ meson may decay into the same final state $D_q \bar{u}_q$. The latter feature leads to interference effects between B_q^0–$\bar{B}_q^0$ mixing and decay processes, providing valuable information about the CP-violating phase $\phi_q + \gamma$.

8.4.2 Rate Asymmetries

Let us first consider B_q decays into $D_q \bar{u}_q$. Since both a B_q^0 and a $\bar{B}_q^0$ meson may decay into this state, we obtain a time-dependent rate asymmetry of the following form:

$$\begin{aligned}&\frac{\Gamma(B_q^0(t) \to D_q \bar{u}_q) - \Gamma(\bar{B}_q^0(t) \to D_q \bar{u}_q)}{\Gamma(B_q^0(t) \to D_q \bar{u}_q) + \Gamma(\bar{B}_q^0(t) \to D_q \bar{u}_q)} \\ &\qquad = \left[\frac{C(B_q \to D_q \bar{u}_q)\cos(\Delta M_q t) + S(B_q \to D_q \bar{u}_q)\sin(\Delta M_q t)}{\cosh(\Delta\Gamma_q t/2) - \mathcal{A}_{\Delta\Gamma}(B_q \to D_q \bar{u}_q)\sinh(\Delta\Gamma_q t/2)}\right],\end{aligned} \tag{8.26}$$

having a structure that is completely analogous to the one of (5.30). Applying the formalism discussed in Section 5, we find that these observables are given by

$$C(B_q \to D_q \bar{u}_q) \equiv C_q = \frac{1 - |\xi_q|^2}{1 + |\xi_q|^2}, \quad S(B_q \to D_q \bar{u}_q) \equiv S_q = \frac{2\,\mathrm{Im}\,\xi_q}{1 + |\xi_q|^2}, \tag{8.27}$$

where

$$\xi_q \equiv -e^{-i\phi_q}\left[e^{i\phi_{\rm CP}(B_q)}\frac{A(\bar{B}_q^0 \to D_q \bar{u}_q)}{A(B_q^0 \to D_q \bar{u}_q)}\right] \tag{8.28}$$

measures the strength of the interference effects between the B_q^0–$\bar{B}_q^0$ mixing and decay processes.

If we take the Feynman diagrams shown in Fig. 25 into account and use an appropriate low-energy effecitve Hamiltonian of the kind discussed in Subsection 4.3.2, we may write

$$A(\bar{B}_q^0 \to D_q \bar{u}_q) = \langle \bar{u}_q D_q | \mathcal{H}_{\rm eff}(\bar{B}_q^0 \to D_q \bar{u}_q) | \bar{B}_q^0 \rangle = \frac{G_{\rm F}}{\sqrt{2}} \bar{v}_q \bar{M}_q, \tag{8.29}$$

where the hadronic matrix element

$$\bar{M}_q \equiv \langle \bar{u}_q D_q | \bar{\mathcal{O}}_1^q\, C_1(\mu) + \bar{\mathcal{O}}_2^q\, C_2(\mu) | \bar{B}_q^0 \rangle \tag{8.30}$$

involves the current–current operators

$$\bar{\mathcal{O}}_1^q \equiv (\bar{q}_\alpha u_\beta)_{\rm V\text{–}A}\,(\bar{c}_\beta b_\alpha)_{\rm V\text{–}A}\,, \quad \bar{\mathcal{O}}_2^q \equiv (\bar{q}_\alpha u_\alpha)_{\rm V\text{–}A}\,(\bar{c}_\beta b_\beta)_{\rm V\text{–}A}\,, \tag{8.31}$$

and the CKM factors $\bar{v}_q$ are given by

$$\bar{v}_s \equiv V_{us}^* V_{cb} = A\lambda^3, \quad \bar{v}_d \equiv V_{ud}^* V_{cb} = A\lambda^2(1-\lambda^2/2). \tag{8.32}$$

On the other hand, the $B_q^0 \to D_q \bar{u}_q$ decay amplitude takes the following form:

$$A(B_q^0 \to D_q \bar{u}_q) = \langle \bar{u}_q D_q | \mathcal{H}_{\rm eff}(B_q^0 \to D_q \bar{u}_q) | B_q^0 \rangle = \frac{G_{\rm F}}{\sqrt{2}} v_q^* \langle \bar{u}_q D_q | \mathcal{O}_1^{q\dagger}\, C_1(\mu) + \mathcal{O}_2^{q\dagger}\, C_2(\mu) | B_q^0 \rangle, \tag{8.33}$$

where we have to deal with the current–current operators

$$\mathcal{O}_1^q \equiv (\bar{q}_\alpha c_\beta)_{\rm V\text{–}A}\, (\bar{u}_\beta b_\alpha)_{\rm V\text{–}A}\,, \quad \mathcal{O}_2^q \equiv (\bar{q}_\alpha c_\alpha)_{\rm V\text{–}A}\, (\bar{u}_\beta b_\beta)_{\rm V\text{–}A}\,, \tag{8.34}$$

and the CKM factors v_q are defined as

$$v_s \equiv V_{cs}^* V_{ub} = A\lambda^3 R_b e^{-i\gamma}, \quad v_d \equiv V_{cd}^* V_{ub} = -\left(\frac{A\lambda^4 R_b}{1-\lambda^2/2}\right) e^{-i\gamma}. \tag{8.35}$$

If we introduce CP phases for the D_q and u_q mesons in analogy to (5.9), we obtain

$$(\mathcal{CP})|D_q \bar{u}_q\rangle = (-1)^L e^{i[\phi_{\rm CP}(D_q) - \phi_{\rm CP}(u_q)]} |\bar{D}_q u_q\rangle, \tag{8.36}$$

where L denotes the angular momentum of the $D_q \bar{u}_q$ state. Using now the relations $(\mathcal{CP})^\dagger(\mathcal{CP}) = \hat{1}$ and $(\mathcal{CP})\mathcal{O}_k^{q\dagger}(\mathcal{CP})^\dagger = \mathcal{O}_k^q$ as in Subsection 5.2, we may rewrite (8.33) as

$$A(B_q^0 \to D_q \bar{u}_q) = (-1)^L e^{i[\phi_{\rm CP}(B_q) - \phi_{\rm CP}(D_q) + \phi_{\rm CP}(u_q)]} \frac{G_{\rm F}}{\sqrt{2}} v_q^* M_q, \tag{8.37}$$

with

$$M_q \equiv \langle u_q \bar{D}_q | \mathcal{O}_1^q\, C_1(\mu) + \mathcal{O}_2^q\, C_2(\mu) | \bar{B}_q^0 \rangle. \tag{8.38}$$

An analogous calculation for the $\bar{B}_q^0 \to \bar{D}_q u_q$ and $B_q^0 \to \bar{D}_q u_q$ transitions yields

$$A(\bar{B}_q^0 \to \bar{D}_q u_q) = \frac{G_{\rm F}}{\sqrt{2}} v_q M_q \tag{8.39}$$

$$A(B_q^0 \to \bar{D}_q u_q) = (-1)^L e^{i[\phi_{\rm CP}(B_q) + \phi_{\rm CP}(D_q) - \phi_{\rm CP}(u_q)]} \frac{G_{\rm F}}{\sqrt{2}} \bar{v}_q^* \bar{M}_q, \tag{8.40}$$

where the same hadronic matrix elements as in the $B_q^0 \to D_q \bar{u}_q$ and $\bar{B}_q^0 \to D_q \bar{u}_q$ modes arise.

If we now insert (8.29) and (8.37) into (8.28), we observe that the convention-dependent phase $\phi_{\rm CP}(B_q)$ is cancelled through the amplitude ratio, and arrive at

$$\xi_q = -(-1)^L e^{-i(\phi_q + \gamma)} \left[\frac{1}{x_q e^{i\delta_q}}\right], \tag{8.41}$$

where

$$x_s \equiv R_b a_s, \quad x_d \equiv -\left(\frac{\lambda^2 R_b}{1-\lambda^2}\right) a_d, \tag{8.42}$$

with

$$a_q e^{i\delta_q} \equiv e^{-i[\phi_{\rm CP}(D_q) - \phi_{\rm CP}(u_q)]} \frac{M_q}{\bar{M}_q}. \tag{8.43}$$

It should be noted that the convention-dependent phases $\phi_{\rm CP}(D_q)$ and $\phi_{\rm CP}(u_q)$ in (8.43) are cancelled through the ratio of hadronic matrix elements, so that $a_q e^{i\delta_q}$ is actually a physical observable (this is shown explicitly in [170]). Applying now (8.27), we finally arrive at

$$C_q = -\left[\frac{1-x_q^2}{1+x_q^2}\right], \quad S_q = (-1)^L \left[\frac{2\,x_q \sin(\phi_q+\gamma+\delta_q)}{1+x_q^2}\right]. \tag{8.44}$$

An analogous calculation for the decays into the CP-conjugate final state $\bar{D}_q u_q$ yields

$$\bar{\xi}_q = -e^{-i\phi_q}\left[e^{i\phi_{\rm CP}(B_q)}\frac{A(\bar{B}_q^0\to\bar{D}_q u_q)}{A(B_q^0\to\bar{D}_q u_q)}\right] = -(-1)^L e^{-i(\phi_q+\gamma)}\left[x_q e^{i\delta_q}\right], \tag{8.45}$$

which implies

$$\bar{C}_q = +\left[\frac{1-x_q^2}{1+x_q^2}\right], \quad \bar{S}_q = (-1)^L \left[\frac{2\,x_q \sin(\phi_q+\gamma-\delta_q)}{1+x_q^2}\right], \tag{8.46}$$

where $\bar{C}_q \equiv C(B_q\to\bar{D}_q u_q)$ and $\bar{S}_q \equiv S(B_q\to\bar{D}_q u_q)$. Note that $\bar{\xi}_q$ and ξ_q satisfy the relation

$$\bar{\xi}_q \times \xi_q = e^{-i2(\phi_q+\gamma)}, \tag{8.47}$$

where the hadronic parameter $x_q e^{i\delta_q}$ *cancels*. Consequently, we may extract $\phi_q+\gamma$ in a *theoretically clean* way from the corresponding observables.

8.4.3 Conventional Extraction of $\phi_q+\gamma$

It is convenient to introduce the following combinations of observables:

$$\langle C_q\rangle_+ \equiv \frac{\bar{C}_q + C_q}{2} = 0 \tag{8.48}$$

$$\langle C_q\rangle_- \equiv \frac{\bar{C}_q - C_q}{2} = \frac{1-x_q^2}{1+x_q^2} \tag{8.49}$$

$$\langle S_q\rangle_+ \equiv \frac{\bar{S}_q + S_q}{2} = +(-1)^L\left[\frac{2\,x_q\cos\delta_q}{1+x_q^2}\right]\sin(\phi_q+\gamma) \tag{8.50}$$

$$\langle S_q\rangle_- \equiv \frac{\bar{S}_q - S_q}{2} = -(-1)^L\left[\frac{2\,x_q\sin\delta_q}{1+x_q^2}\right]\cos(\phi_q+\gamma). \tag{8.51}$$

We observe that (8.49) allows us – in principle – to determine x_q from $\langle C_q\rangle_-$. However, to this end, terms entering at the x_q^2 level have to be resolved experimentally. In the case of $q=s$, we have $x_s = \mathcal{O}(R_b)$, implying $x_s^2 = \mathcal{O}(0.16)$, so that this may actually be possible, although challenging [168]. On the other hand, $x_d = \mathcal{O}(-\lambda^2 R_b)$ is doubly Cabibbo-suppressed. Although it should be possible to resolve terms of $\mathcal{O}(x_d)$, this will be impossible for the vanishingly small $x_d^2 = \mathcal{O}(0.0004)$ terms, so that alternative approaches to fix x_d are required [169].

In contrast to the observables associated with the $\cos(\Delta M_q t)$ terms, the mixing-induced observables entering the rate asymmetries with $\sin(\Delta M_q t)$ provide information on $\phi_q+\gamma$. Let us now assume that x_q is known. We may then consider

$$s_+ \equiv (-1)^L\left[\frac{1+x_q^2}{2x_q}\right]\langle S_q\rangle_+ = +\cos\delta_q\sin(\phi_q+\gamma) \tag{8.52}$$

$$s_- \equiv (-1)^L\left[\frac{1+x_q^2}{2x_q}\right]\langle S_q\rangle_- = -\sin\delta_q\cos(\phi_q+\gamma), \tag{8.53}$$

yielding

$$\sin^2(\phi_q+\gamma)=\frac{1}{2}\left[(1+s_+^2-s_-^2)\pm\sqrt{(1+s_+^2-s_-^2)^2-4s_+^2}\right]. \tag{8.54}$$

This expression implies an eightfold solution for $\phi_q+\gamma$. If we fix the sign of $\cos\delta_q$ with the help of factorization, a fourfold discrete ambiguity emerges. Since we may determine ϕ_d and ϕ_s through analyses of $B_d\to J/\psi K_{\rm S}$ and $B_s\to J/\psi\phi$ decays, respectively, we may extract γ from $\phi_q+\gamma$.

8.4.4 New Strategies and Recent Developments

Let us now discuss new strategies to explore the $B_q\to D_q\bar{u}_q$ modes [170]. If the width difference $\Delta\Gamma_s$ is sizeable, the time-dependent untagged rates (see (8.11))

$$\langle\Gamma(B_q(t)\to D_q\bar{u}_q)\rangle=\langle\Gamma(B_q\to D_q\bar{u}_q)\rangle\left[\cosh(\Delta\Gamma_q t/2)-\mathcal{A}_{\Delta\Gamma}(B_q\to D_q\overline{u}_q)\,\sinh(\Delta\Gamma_q t/2)\right]e^{-\Gamma_q t} \tag{8.55}$$

and their CP conjugates provide $\mathcal{A}_{\Delta\Gamma}(B_s\to D_s\bar{u}_s)\equiv\mathcal{A}_{\Delta\Gamma_{\rm s}}$ and $\mathcal{A}_{\Delta\Gamma}(B_s\to\bar{D}_s u_s)\equiv\bar{\mathcal{A}}_{\Delta\Gamma_{\rm s}}$. It can be shown that these "untagged" observables can be combined with their "tagged" counterparts $\langle S_s\rangle_\pm$ in the form of the following simple relation:

$$\tan(\phi_s+\gamma)=-\left[\frac{\langle S_s\rangle_+}{\langle\mathcal{A}_{\Delta\Gamma_{\rm s}}\rangle_+}\right]=+\left[\frac{\langle\mathcal{A}_{\Delta\Gamma_{\rm s}}\rangle_-}{\langle S_s\rangle_-}\right], \tag{8.56}$$

where $\langle\mathcal{A}_{\Delta\Gamma_{\rm s}}\rangle_+$ and $\langle\mathcal{A}_{\Delta\Gamma_{\rm s}}\rangle_-$ are defined in analogy to (8.50) and (8.51), respectively. Obviously, (8.56) offers an elegant extraction of $\phi_s+\gamma$, up to a twofold ambiguity. If we fix again the sign of $\cos\delta_q$ through factorization, we may determine $\phi_s+\gamma$ in an *unambiguous* manner, which should be compared with the fourfold ambiguity arising in this case from (8.54). In particular, we may decide whether $\gamma\in[0^\circ,180^\circ]$, as in the SM, or $\gamma\in[180^\circ,360^\circ]$. Another important advantage of (8.56) is that we do *not* have to rely on the resolution of $\mathcal{O}(x_s^2)$ terms, as $\langle S_s\rangle_\pm$ and $\langle\mathcal{A}_{\Delta\Gamma_{\rm s}}\rangle_\pm$ are both proportional to x_s. On the other hand, we need a sizeable value of $\Delta\Gamma_s$. Measurements of untagged rates are also very useful in the case of a vanishingly small $\Delta\Gamma_q$, since the "unevolved" (i.e. time-independent) untagged rates in (8.55) offer various interesting strategies to determine x_q from the ratio of $\langle\Gamma(B_q\to D_q\bar{u}_q)\rangle+\langle\Gamma(B_q\to\bar{D}_q u_q)\rangle$ to CP-averaged rates of appropriate $B^\pm$ or flavour-specific B_q decays.

If we keep the hadronic parameter x_q and the associated strong phase δ_q as "unknown", free parameters in the expressions for the $\langle S_q\rangle_\pm$, we may derive the relations

$$|\sin(\phi_q+\gamma)|\geq|\langle S_q\rangle_+|,\quad|\cos(\phi_q+\gamma)|\geq|\langle S_q\rangle_-|, \tag{8.57}$$

which can straightforwardly be converted into bounds on $\phi_q+\gamma$. If x_q is known, stronger constraints are implied by

$$|\sin(\phi_q+\gamma)|\geq|s_+|,\quad|\cos(\phi_q+\gamma)|\geq|s_-|. \tag{8.58}$$

Once s_+ and s_- are known, we may of course determine $\phi_q+\gamma$ through the "conventional" approach, using (8.54). However, the bounds following from (8.58) provide essentially the same information and are much simpler to implement. Moreover, as discussed in detail in [170] for several examples, the bounds following from the B_s and B_d modes may be highly complementary, thereby providing particularly narrow, theoretically clean ranges for γ. Whereas the B_s decays are not yet accessible, first results for the $B_d\to D^{(*)\pm}\pi^\mp$ modes obtained by BaBar give $|\sin(\phi_d+\gamma)|>0.87$ (0.58) at the 68% (95%) C.L. [171]. Looking at (8.50), we observe that we may extract the sign of $\sin(\phi_q+\gamma)$ from $\langle S_q\rangle_+$ if we assume that the sign of $\cos\delta_q$ is as in factorization. To this end, the factor $(-1)^L$ has to be properly taken into account. The information on the sign of $\sin(\phi_d+\gamma)$ is very useful, as it allows us to distinguish directly between the two solutions for (ϕ_d,γ) discussed in Subsection 8.3.3. If we apply (8.24), the analysis of CP violation in $B_d\to\pi^+\pi^-$ gives $(\phi_d,\gamma)\sim(47^\circ,65^\circ)$ or $(133^\circ,115^\circ)$ [47, 105], corresponding to $\sin(\phi_q+\gamma)\sim+0.9$ or -0.9, respectively. The BaBar analysis favours the former case [170], i.e. the

picture of the SM, in accordance with the discussion after (8.24). The exploration of $B_d \to D^{(*)\pm}\pi^{\mp}$ modes is also in progress at Belle [172]. Unfortunately, the current Belle results for (fully reconstructed) $B_d \to D^{(*)\pm}\pi^{\mp}$ decays favour the sign opposite to the one obtained by BaBar (see also [86]), so that the experimental picture is not yet conclusive.

Let us now further exploit the complementarity between the $B_s^0 \to D_s^{(*)+}K^-$ and $B_d^0 \to D^{(*)+}\pi^-$ modes. If we look at their decay topologies, we observe that these channels are related to each other through an interchange of all down and strange quarks. Consequently, the U-spin flavour symmetry of strong interactions implies $a_s = a_d$ and $\delta_s = \delta_d$. There are various possibilities to implement these relations. A particularly simple picture emerges if we assume that $a_s = a_d$ *and* $\delta_s = \delta_d$, which yields

$$\tan\gamma = -\left[\frac{\sin\phi_d - S\sin\phi_s}{\cos\phi_d - S\cos\phi_s}\right] \stackrel{\phi_s=0^\circ}{=} -\left[\frac{\sin\phi_d}{\cos\phi_d - S}\right]. \tag{8.59}$$

Here we have introduced

$$S \equiv -R\left[\frac{\langle S_d\rangle_+}{\langle S_s\rangle_+}\right] \tag{8.60}$$

with

$$R \equiv \left(\frac{1-\lambda^2}{\lambda^2}\right)\left[\frac{1}{1+x_s^2}\right], \tag{8.61}$$

which can be fixed from untagged B_s rates through

$$R = \left(\frac{f_K}{f_\pi}\right)^2\left[\frac{\Gamma(\bar{B}_s^0 \to D_s^{(*)+}\pi^-) + \Gamma(B_s^0 \to D_s^{(*)-}\pi^+)}{\langle\Gamma(B_s \to D_s^{(*)+}K^-)\rangle + \langle\Gamma(B_s \to D_s^{(*)-}K^+)\rangle}\right]. \tag{8.62}$$

Alternatively, we may *only* assume that $\delta_s = \delta_d$ *or* that $a_s = a_d$. Apart from features related to multiple discrete ambiguities, the most important advantage with respect to the "conventional" approach is that the experimental resolution of the x_q^2 terms is not required. In particular, x_d does *not* have to be fixed, and x_s may only enter through a $1 + x_s^2$ correction, which can straightforwardly be determined through untagged B_s rate measurements. In the most refined implementation of this strategy, the measurement of x_d/x_s would *only* be interesting for the inclusion of U-spin-breaking effects in a_d/a_s.

9 RARE DECAYS

9.1 General Features and Impact of New Physics in Models with Minimal Flavour Violation

In order to complement the exploration of flavour physics through the CP-violating phenomena discussed above, also various rare decays of B and K mesons offer very interesting strategies. As we have already noted, by "rare" decays we mean transitions that do *not* arise at the tree level in the SM, but may originate through loop effects. Consequently, rare B decays are mediated by FCNC processes of the kind $\bar{b} \to \bar{s}$ or $\bar{b} \to \bar{d}$, whereas rare K decays originate from their $\bar{s} \to \bar{d}$ counterparts. Prominent examples of rare B decays are the following exclusive decay modes:

- $B \to K^*\gamma$, $B \to \rho\gamma$, ...
- $B \to K\mu^+\mu^-$, $B \to \pi\mu^+\mu^-$, ...
- $B_{s,d} \to \mu^+\mu^-$.

While the $B_{s,d} \to \mu^+\mu^-$ transitions are very clean, the former two decay classes suffer from theoretical uncertainties that are related to hadronic form factors and long-distance contributions. On the other hand, the hadronic uncertainties are much smaller in the corresponding inclusive decays, $B \to X_{s,d}\gamma$ and $B \to X_{s,d}\mu^+\mu^-$, which are therefore more promising from the theoretical point of view, but are unfortunately more difficult to measure; the cleanest rare B decays are given by $B \to X_{s,d}\nu\bar{\nu}$ processes. Let us note that a tremendous amount of work went into the calculation of the branching ratio of the prominent $B \to X_s\gamma$ channel (for an overview, see [173]); the agreement of the experimental value with the SM expectation implies important constraints for the allowed parameter space of popular NP scenarios. The phenomenology of the kaon system includes also interesting rare decays:

- $K_{\rm L} \to \mu^+\mu^-$
- $K_{\rm L} \to \pi^0 e^+ e^-$
- $K_{\rm L} \to \pi^0\nu\bar{\nu}$, $K^+ \to \pi^+\nu\bar{\nu}$,

where the "golden" modes are given by the $K \to \pi\nu\bar{\nu}$ processes, which are essentially theoretically clean, as we have already noted in Subsection 3.2.

In order to deal with rare decays theoretically, appropriate low-energy effective Hamiltonians are used, in analogy to the analysis of non-leptonic B decays. The structure of the corresponding transition amplitudes is similar to the one of (4.26), i.e. the short-distance physics is described by perturbatively calculable Wilson coefficient functions, whereas the long-distance dynamics is encoded in non-perturbative hadronic matrix elements of local operators. It is useful to follow [174, 175], and to rewrite the rare-decay implementation of (4.26) as

$$A(\text{decay}) = P_0(\text{decay}) + \sum_r P_r(\text{decay}) F_r(v). \tag{9.1}$$

For the derivation of this expression, we choose $\mu = \mu_0 = \mathcal{O}(M_W)$, and rewrite the corresponding Wilson coefficients $C_k(\mu_0)$ as linear combinations of "master functions" $F_r(v)$, which follow from the evaluation of penguin and box diagrams with heavy particle exchanges. Expression (9.1) does not only apply to the SM, but also to NP scenarios with MFV (see Subsection 6.4.4), where the parameters involved are collectively denoted by v. In the SM, the functions $F_r(v)$ reduce to the well-known Inami–Lim functions [81], with $v = x_t = m_t^2/M_W^2$. The term P_0 summarizes the contributions that originate from light internal quarks, such as the charm and up quarks, and the sum takes the remaining contributions into account. For a detailed discussion of this formalism and the general features of the P_0, P_r and F_r, we refer the reader to [122]. Let us here just emphasize the following important points:

- The $F_r(v)$ are *process-independent, universal* functions that depend on the particular model considered. NP enters the decay amplitudes only through these functions.
- The P_0 and P_r are *process-dependent* quantities. In particular, they depend on the hadronic matrix elements of the operators Q_k.

In models with MFV, the set of the $F_r(v)$ consists of seven functions

$$S(v),\ X(v),\ Y(v),\ Z(v),\ E(v),\ D'(v),\ E'(v), \tag{9.2}$$

which are discussed in detail in [122]. In (6.44), we encountered already one of them, the function $S(v)$, which governs B_q^0–$\bar{B}_q^0$ and K^0–$\bar{K}^0$ mixing; below, we will come across $X(v)$ and $Y(v)$, which characterize rare K, B decays with $\nu\bar{\nu}$ and $\ell^+\ell^-$ in the final states, respectively. The important property of the functions in (9.2) is that they do not – within the framework of MFV – contain complex phases, so that the CP-violating effects are governed *entirely* by the KM phase hiding in the parameters P_r.

For detailed discussions of the many interesting aspects of rare B and K decays and recent developments, we refer the reader to [21, 22, 173, 176]. Let us here choose $B_{s,d} \to \mu^+\mu^-$ and $K \to \pi\nu\bar{\nu}$ processes as representative examples, which are particularly clean from the theoretical point of view; the former channels are also an important element of the B-physics programme of the LHC [19]. Finally, we shall illustrate the impact of NP that does *not* belong to the class of MFV models on rare decays. To this end, we consider a NP scenario that is suggested by the "$B \to \pi K$ puzzle" discussed in Subsection 7.2.3.

9.2 $B_{s,d} \to \mu^+\mu^-$

As can be seen in Fig. 26, within the framework of the SM, the decays $B_{s,d} \to \mu^+\mu^-$ originate from Z^0 penguins and box diagrams. These transitions belong to the cleanest modes in the category of rare B decays, since they involve only the hadronic matrix element of a quark current between a B_q-meson and the vacuum state, i.e. the decay constant f_{B_q} that we introduced in (4.5), NLO QCD corrections were

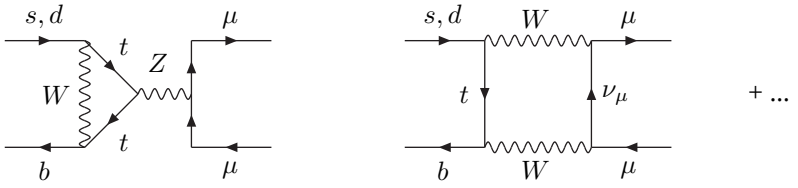

Fig. 26: Decay processes contributing to $B_{s,d} \to \mu^+\mu^-$ in the SM.

calculated, and long-distance contributions are expected to play a negligible rôle [177]. The low-energy effective Hamiltonian describing $B_q \to \mu^+\mu^-$ decays is given as follows ($q \in \{s, d\}$):

$$\mathcal{H}_{\text{eff}} = -\frac{G_{\text{F}}}{\sqrt{2}}\left[\frac{\alpha}{2\pi \sin^2\Theta_{\text{W}}}\right] V_{tb}^* V_{tq} \eta_Y Y_0(x_t) (\bar{b}q)_{\text{V}-\text{A}} (\bar{\mu}\mu)_{\text{V}-\text{A}} \,+\, \text{h.c.}, \tag{9.3}$$

where α denotes the QED coupling and Θ_{W} is the Weinberg angle. Here the short-distance physics is described by

$$Y(x_t) = \eta_Y Y_0(x_t), \tag{9.4}$$

where $\eta_Y = 1.012$ is a perturbative QCD correction factor [177, 178, 179], and $Y_0(x_t)$, which is another Inami–Lim function [81], describes the top-quark mass dependence of the Feynman diagrams shown in Fig. 26. In the SM, we may write $Y_0(x_t)$ – to a very good approximation – as follows [122]:

$$Y_0(x_t) = 0.98 \times \left[\frac{m_t}{167\,\text{GeV}}\right]^{1.56}. \tag{9.5}$$

We observe that the matrix element of (9.3) between a $\langle\mu^-\mu^+|$ final state and a $|B_q\rangle$ initial state indeed involves the decay constant f_{B_q}. The corresponding SM branching ratios then take the following form [37]:

$$\text{BR}(B_s \to \mu^+\mu^-) = 4.1 \times 10^{-9} \left[\frac{f_{B_s}}{0.24\,\text{GeV}}\right]^2 \left[\frac{|V_{ts}|}{0.040}\right]^2 \left[\frac{\tau_{B_s}}{1.5\,\text{ps}}\right] \left[\frac{m_t}{167\,\text{GeV}}\right]^{3.12} \tag{9.6}$$

$$\text{BR}(B_d \to \mu^+\mu^-) = 1.1 \times 10^{-10} \left[\frac{f_{B_d}}{0.20\,\text{GeV}}\right]^2 \left[\frac{|V_{td}|}{0.008}\right]^2 \left[\frac{\tau_{B_d}}{1.5\,\text{ps}}\right] \left[\frac{m_t}{167\,\text{GeV}}\right]^{3.12}, \tag{9.7}$$

which should be compared with the experimental 90% C.L. bounds

$$\text{BR}(B_s \to \mu^+\mu^-) < 5.8 \times 10^{-7}, \quad \text{BR}(B_d \to \mu^+\mu^-) < 1.5\,(1.6) \times 10^{-7} \tag{9.8}$$

obtained by the CDF (Belle) collaboration [180]. Looking at (9.6) and (9.7), we see that a measurement of these branching ratios would allow clean determinations of $|V_{ts}|$ and $|V_{td}|$, respectively, provided the non-perturbative decay constants f_{B_s} and f_{B_d} were known reliably. The current status following from lattice QCD studies is given as follows [41]:

$$f_{B_d} = (203 \pm 27^{+0}_{-20})\,\text{MeV}, \quad f_{B_s} = (238 \pm 31)\,\text{MeV}; \tag{9.9}$$

similar results were obtained with the help of QCD sum rules [150]. If we consider the ratio

$$\frac{\text{BR}(B_d \to \mu^+\mu^-)}{\text{BR}(B_s \to \mu^+\mu^-)} = \left[\frac{\tau_{B_d}}{\tau_{B_s}}\right] \left[\frac{M_{B_d}}{M_{B_s}}\right] \left[\frac{f_{B_d}}{f_{B_s}}\right]^2 \left|\frac{V_{td}}{V_{ts}}\right|^2, \tag{9.10}$$

these parameters enter only in the form of the following $SU(3)$-breaking ratio (see also (8.9)):

$$\frac{f_{B_s}}{f_{B_d}} = 1.18 \pm 0.04^{+0.12}_{-0}. \tag{9.11}$$

Using now (8.6), the relation in (9.10) allows a determination of the side R_t of the UT. On the other hand, we may also write (see (8.4))

$$\frac{\Delta M_d}{\Delta M_s} = \left[\frac{M_{B_d}}{M_{B_s}}\right] \left[\frac{\hat{B}_{B_d}}{\hat{B}_{B_s}}\right] \left[\frac{f_{B_d}}{f_{B_s}}\right]^2 \left|\frac{V_{td}}{V_{ts}}\right|^2, \tag{9.12}$$

allowing us to fix R_t with the help of (8.7). Consequently, (9.10) and (9.12) provide complementary determinations of the UT side R_t. Moreover, these expressions imply also the following relation:

$$\frac{\mathrm{BR}(B_s \to \mu^+\mu^-)}{\mathrm{BR}(B_d \to \mu^+\mu^-)} = \left[\frac{\tau_{B_s}}{\tau_{B_d}}\right] \left[\frac{\hat{B}_{B_d}}{\hat{B}_{B_s}}\right] \left[\frac{\Delta M_s}{\Delta M_d}\right], \tag{9.13}$$

which suffers from theoretical uncertainties that are smaller than those affecting (9.10) and (9.12), since the dependence on $(f_{B_d}/f_{B_s})^2$ cancels, and $\hat{B}_{B_d}/\hat{B}_{B_s} = 1$ up to tiny $SU(3)$-breaking corrections [181]. In particular, QCD lattice simulations give the following numbers [41]:

$$\hat{B}_{B_d} = 1.34 \pm 0.12, \quad \hat{B}_{B_s} = 1.34 \pm 0.12, \quad \frac{\hat{B}_{B_s}}{\hat{B}_{B_d}} = 1.00 \pm 0.03. \tag{9.14}$$

Moreover, we may also use the (future) experimental data for $\Delta M_{(s)d}$ to reduce the hadronic uncertainties in the SM predictions for the $B_q \to \mu^+\mu^-$ branching ratios [181], yielding

$$\mathrm{BR}(B_s \to \mu^+\mu^-)\big|_{\mathrm{SM}} = (3.42 \pm 0.53) \times \left[\frac{\Delta M_s}{18.0\,\mathrm{ps}^{-1}}\right] \times 10^{-9} \tag{9.15}$$

$$\mathrm{BR}(B_d \to \mu^+\mu^-)\big|_{\mathrm{SM}} = (1.00 \pm 0.14) \times 10^{-10}. \tag{9.16}$$

Since these branching ratios are very small, we could only hope to observe the $B_q \to \mu^+\mu^-$ decays at the LHC, should they actually be governed by their SM contributions [19]. However, as these transitions are mediated by rare FCNC processes, they are sensitive probes for NP. In particular, as was recently reviewed in [182], the $B_q \to \mu^+\mu^-$ branching ratios may be dramatically enhanced in specific NP (SUSY) scenarios. Should this actually be the case, these decays may be seen at run II of the Tevatron, and the e^+e^- B factories could observe $B_d \to \mu^+\mu^-$. In the case of models with MFV, we just have to make the replacement

$$Y(x_t) \to Y(v) \tag{9.17}$$

in order to take the NP contributions to the $B_q \to \mu^+\mu^-$ decays into account. In particular, the *same* $Y(v)$ enters the $B_s \to \mu^+\mu^-$ and $B_d \to \mu^+\mu^-$ channels (see (9.2)). In analogy, the *same* generalized function $S(v)$ governs the mass differences ΔM_s and ΔM_d, as we have seen in Subsection 6.4.4. Consequently, within MFV scenarios, the NP effects cancel in (9.10), (9.12) and (9.13), where in particular the latter relation offers an interesting test of this picture.

9.3 $K \to \pi\nu\bar{\nu}$

As we discussed in Subsection 3.2, $K \to \pi\nu\bar{\nu}$ decays originate from Z^0 penguins and box diagrams. Let us first have a closer look at the charged mode $K^+ \to \pi^+\nu\bar{\nu}$. The low-energy effective Hamiltonian describing this decay is given as follows [37]:

$$\mathcal{H}_{\mathrm{eff}} = \frac{G_{\mathrm{F}}}{\sqrt{2}} \left[\frac{\alpha}{2\pi \sin^2\Theta_{\mathrm{W}}}\right] \sum_{\ell=e,\mu,\tau} \left[\lambda_c X^{\ell}_{\mathrm{NL}} + \lambda_t X(x_t)\right] (\bar{s}d)_{\mathrm{V-A}} (\bar{\nu}_\ell \nu_\ell)_{\mathrm{V-A}}, \tag{9.18}$$

where

$$\lambda_c \equiv V^*_{cs} V_{cd} = -\lambda \left(1 - \frac{\lambda^2}{2}\right) \tag{9.19}$$

and $\lambda_t \equiv V_{ts}^* V_{td}$ with

$$\mathrm{Im}\,\lambda_t = \eta A^2\lambda^5, \quad \mathrm{Re}\,\lambda_t = -\left(1-\frac{\lambda^2}{2}\right)A^2\lambda^5(1-\bar{\rho}) \tag{9.20}$$

are CKM factors, and

$$X(x_t) = \eta_X X_0(x_t) \tag{9.21}$$

describes the top-quark mass dependence originating from the Z^0 penguin and box diagrams, where $X_0(x_t)$ is another Inam–Lim function [81], and $\eta_X = 0.994$ is a perturbative NLO QCD correction factor [177, 178, 179, 183]. Within the SM, we may write $X_0(x_t)$ – to a very good approximation – as follows [122]:

$$X_0(x_t) = 1.53 \times \left[\frac{m_t}{167\,\mathrm{GeV}}\right]^{1.15}. \tag{9.22}$$

The counterpart of $X(x_t)$ in the charm sector is given by X_{NL}^{ℓ}. For the analysis of $K^+ \to \pi^+\nu\bar{\nu}$, the following combination is relevant:[13]

$$P_c(\nu\bar{\nu}) = \frac{1}{\lambda^4}\left[\frac{2}{3}X_{\mathrm{NL}}^{e} + \frac{1}{3}X_{\mathrm{NL}}^{\tau}\right] = 0.39 \pm 0.06. \tag{9.23}$$

If we calculate the matrix element of (9.18) between the $\langle\bar{\nu}\nu\pi^+|$ final state and the $|K^+\rangle$ initial state, we encounter a hadronic matrix element of the $(\bar{s}d)_{\mathrm{V-A}}$ current that can be extracted – with the help of the isospin flavour symmetry of strong interactions – from the semileptonic decay $K^+ \to \pi^0 e^+\nu$, which is a tree decay that is described by the following Hamiltonian [37]:

$$\mathcal{H}_{\mathrm{eff}}(K^+ \to \pi^0 e^+\nu) = \frac{G_{\mathrm{F}}}{\sqrt{2}}V_{us}^*(\bar{s}u)_{\mathrm{V-A}}(\bar{\nu}_e e)_{\mathrm{V-A}}. \tag{9.24}$$

Using the isospin relation

$$\langle\pi^+|(\bar{s}d)_{\mathrm{V-A}}|K^+\rangle = \sqrt{2}\langle\pi^0|(\bar{s}u)_{\mathrm{V-A}}|K^+\rangle, \tag{9.25}$$

and neglecting the phase-space differences due to $M_{\pi^+} \neq M_{\pi^0}$ and $M_e \neq 0$, we obtain

$$\frac{\mathrm{BR}(K^+ \to \pi^+\nu\bar{\nu})}{\mathrm{BR}(K^+ \to \pi^0 e^+\nu)} = \frac{\alpha^2}{|V_{us}|^2 2\pi^2\sin^4\Theta_{\mathrm{W}}}\sum_{\ell=e,\mu,\tau}|\lambda_c X_{\mathrm{NL}}^{\ell} + \lambda_t X(x_t)|^2. \tag{9.26}$$

Consequently, we may determine the hadronic matrix element relevant to the rare decay $K^+ \to \pi^+\nu\bar{\nu}$ through the experimental data for the (non-rare) decay $K^+ \to \pi^0 e^+\nu$. Because of this important feature, $K^+ \to \pi^+\nu\bar{\nu}$ is a very *clean* decay.

It is useful to write the $K^+ \to \pi^+\nu\bar{\nu}$ branching ratio as

$$B_1 \equiv \frac{1}{\kappa_+}\mathrm{BR}(K^+ \to \pi^+\nu\bar{\nu}), \tag{9.27}$$

with

$$\kappa_+ = r_{K^+}\left[\frac{3\alpha^2\mathrm{BR}(K^+ \to \pi^0 e^+\nu)}{2\pi^2\sin^4\Theta_{\mathrm{W}}}\right]\lambda^8 = 4.78 \times 10^{-11}, \tag{9.28}$$

where $r_{K^+} = 0.901$ describes the isospin-breaking corrections that arise in relating $K^+ \to \pi^+\nu\bar{\nu}$ to $K^+ \to \pi^0 e^+\nu$. Let us now consider the general MFV case, where

$$X(x_t) \to X(v). \tag{9.29}$$

[13] The small numerical difference of $P_c(\nu\bar{\nu})$ with respect to the value given in [37], where $\lambda = 0.2205$ was used, is related to the very recent value of $\lambda = 0.2240$ [41]. A similar comment applies to the quantities κ_+ and κ_{L}, to be introduced below.

The "reduced" $K^+ \to \pi^+\nu\bar{\nu}$ branching ratio B_1 can then be expressed as follows [126]:

$$B_1 = \left[\frac{\mathrm{Im}\lambda_t}{\lambda^5}|X(v)|\right]^2 + \left[\frac{\mathrm{Re}\lambda_c}{\lambda}\mathrm{sgn}(X(v))P_c(\nu\bar{\nu}) + \frac{\mathrm{Re}\lambda_t}{\lambda^5}|X(v)|\right]^2; \tag{9.30}$$

the corresponding SM prediction following from the very recent update in [48] was given in (3.6). It is now an easy exercise to show that the measured $K^+ \to \pi^+\nu\bar{\nu}$ branching ratio determines an ellipse in the $\bar{\rho}$–$\bar{\eta}$ plane,

$$\left(\frac{\bar{\rho}-\rho_0}{\bar{\rho}_1}\right)^2 + \left(\frac{\bar{\eta}}{\bar{\eta}_1}\right)^2 = 1, \tag{9.31}$$

centred at $(\rho_0, 0)$ with

$$\rho_0 = 1 + \mathrm{sgn}(X(v))\frac{P_c(\nu\bar{\nu})}{A^2|X(v)|}, \tag{9.32}$$

and having the squared axes

$$\bar{\rho}_1^2 = r_0^2, \quad \bar{\eta}_1^2 = \left(\frac{r_0}{\sigma}\right)^2, \tag{9.33}$$

with

$$r_0^2 = \frac{\sigma B_1}{A^4|X(v)|^2}, \quad \sigma = \frac{1}{(1-\lambda^2/2)^2}. \tag{9.34}$$

Concerning $K_\mathrm{L} \to \pi^0\nu\bar{\nu}$, we may introduce – in analogy to (9.27) – the reduced branching ratio

$$B_2 \equiv \frac{1}{\kappa_\mathrm{L}}\mathrm{BR}(K_\mathrm{L} \to \pi^0\nu\bar{\nu}), \tag{9.35}$$

which is characterized by

$$\kappa_\mathrm{L} = \left[\frac{r_{K_\mathrm{L}}}{r_{K^+}}\frac{\tau_{K_\mathrm{L}}}{\tau_{K^+}}\right]\kappa_+ = 2.09 \times 10^{-10}, \tag{9.36}$$

where $r_{K_\mathrm{L}} = 0.944$ describes the isospin-breaking corrections that arise in relating $K_\mathrm{L} \to \pi^0\nu\bar{\nu}$ to $K^+ \to \pi^0 e^+\nu$. As discussed in detail in [37], the decay $K_\mathrm{L} \to \pi^0\nu\bar{\nu}$ is dominated in the SM by direct CP violation, and is completely governed by the short-distance loop diagrams with internal top-quark exchanges. Since the charm contribution can be fully neglected, the decay $K_\mathrm{L} \to \pi^0\nu\bar{\nu}$ is *even cleaner* than $K^+ \to \pi^+\nu\bar{\nu}$. In models with MFV, the reduced $K_\mathrm{L} \to \pi^0\nu\bar{\nu}$ branching ratio is given as follows:

$$B_2 = \left[\frac{\mathrm{Im}\lambda_t}{\lambda^5}|X(v)|\right]^2; \tag{9.37}$$

the SM corresponds to (3.6). If we now follow [45], but admit both signs of $X(v)$ and $S(v)$, we obtain

$$\bar{\rho} = 1 + \left[\frac{\pm\sqrt{\sigma(B_1 - B_2)} + \mathrm{sgn}(X(v))P_c(\nu\bar{\nu})}{A^2|X(v)|}\right], \quad \bar{\eta} = \mathrm{sgn}(S(v))\frac{\sqrt{B_2}}{\sqrt{\sigma}A^2|X(v)|}. \tag{9.38}$$

The dependence on $|X(v)|$ cancels in the following quantity [126]:

$$r_s \equiv \frac{1-\overline{\rho}}{\overline{\eta}} = \mathrm{ctg}\beta = \mathrm{sgn}(S(v))\sqrt{\sigma}\left[\frac{\mp\sqrt{\sigma(B_1 - B_2)} - \mathrm{sgn}(X(v))P_c(\nu\bar{\nu})}{\sqrt{B_2}}\right], \tag{9.39}$$

which allows the determination of $(\sin 2\beta)_{\pi\nu\bar{\nu}}$ in (3.5) through

$$\sin 2\beta = \frac{2r_s}{1+r_s^2}. \tag{9.40}$$

Note that (9.39) reduces to

$$r_s = \sqrt{\sigma}\left[\frac{\sqrt{\sigma(B_1 - B_2)} - P_c(\nu\bar{\nu})}{\sqrt{B_2}}\right] \tag{9.41}$$

in the case of positive values of $S(v)$ and $X(v)$ [45]. Because of the relation in (6.46), it is actually more appropriate to consider the CP-violating observable $a_{\psi K_S}$ instead of $\sin 2\beta$. Consequently, we obtain a very interesting link between the mixing-induced CP violation in the "golden" mode $B_d \to J/\psi K_S$ and the branching ratios of the rare $K \to \pi\nu\bar{\nu}$ decays.

Since $a_{\psi K_S}$ has already been measured with impressive accuracy and BR$(K^+ \to \pi^+\nu\bar{\nu})$ will be known rather accurately prior to the measurement of BR$(K_L \to \pi^0\nu\bar{\nu})$, it is of particular interest to calculate BR$(K_L \to \pi^0\nu\bar{\nu})$ as a function of BR$(K^+ \to \pi^+\nu\bar{\nu})$ for a given value of $a_{\psi K_S}$ [126]. To this end, it is useful to introduce the quantity

$$f(\beta) \equiv \mathrm{sgn}(S(v))\,\mathrm{ctg}\beta = \frac{1-\bar{\rho}}{|\bar{\eta}|}, \tag{9.42}$$

which can be determined *unambiguously* through

$$f(\beta) = \frac{1+\sqrt{1-a_{\psi K_S}^2}}{a_{\psi K_S}} = 2.279^{+0.235}_{-0.215}; \tag{9.43}$$

the numerical value corresponds to $a_{\psi K_S} = 0.736 \pm 0.049$. We then obtain the following expression:

$$B_1 = B_2 + \left[\frac{f(\beta)\sqrt{B_2} + \mathrm{sgn}(X(v))\sqrt{\sigma}P_c(\nu\bar{\nu})}{\sigma}\right]^2. \tag{9.44}$$

In comparison with (9.39), the advantage of (9.44) is the absence of the sign ambiguities due to $\mathrm{sgn}(S(v))$ and the $\mp$ in front of $\sqrt{\sigma(B_1-B_2)}$. Consequently, for given values of $a_{\psi K_S}$ and BR$(K^+ \to \pi^+\nu\bar{\nu})$, only two values of BR$(K_L \to \pi^0\nu\bar{\nu})$ are allowed for the full class of MFV models, independently of any new parameter present in these models. These two values of the $K_L \to \pi^0\nu\bar{\nu}$ branching ratio correspond to the two possible signs of $X(v)$. The measurement of BR$(K_L \to \pi^0\nu\bar{\nu})$ will therefore either select one of these two possible values or will rule out all MFV models.

9.4 New Physics Beyond Minimal Flavour Violation: An Example

As we have seen in Subsection 7.2.3, the pattern of the current B-factory data for the $B \to \pi K$ system suggests an enhancement of the corresponding EW penguin parameter q, and the presence of a CP-violating NP phase ϕ in the EW penguin sector, as summarized in (7.26). Since we encounter here CP-violating effects that are *not* associated with the CKM matrix, the corresponding NP does *not* belong to the category of MFV models considered above. In order to explore the implications for rare B and K decays, let us follow [48, 54], and consider a specific scenario, where the NP effects enter through enhanced Z^0 penguins, which are described by a short-distance function C.

The implications of enhanced Z^0 penguins with a large new complex phase for rare and CP-violating K and B decays were already discussed in [184]–[186], where model-independent analyses and studies within particular supersymmetric scenarios were presented. Here we determine the size of the enhancement of the Z^0-penguin function C and the magnitude of its complex phase through the $B \to \pi K$ data. As was pointed out in [146], a connection between rare decays and the $B \to \pi K$ system can be established by relating the EW penguin parameter q to the Z^0-penguin function C, which can be properly done with the help of a renormalization-group analysis. In the case of a complex EW penguin parameter, with a non-vanishing weak phase ϕ, we obtain the following relation [48, 54]:

$$C \equiv |C|e^{i\theta_C} = 2.35\,\bar{q}e^{i\phi} - 0.82, \quad \bar{q} = q\left[\frac{|V_{ub}/V_{cb}|}{0.086}\right]. \tag{9.45}$$

This quantity enters the short-distance functions X and Y, which govern the rare K, B decays with $\nu\bar{\nu}$ and $\mu^+\mu^-$ in the final states, respectively, in the linear combinations

$$X \equiv |X|e^{i\theta_X} = C + B^{\nu\bar{\nu}}, \quad Y \equiv |Y|e^{i\theta_Y} = C + B^{\mu^+\mu^-}, \tag{9.46}$$

where $B^{\nu\bar{\nu}}$ and $B^{\mu^+\mu^-}$ describe the box diagrams with $\nu\bar{\nu}$ and $\mu^+\mu^-$, respectively. If we evaluate, in the spirit of [146, 184, 185], these box-diagram contributions in the SM and use (9.45), we obtain

$$|X|e^{i\theta_X} = |C|e^{i\theta_C} + 0.73 \quad \text{and} \quad |Y|e^{i\theta_Y} = |C|e^{i\theta_C} + 0.18. \tag{9.47}$$

While the analysis described here does not rely on a particular model, concrete models with enhanced CP-violating Z^0-mediated FCNC couplings, generated either at the one-loop level or even at the tree level, were discussed in the literature (see, for instance, [9, 148, 184, 185, 186]). Let us also note that models with Z'-mediated FCNCs could be put in this class, provided their contributions can effectively be absorbed in the function C (for a recent analysis, see [187]).

If we now insert the numerical values in (7.26) into (9.47), we obtain a central value for $|Y|$ that violates the upper bound $|Y| \leq 2.2$ following from the BaBar and Belle data on $B \to X_s\mu^+\mu^-$ [188], and the upper bound on $\text{BR}(K_{\rm L} \to \pi^0 e^+ e^-)$ of 2.8×10^{-10} from KTeV [189]. However, we may still encounter significant deviations from the SM. In order to illustrate this exciting feature, we consider only the subset of those values of (q, ϕ) in (7.26) that satisfy the constraint of $|Y| = 2.2$. If we then use (9.45) and (9.47), we obtain

$$\begin{array}{rclcrcl} |C| &=& 2.24 \pm 0.04, & \qquad & \theta_C &=& -(105 \pm 12)^\circ, \\ |X| &=& 2.17 \pm 0.12, & & \theta_X &=& -(87 \pm 12)^\circ, \\ |Y| &=& 2.2 \ (\text{input}), & & \theta_Y &=& -(103 \pm 12)^\circ, \end{array} \tag{9.48}$$

which should be compared with the SM values $C(x_t) = 0.79$, $X(x_t) = 1.53$ and $Y(x_t) = 0.98$, corresponding to $m_t = 167$ GeV.

Going now back to the $B_q \to \mu^+\mu^-$ decays, we find

$$\frac{\text{BR}(B_s \to \mu^+\mu^-)}{\text{BR}(B_s \to \mu^+\mu^-)_{\rm SM}} = \frac{\text{BR}(B_d \to \mu^+\mu^-)}{\text{BR}(B_d \to \mu^+\mu^-)_{\rm SM}} = \left|\frac{Y}{Y_{\rm SM}}\right|^2 \approx 5.0. \tag{9.49}$$

This significant enhancement corresponds to the branching ratios

$$\text{BR}(B_s \to \mu^+\mu^-) \approx 17 \times 10^{-9}, \quad \text{BR}(B_d \to \mu^+\mu^-) \approx 5 \times 10^{-10}, \tag{9.50}$$

which are still well below the experimental bounds summarized in (9.8).

As far as the $K \to \pi\nu\bar{\nu}$ decays are concerned, this NP analysis implies

$$\text{BR}(K^+ \to \pi^+\nu\bar{\nu}) = (7.5 \pm 2.1) \times 10^{-11}, \quad \text{BR}(K_{\rm L} \to \pi^0\nu\bar{\nu}) = (3.1 \pm 1.0) \times 10^{-10}, \tag{9.51}$$

which should be compared with the SM predictions in (3.6). We observe that the impact of NP on the $K^+ \to \pi^+\nu\bar{\nu}$ branching ratio would be small, whereas $\text{BR}(K_{\rm L} \to \pi^0\nu\bar{\nu})$ would be dramatically enhanced. If we introduce

$$\beta_X \equiv \beta - \beta_s - \theta_X \quad \text{with} \quad \beta_s \equiv -\delta\gamma = -\lambda^2\eta, \tag{9.52}$$

we see that this exciting pattern is dominantly the consequence of $\beta_X \approx 111^\circ$, as

$$\frac{\text{BR}(K_{\rm L} \to \pi^0\nu\bar{\nu})}{\text{BR}(K_{\rm L} \to \pi^0\nu\bar{\nu})_{\rm SM}} = \left|\frac{X}{X_{\rm SM}}\right|^2 \left[\frac{\sin\beta_X}{\sin(\beta - \beta_s)}\right]^2 \tag{9.53}$$

and

$$\frac{\text{BR}(K_{\rm L} \to \pi^0\nu\bar{\nu})}{\text{BR}(K^+ \to \pi^+\nu\bar{\nu})} \approx 4.4 \times (\sin\beta_X)^2 \approx 4.2 \pm 0.2. \tag{9.54}$$

It is interesting to note that $\text{BR}(K_{\rm L} \to \pi^0\nu\bar{\nu})$ is very close to its model-independent upper bound [190]:

$$\text{BR}(K_{\rm L} \to \pi^0\nu\bar{\nu}) \leq 4.4 \times \text{BR}(K^+ \to \pi^+\nu\bar{\nu}). \tag{9.55}$$

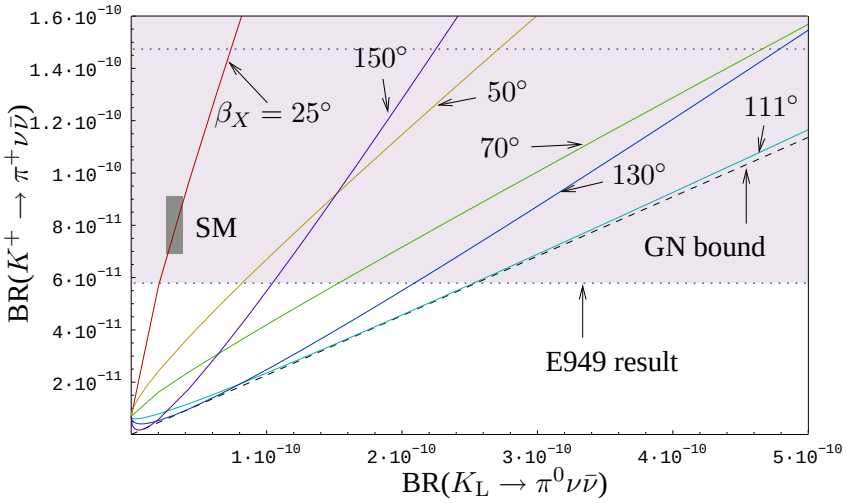

Fig. 27: BR($K^+ \to \pi^+ \nu\bar{\nu}$) as a function of BR($K_{\rm L} \to \pi^0 \nu\bar{\nu}$) for various values of β_X. The dotted horizontal lines indicate the experimental range (3.7) and the grey area the SM prediction. We also show the bound in (9.55).

A spectacular implication of these findings is a strong violation of the relation in (3.5). Indeed,

$$(\sin 2\beta)_{\pi\nu\bar{\nu}} = \sin 2\beta_X = -(0.69^{+0.23}_{-0.41}), \tag{9.56}$$

in striking disagreement with $(\sin 2\beta)_{\psi K_{\rm S}} = 0.736 \pm 0.049$. In Fig. 27, we plot – in the spirit of [126] – BR($K^+ \to \pi^+ \nu\bar{\nu}$) as a function of BR($K_{\rm L} \to \pi^0 \nu\bar{\nu}$) for fixed values of β_X. As this plot is independent of $|X|$, it offers a direct measurement of the phase β_X. The first line on the left represents the MFV models with $\beta_X = \beta - \beta_s$, whereas the first line on the right corresponds to the model-independent Grossman–Nir bound given in (9.55). The central value $\beta_X = 111^\circ$ found in [48, 54] is very close to this bound. As can be seen in Fig. 27, the measured $K \to \pi\nu\bar{\nu}$ branching ratios allow us to determine β_X up to discrete ambiguities, which can be resolved by considering other rare decays simultaneously. The corresponding plot for different values of β_X that are close to β can be found in [126].

In addition to the significant and – in the case of $K_{\rm L} \to \pi^0 \nu\bar{\nu}$ and $(\sin 2\beta)_{\pi\nu\bar{\nu}}$ – even spectacular NP effects discussed above, there are further interesting implications of this scenario [48, 54]:

- The branching ratio
$$\text{BR}(K_{\rm L} \to \pi^0 e^+ e^-) = (7.8 \pm 1.6) \times 10^{-11} \tag{9.57}$$
is significantly enhanced and governed by direct CP violation. On the other hand, the SM result $(3.2^{+1.2}_{-0.8}) \times 10^{-11}$ [191] is dominated by indirect CP violation. In a very recent analysis [192], the same NP scenario was considered as well, addressing also the decay $K_{\rm L} \to \pi^0 \mu^+ \mu^-$.
- The integrated forward–backward CP asymmetry for $B_d \to K^* \mu^+ \mu^-$ [186], which is given by
$$A_{\rm FB}^{\rm CP} = (0.03 \pm 0.01) \times \tan\theta_Y, \tag{9.58}$$
can be very large in view of $\theta_Y \approx -100^\circ$. The corresponding NP effects for the lepton polarization asymmetries of $B \to X_s \ell^+ \ell^-$ decays were recently studied in [193].
- The $B \to X_{s,d} \nu\bar{\nu}$ branching ratios are enhanced by a factor of 2 with respect to the SM.
- Enhanced Z^0 penguins may also play an important rôle in Re$(\varepsilon'/\varepsilon)$ [184]. As far as the enhancement of $|C|$ and its large negative phase suggested by the $B \to \pi K$ analysis are concerned, the consistency with (3.4) requires a significant enhancement of the hadronic matrix element of the relevant QCD penguin operator with respect to that of the relevant EW penguin operator. The corresponding large hadronic uncertainties leave sufficient room for such effects.

- It is also interesting to explore the implications for $B_d \to J/\psi K_{\rm S}$ and $B_d \to \phi K_{\rm S}$. As far as the former channel is concerned, the NP corrections to the determination of $\sin 2\beta$ from the mixing-induced $B_d \to J/\psi K_{\rm S}$ CP asymmetry are at the 0.05 level, corresponding to a shift of β by at most $\pm 2^\circ$. Such small effects are still beyond the current experimental and theoretical accuracy, but could be reinvestigated in the LHC era. Concerning the decay $B_d \to \phi K_{\rm S}$, large hadronic uncertainties preclude a precise prediction. However, if we assume that the sign of the cosine of a strong phase agrees with factorization, we find

$$\underbrace{(\sin 2\beta)_{\phi K_{\rm S}}}_{-\mathcal{A}_{\rm CP}^{\rm mix}(B_d \to \phi K_{\rm S})} \;>\; \underbrace{(\sin 2\beta)_{\psi K_{\rm S}} = 0.736 \pm 0.049}_{-\mathcal{A}_{\rm CP}^{\rm mix}(B_d \to J/\psi K_{\rm S})}, \tag{9.59}$$

  where $(\sin 2\beta)_{\phi K_{\rm S}} \sim 1$ may well be possible. This pattern is qualitatively different from the present B-factory data summarized in (6.39), which are, however, not yet conclusive. In particular, we could easily accommodate a value of $(\sin 2\beta)_{\phi K_{\rm S}}$ of the same magnitude as the central value found by Belle but of *opposite* sign. On the other hand, a future confirmation of the pattern in (9.59) would be another signal of enhanced CP-violating Z^0 penguins at work.

If future, more accurate $B \to \pi\pi, \pi K$ data will not significantly modify the currently observed patterns in these decays discussed in Subsections 6.2.2 and 7.2.3, the scenario of enhanced Z^0 penguins with a large CP-violating NP phase ϕ will remain an attractive possibility for physics beyond the SM. It will then be very interesting to confront the corresponding predictions for the rare B and K decays discussed above with experiment.

10 CONCLUSIONS

The field of flavour physics and CP violation is very rich and represents an exciting topic for theoretical and experimental research. In these lectures, we have put our focus on the B-meson system, which provides a particularly fertile testing ground for the SM picture of flavour physics, where CP violation can be accommodated by means of the KM mechanism through a single phase in the parametrization of the quark-mixing matrix. The corresponding UT represents one of the central targets of the B factories, which govern the current experimental stage of quark-flavour physics, run II of the Tevatron, and of the LHCb and BTeV experiments, which will join these efforts in the not too distant future.

In 1964, the observation of indirect CP violation, which originates from the fact that the mass eigenstates of the neutral kaon system are not eigenstates of the CP operator, came as a big surprise. After tremendous efforts, also direct CP violation could be established in neutral K decays in 1999 by the NA48 and KTeV collaborations. Unfortunately, the calculations of the corresponding observable ${\rm Re}(\varepsilon'/\varepsilon)$, which is governed by the competition between QCD and EW penguins, suffer from large theoretical uncertainties. Consequently, unless better techniques to deal with the relevant hadronic matrix elements will be available, ${\rm Re}(\varepsilon'/\varepsilon)$ does unfortunately not provide a stringent test of the SM, although the SM analyses give results of the same order of magnitude as the experimental value. From the theoretical point of view, the rare decays $K^+ \to \pi^+ \nu\bar{\nu}$ and $K_{\rm L} \to \pi^0 \nu\bar{\nu}$ are much more promising. On the other hand, these decays exhibit extremely tiny branching ratios at the 10^{-10} and 10^{-11} levels in the SM, respectively, and are extremely challenging from the experimental point of view. Nevertheless, three events for $K^+ \to \pi^+ \nu\bar{\nu}$ were already observed at BNL.

Concerning the decays of B mesons, we distinguish between leptonic, semileptonic and non-leptonic transitions. The former exhibit the simplest structure and would be interesting to measure the non-perturbative decay constants f_B, but suffer from tiny branching ratios. The semileptonic B decays are more complicated than the leptonic ones. However, applications of the HQET and heavy-quark expansions allow us to determine $|V_{cb}|$ and $|V_{ub}|$, which are important ingredients for theoretical predictions and the analysis of the UT in the $\bar{\rho}$–$\bar{\eta}$ plane. Finally, the non-leptonic decays are the most complicated transitions, as far as the impact of strong interactions is concerned. In order to deal with them theoretically, low-energy effective Hamiltonians are used, which consist of perturbatively calculable Wilson

coefficients and local four-quark operators. The former encode the whole short-distance dynamics of the decay class at hand, whereas the long-distance contributions of a specific channel show up as the corresponding hadronic matrix elements of the four-quark operators. The same formalism applies of course also to non-leptonic kaon decays and is at the basis of the calculations of $\mathrm{Re}(\varepsilon'/\varepsilon)$. The non-leptonic B decays play the key rôle for the exploration of CP violation, since non-vanishing CP asymmetries may be induced by interference effects in such transitions. In general, the theoretical interpretation of such CP asymmetries is affected by large hadronic uncertainties, in analogy to $\mathrm{Re}(\varepsilon'/\varepsilon)$. However, the B-meson system provides tools to deal with these uncertainties: there are fortunate cases, where relations between various decay amplitudes allow us to *eliminate* the – essentially unknown – hadronic matrix elements, and we may exploit mixing-induced CP asymmetries, where the hadronic matrix elements *cancel* if the decay is governed by a single CKM amplitude. The latter observables can also be nicely combined with amplitude relations. Following these lines, we may also determine – in addition to the angles of the UT – certain hadronic parameters, which can then be compared with the corresponding theoretical calculations, where also a lot of progress could be made over the recent years.

Thanks to the efforts of the BaBar and Belle collaborations, CP violation could be established in the B-meson system in 2001, with the help of the "golden" mode $B_d \to J/\psi K_{\rm S}$, thereby opening a new era in the exploration of this phenomenon. The current experimental status of the mixing-induced CP asymmetry of this (and similar) channel(s) implies $\sin 2\beta = 0.736 \pm 0.049$, in impressive accordance with the indirect value following from the CKM fits of the UT in the $\bar\rho$–$\bar\eta$ plane. The physics potential of the B factories goes far beyond the famous $B_d \to J/\psi K_{\rm S}$ decay, allowing us now to confront many more strategies to explore CP violation with data. Here the main goal is to overconstrain the UT as much as possible, thereby performing a stringent test of the KM mechanism of CP violation. Important B-factory benchmark modes to complement the $B \to J/\psi K$ system are given by $B \to \pi\pi$ and $B \to \phi K$ decays, and exciting data on these channels are already available. The pattern of the $B \to \pi\pi$ data favours large non-factorizable effects, and the analyses of CP violation in $B_d \to \pi^+\pi^-$ point towards large direct and mixing-induced CP asymmetries, which can be interpreted in terms of $\gamma \sim 65^\circ$, in accordance with the CKM fits. Although the BaBar and Belle measurements of these asymmetries are not yet in full accordance, they already moved towards each other and it seems plausible that they will meet close to the current averages. On the other hand, the Belle measurement of the mixing-induced CP asymmetry of $B_d \to \phi K_{\rm S}$ raises the exciting possibility of having large NP effects in the $\bar b \to \bar s s \bar s$ quark-level processes. However, the corresponding BaBar analysis is consistent with the SM, so that we cannot yet draw firm conclusions. Let us hope that this unsatisfactory experimental situation will be clarified soon.

As far as the exploration of CP violation with the help of amplitude relations is concerned, we distinguish between exact and flavour-symmetry relations. The prototype of the former is provided by $B^\pm \to K^\pm D$ decays, whereas $B_c^\pm \to D_s^\pm D$ transitions offer the ideal theoretical realization of the corresponding triangle strategy to determine the angle γ of the UT. An important example for the application of flavour-symmetry relations is given by $B \to \pi K$ decays. Here the corresponding B-factory data point again to a puzzling pattern, which may be due to the presence of enhanced EW penguins with a large CP-violating NP phase. Although BaBar, Belle and CLEO indicate separately the corresponding "$B \to \pi K$ puzzle", it is still too early for definite conclusions. This kind of NP would yield striking effects in various rare B and K decays, of which an enhancement of the $K_{\rm L} \to \pi^0\nu\bar\nu$ branching ratio by one order of magnitude and a negative value of $(\sin 2\beta)_{\pi\nu\bar\nu}$ would be the most spectacular ones.

Another key element for the testing of the SM description of CP violation is the B_s-meson system, which is not accessible at the e^+e^- B factories operating at the $\Upsilon(4S)$ resonance, BaBar and Belle, but can be studied nicely at hadron collider experiments. Interesting results on B_s physics are soon expected from run II of the Tevatron, where B_s^0–$\bar B_s^0$ mixing should be discovered, which is an important ingredient for the CKM fits of the UT. The most prominent B_s decays include $B_s \to J/\psi\phi$, which is a powerful probe for NP contributions to B_s^0–$\bar B_s^0$ mixing manifesting themselves through a sizeable value of ϕ_s; $B_s \to K^+K^-$, which can be combined with $B_d \to \pi^+\pi^-$ through the U-spin flavour symmetry to

determine γ; and $B_s \to D_s^{(*)\pm} K^{\mp}$ modes, which allow clean determinations of $\phi_s + \gamma$ and can be combined in a variety of ways with their $B_d \to D^{(*)\pm}\pi^{\mp}$ counterparts, offering advantages from the practical point of view. Although the Tevatron will provide first insights into these decays, they can only be fully exploited at the experiments of the LHC era, in particular LHCb and BTeV.

Finally, it should be emphasized again that it is crucial to complement the studies of CP violation with measurements of rare B and K decays, which are sensitive probes for NP. Moreover, it is important to keep also an eye on the D-meson system, which exhibits tiny mixing and CP-violating effects in the SM [121], as well as on various other interesting aspects of flavour physics, such as flavour-violating charged-lepton decays (for a very recent study, see [194]), which we could not cover in these lectures.

In this decade, the successful exploration of flavour physics and CP violation will certainly be continued, thereby leading to many further exciting results and valuable new insights. Let us hope that eventually also several "surprises" can be established, shedding light on the physics beyond the SM!

ACKNOWLEDGEMENTS

I would like to thank the students for their interest in my lectures, the discussion leaders for their efforts to complement them in the discussion sessions, and the local organizers for hosting this exciting school in Armenia. I am also grateful to my collaborators for the fun we had working on many of the topics addressed in these lectures.

References

[1] J.H. Christenson, J.W. Cronin, V.L. Fitch and R. Turlay, Phys. Rev. Lett. **13** (1964) 138.

[2] V. Fanti *et al.* [NA48 Collaboration], Phys. Lett. **B465** (1999) 335.

[3] A. Alavi-Harati *et al.* [KTeV Collaboration], Phys. Rev. Lett. **83** (1999) 22.

[4] B. Aubert *et al.* [BaBar Collaboration], Phys. Rev. Lett. **87** (2001) 091801.

[5] K. Abe *et al.* [Belle Collaboration], Phys. Rev. Lett. **87** (2001) 091802.

[6] I. Aitchison, lectures given at this school.

[7] G. Gabadadze, lectures given at this school.

[8] Y. Grossman, Int. J. Mod. Phys. **A19** (2004) 907;
J.R. Ellis, CERN-TH/2002-339 [hep-ph/0211322], talk given at 1st International Workshop on Frontier Science: Charm, Beauty, and CP, Frascati, Rome, Italy, 6–11 October 2002;
A. Masiero and O. Vives, Annu. Rev. Nucl. Part. Sci. **51** (2001) 161;
L. Wolfenstein, Phys. Rev. **D57** (1998) 6857;
M. Gronau and D. London, Phys. Rev. **D55** (1997) 2845;
Y. Nir and H.R. Quinn, Annu. Rev. Nucl. Part. Sci. **42** (1992) 211.

[9] Y. Grossman, Y. Nir and R. Rattazzi, Adv. Ser. Direct. High Energy Phys. **15** (1998) 755.

[10] S. Petkov, lectures given at this school.

[11] G. Altarelli and F. Feruglio, hep-ph/0306265.

[12] A. De Rujula, M.B. Gavela and P. Hernandez, *Nucl. Phys.* **B547** (1999) 21;
K. Dick, M. Freund, M. Lindner and A. Romanino, *Nucl. Phys.* **B562** (1999) 29;
P. Huber, M. Lindner, M. Rolinec, T. Schwetz and W. Winter, hep-ph/0403068.

[13] I. Tkachev, lectures given at this school.

[14] For a recent discussion, see also W. Buchmüller, DESY-03-068 [hep-ph/0306047].

[15] A.D. Sakharov, JETP Lett. **5** (1967) 24.

[16] V.A. Rubakov, M.E. Shaposhnikov, Usp. Fiz. Nauk **166** (1996) 493; Phys. Usp. **39** (1996) 461; A. Riotto and M. Trodden, Annu. Rev. Nucl. Part. Sci. **49** (1999) 35.

[17] *The BaBar Physics Book*, eds. P. Harrison and H.R. Quinn, SLAC-R-504 (1998).

[18] K. Anikeev *et al.*, FERMILAB-Pub-01/197 [hep-ph/0201071].

[19] P. Ball *et al.*, CERN-TH/2000-101 [hep-ph/0003238], in CERN Report on *Standard Model physics (and more) at the LHC* (CERN, Geneva, 2000), p. 305.

[20] G. Branco, L. Lavoura and J. Silva, *CP Violation* (Oxford Science Publications, Clarendon Press, Oxford, 1999); I.I. Bigi and A.I. Sanda, *CP Violation* (Cambridge Monographs on Particle Physics, Nuclear Physics and Cosmology, Cambridge University Press, Cambridge, 2000).

[21] A.J. Buras and R. Fleischer, Adv. Ser. Direct. High Energy Phys. **15** (1998) 65.

[22] A.J. Buras, hep-ph/9806471, lectures given at Summer School on Theoretical Physics: Probing the Standard Model of Particle Interactions, Les Houches, France, 28 July – 5 September 1997.

[23] Y. Nir, hep-ph/9911321, lectures given at 27th SLAC Summer Institute on Particle Physics: CP Violation in and Beyond the Standard Model (SSI 99), Stanford, CA, 7–16 July 1999.

[24] J. Rosner, hep-ph/0011355, lectures given at Theoretical Advanced Study Institute in Elementary Particle Physics (TASI 2000): Flavor Physics for the Millenium, Boulder, CO, 4–30 June 2000.

[25] Z. Ligeti, hep-ph/0302031, lectures given at 30th SLAC Summer Institute on Particle Physics: Secrets of the B Meson (SSI 2002), Stanford, CA, 5–16 August 2002.

[26] R. Fleischer, Phys. Rep. **370** (2002) 531.

[27] S.L. Glashow, Nucl. Phys. **22** (1961) 579;
S. Weinberg, Phys. Rev. Lett. **19** (1967) 1264;
A. Salam, in *Elementary Particle Theory*, ed. N. Svartholm (Almqvist and Wiksell, Stockholm, 1968).

[28] N. Cabibbo, Phys. Rev. Lett. **10** (1963) 531.

[29] M. Kobayashi and T. Maskawa, Progr. Theor. Phys. **49** (1973) 652.

[30] S.L. Glashow, J. Iliopoulos and L. Maiani, Phys. Rev. **D2** (1970) 1285.

[31] K. Hagiwara *et al.* [Particle Data Group], Phys. Rev. **D66** (2002) 010001.

[32] H. Fritzsch and Z.-Z. Xing, Phys. Lett. **B413** (1997) 396.

[33] C. Jarlskog, Phys. Rev. Lett. **55** (1985) 1039; Z. Phys. **C29** (1985) 491.

[34] J. Bernabeu, G. Branco and M. Gronau, Phys. Lett. **B169** (1986) 243.

[35] L. Wolfenstein, Phys. Rev. Lett. **51** (1983) 1945.

[36] A.J. Buras, M.E. Lautenbacher and G. Ostermaier, Phys. Rev. **D50** (1994) 3433.

[37] A.J. Buras, hep-ph/0101336, lectures given at Erice International School of Subnuclear Physics: Theory and Experiment Heading for New Physics, Erice, Italy, 27 August – 5 September 2000.

[38] R. Aleksan, B. Kayser and D. London, Phys. Rev. Lett. **73** (1994) 18.

[39] C. Jarlskog and R. Stora, Phys. Lett. **B208** (1988) 268.

[40] L.L. Chau and W.-Y. Keung, Phys. Rev. Lett. **53** (1984) 1802.

[41] M. Battaglia *et al.*, CERN 2003-002-corr [hep-ph/0304132].

[42] J.R. Batley *et al.* [NA48 Collaboration], Phys. Lett. **B544** (2002) 97.

[43] A. Alavi-Harati *et al.* [KTeV Collaboration], Phys. Rev. **D67** (2003) 012005.

[44] A.J. Buras and M. Jamin, JHEP **0401** (2004) 048.

[45] G. Buchalla and A.J. Buras, Phys. Lett. **B333** (1994) 221; Phys. Rev. **D54** (1996) 6782.

[46] G. D'Ambrosio and G. Isidori, Phys. Lett. **B530** (2002) 108.

[47] R. Fleischer, G. Isidori and J. Matias, JHEP **0305** (2003) 053.

[48] A.J. Buras, R. Fleischer, S. Recksiegel, F. Schwab, CERN-PH-TH/2004-020 [hep-ph/0402112].

[49] G. Isidori, eConf **C0304052** (2003) WG304 [hep-ph/0307014].

[50] S.H. Kettell, L.G. Landsberg and H.H. Nguyen, FERMILAB-FN-0727 [hep-ph/0212321].

[51] V.V. Anisimovsky *et al.* [E949 Collaboration], BNL/72164-2004-JA [hep-ex/0403036].

[52] S. Adler *et al.* [E787 Collaboration], Phys. Rev. Lett. **88** (2002) 041803; BNL-72163-2004-JA [hep-ex/0403034].

[53] A. Alavi-Harati *et al.* [E799-II/KTeV Collaboration], Phys. Rev. **D61** (2000) 072006.

[54] A.J. Buras, R. Fleischer, S. Recksiegel and F. Schwab, *Phys. Rev. Lett.* **92** (2004) 101804.

[55] D.E. Jaffe, hep-ex/0311053.

[56] M. Lüscher, Annales Henri Poincare **4** (2003) S197 [hep-ph/0211220].

[57] A. Khodjamirian, lectures given at this school [hep-ph/0403145].

[58] F. De Fazio, hep-ph/0010007.

[59] D.G. Cassel, eConf **C0304052** (2003) WG501 [hep-ex/0307038].

[60] N. Isgur and M.B. Wise, Phys. Lett. **B232** (1989) 113 and **B237** (1990) 527.

[61] M. Neubert, Phys. Rep. **245** (1994) 259.

[62] M. Neubert, Phys. Lett. **B264** (1991) 455.

[63] M.E. Luke, Phys. Lett. **B252** (1990) 447.

[64] F.J. Gilman and M.B. Wise, Phys. Rev. **D20** (1979) 2392;
G. Altarelli, G. Curci, G. Martinelli and S. Petrarca, Phys. Lett. **B99** (1981) 141;
A.J. Buras and P.H. Weisz, Nucl. Phys. **B333** (1990) 66.

[65] G. Buchalla, A.J. Buras and M.E. Lautenbacher, Rev. Mod. Phys. **68** (1996) 1125.

[66] M. Bander, D. Silverman and A. Soni, Phys. Rev. Lett. **43** (1979) 242.

[67] R. Fleischer, Z. Phys. **C58** (1993) 483.

[68] A.J. Buras and R. Fleischer, Phys. Lett. **B341** (1995) 379.

[69] M. Ciuchini, E. Franco, G. Martinelli, M. Pierini and L. Silvestrini, Phys. Lett. **B515** (2001) 33;
C. Isola, M. Ladisa, G. Nardulli, T.N. Pham and P. Santorelli, Phys. Rev. **D65** (2002) 094005;
C.W. Bauer, D. Pirjol, I.Z. Rothstein and I.W. Stewart, MIT-CTP-3469 [hep-ph/0401188].

[70] R. Fleischer, Z. Phys. **C62** (1994) 81; Phys. Lett. **B321** (1994) 259 and **B332** (1994) 419.

[71] R. Fleischer, Int. J. Mod. Phys. **A12** (1997) 2459.

[72] N.G. Deshpande and X.-G. He, Phys. Rev. Lett. **74** (1995) 26 [E: ibid., p. 4099];
M. Gronau, O.F. Hernandez, D. London and J.L. Rosner, Phys. Rev. **D52** (1995) 6374.

[73] M. Neubert, B. Stech, Adv. Ser. Direct. High Energy Phys. **15** (1998) 294, and references therein.

[74] A.J. Buras and J.-M. Gérard, Nucl. Phys. **B264** (1986) 371;
A.J. Buras, J.-M. Gérard and R. Rückl, Nucl. Phys. **B268** (1986) 16.

[75] M. Beneke, G. Buchalla, M. Neubert and C. Sachrajda, Phys. Rev. Lett. **83** (1999) 1914; Nucl. Phys. **B591** (2000) 313; Nucl. Phys. **B606** (2001) 245.

[76] J.D. Bjorken, Nucl. Phys. (Proc. Suppl.) **B11** (1989) 325;
M. Dugan and B. Grinstein, Phys. Lett. **B255** (1991) 583;
H.D. Politzer and M.B. Wise, Phys. Lett. **B257** (1991) 399.

[77] H.-n. Li and H.L. Yu, Phys. Rev. **D53** (1996) 2480;
Y.Y. Keum, H.-n. Li and A.I. Sanda, Phys. Lett. **B504** (2001) 6;
Y.Y. Keum and H.-n. Li, Phys. Rev. **D63** (2001) 074006;
Y.Y. Keum and A.I. Sanda, eConf **C0304052** (2003) WG420 [hep-ph/0306004].

[78] C.W. Bauer, D. Pirjol and I.W. Stewart, Phys. Rev. Lett. **87** (2001) 201806;
C.W. Bauer, B. Grinstein, D. Pirjol and I.W. Stewart, Phys. Rev. **D67** (2003) 014010.

[79] A. Khodjamirian, Nucl. Phys. **B605** (2001) 558;
A. Khodjamirian, T. Mannel and B. Melic, Phys. Lett. **B571** (2003) 75.

[80] A.J. Buras, M. Jamin and P.H. Weisz, Nucl. Phys. **B347** (1990) 491;
J. Urban, F. Krauss, U. Jentschura and G. Soff, Nucl. Phys. **B523** (1998) 40.

[81] T. Inami and C.S. Lim, Prog. Theor. Phys. **65** (1981) 297 [E: ibid., p. 1772].

[82] A.J. Buras, hep-ph/0307203, lectures given at 41st International University School of Theoretical Physics: Flavour Physics (IUTP 41), Schladming, Styria, Austria, 22–28 February 2003.

[83] S. Laplace, Z. Ligeti, Y. Nir and G. Perez, Phys. Rev. **D65** (2002) 094040.

[84] M. Beneke, G. Buchalla, A. Lenz and U. Nierste, Phys. Lett. **B576** (2003) 173;
M. Ciuchini, E. Franco, V. Lubicz, F. Mescia and C. Tarantino, JHEP **0308** (2003) 031.

[85] B Oscillations Working Group: `http://lepbosc.web.cern.ch/LEPBOSC/`.

[86] Heavy Flavour Averaging Group: `http://www.slac.stanford.edu/xorg/hfag/`.

[87] R. Fleischer, Eur. Phys. J. **C10** (1999) 299.

[88] A.B. Carter and A.I. Sanda, Phys. Rev. Lett. **45** (1980) 952, Phys. Rev. **D23** (1981) 1567;
I.I. Bigi and A.I. Sanda, Nucl. Phys. **B193** (1981) 85.

[89] B. Aubert *et al.* [BABAR Collaboration], Phys. Rev. Lett. **89** (2002) 201802.

[90] K. Abe *et al.* [Belle Collaboration], BELLE-CONF-0353 [hep-ex/0308036].

[91] R. Fleischer and T. Mannel, Phys. Lett. **B506** (2001) 311.

[92] H. Boos, T. Mannel and J. Reuter, SI-HEP-2004-04 [hep-ph/0403085].

[93] Ya.I. Azimov, V.L. Rappoport and V.V. Sarantsev, Z. Phys. **A356** (1997) 437;
Y. Grossman and H.R. Quinn, Phys. Rev. **D56** (1997) 7259;
J. Charles *et al.*, Phys. Lett. **B425** (1998) 375 [E: **B433** (1998) 441];
B. Kayser and D. London, Phys. Rev. **D61** (2000) 116012;
H.R. Quinn, T. Schietinger, J.P. Silva and A.E. Snyder, Phys. Rev. Lett. **85** (2000) 5284.

[94] A.S. Dighe, I. Dunietz and R. Fleischer, Phys. Lett. **B433** (1998) 147.

[95] I. Dunietz, R. Fleischer and U. Nierste, Phys. Rev. **D63** (2001) 114015.

[96] R. Fleischer, Phys. Lett. **B459** (1999) 306.

[97] M. Gronau and D. London, Phys. Rev. Lett. **65** (1990) 3381.

[98] J.P. Silva and L. Wolfenstein, Phys. Rev. **D49** (1994) 1151.

[99] R. Fleischer and T. Mannel, Phys. Lett. **B397** (1997) 269.

[100] Y. Grossman and H.R. Quinn, Phys. Rev. **D58** (1998) 017504.

[101] J. Charles, Phys. Rev. **D59** (1999) 054007.

[102] M. Gronau, D. London, N. Sinha and R. Sinha, Phys. Lett. **B514** (2001) 315

[103] H. Jawahery, talk given at Lepton–Photon 2003, Fermilab, Batavia, IL, 11–16 August 2003, `http://conferences.fnal.gov/lp2003/`.

[104] K. Abe *et al.* [Belle Collaboration], Phys. Rev. **D68** (2003) 012001.

[105] R. Fleischer and J. Matias, Phys. Rev. **D66** (2002) 054009.

[106] B. Aubert *et al.* [BaBar Collaboration], Phys. Rev. Lett. **91** (2003) 241801.

[107] K. Abe *et al.* [Belle Collaboration], Phys. Rev. Lett. **91** (2003) 261801.

[108] M. Beneke and M. Neubert, Nucl. Phys. **B675** (2003) 333.

[109] A. Ali, E. Lunghi and A.Y. Parkhomenko, DESY-04-036 [hep-ph/0403275].

[110] C.W. Chiang, M. Gronau, J.L. Rosner and D.A. Suprun, MADPH-04-1372 [hep-ph/0404073].

[111] G. Buchalla and A.S. Safir, LMU-25-03 [hep-ph/0310218];
F.J. Botella and J.P. Silva, hep-ph/0312337.

[112] D. London and R.D. Peccei, Phys. Lett. **B223** (1989) 257;
N.G. Deshpande and J. Trampetic, Phys. Rev. **D41** (1990) 895 and 2926;
J.-M. Gérard and W.-S. Hou, Phys. Rev. **D43** (1991) 2909; Phys. Lett. **B253** (1991) 478.

[113] N.G. Deshpande and X.-G. He, Phys. Lett. **B336** (1994) 471.

[114] Y. Grossman and M.P. Worah, Phys. Lett. **B395** (1997) 241.

[115] D. London and A. Soni, Phys. Lett. **B407** (1997) 61.

[116] R. Fleischer and T. Mannel, Phys. Lett. **B511** (2001) 240.

[117] T. Browder, hep-ex/0312024, talk given at Lepton–Photon 2003, Fermilab, Batavia, IL, 11–16 August 2003, `http://conferences.fnal.gov/lp2003/`.

[118] B. Aubert *et al.* [BaBar Collaboration], BABAR-PUB-04-004 [hep-ex/0403026].

[119] K. Abe *et al.* [Belle Collaboration], Phys. Rev. Lett. **91** (2003) 261602.

[120] G. Hiller, Phys. Rev. **D66** (2002) 071502;
A. Datta, Phys. Rev. **D66** (2002) 071702;
M. Raidal, Phys. Rev. Lett. **89** (2002) 231803;
B. Dutta, C.S. Kim and S. Oh, Phys. Rev. Lett. **90** (2003) 011801;
C.W. Chiang and J.L. Rosner, Phys. Rev. **D68** (2003) 014007;
C.K. Chua, W.S. Hou and M. Nagashima, hep-ph/0308298.

[121] A.A. Petrov, WSU-HEP-0314 [hep-ph/0311371].

[122] A.J. Buras, Acta Phys. Polon. **B34** (2003) 5615.

[123] A.J. Buras, P. Gambino, M. Gorbahn, S. Jäger and L. Silvestrini, Phys. Lett. **B500** (2001) 161.

[124] G. D'Ambrosio, G.F. Giudice, G. Isidori and A. Strumia, Nucl. Phys. **B645** (2002) 155.

[125] C. Bobeth, T. Ewerth, F. Krüger and J. Urban, Phys. Rev. **D66** (2002) 074021.

[126] A.J. Buras and R. Fleischer, Phys. Rev. **D64** (2001) 115010.

[127] A.J. Buras and R. Buras, Phys. Lett. **B501** (2001) 223.

[128] M. Gronau and D. Wyler, Phys. Lett. **B265** (1991) 172.

[129] D. Atwood, I. Dunietz, A. Soni, Phys. Rev. Lett. **78** (1997) 3257; Phys. Rev. **D63** (2001) 036005.

[130] F. Abe *et al.* [CDF Collaboration], Phys. Rev. Lett. **81** (1998) 2432.

[131] M. Masetti, Phys. Lett. **B286** (1992) 160.

[132] R. Fleischer and D. Wyler, Phys. Rev. **D62** (2000) 057503.

[133] M.A. Ivanov, J.G. Körner and O.N. Pakhomova, Phys. Lett. **B555** (2003) 189.

[134] R. Fleischer, Phys. Lett. **B365** (1996) 399.

[135] R. Fleischer and T. Mannel, Phys. Rev. **D57** (1998) 2752.

[136] M. Gronau and J.L. Rosner, Phys. Rev. **D57** (1998) 6843.

[137] R. Fleischer, Eur. Phys. J. **C6** (1999) 451.

[138] M. Neubert and J.L. Rosner, Phys. Lett. **B441** (1998) 403; Phys. Rev. Lett. **81** (1998) 5076.

[139] M. Neubert, JHEP **9902** (1999) 014.

[140] A.J. Buras and R. Fleischer, Eur. Phys. J. **C11** (1999) 93.

[141] A.J. Buras and R. Fleischer, Eur. Phys. J. **C16** (2000) 97.

[142] M. Gronau, J.L. Rosner and D. London, Phys. Rev. Lett. **73** (1994) 21.

[143] R. Fleischer and J. Matias, Phys. Rev. **D61** (2000) 074004.

[144] T. Yoshikawa, Phys. Rev. **D68** (2003) 054023.

[145] M. Gronau and J.L. Rosner, Phys. Lett. **B572** (2003) 43.

[146] A.J. Buras, R. Fleischer, S. Recksiegel and F. Schwab, Eur. Phys. J. **C32** (2003) 45.

[147] R. Fleischer and T. Mannel, TTP-97-22 [hep-ph/9706261].

[148] Y. Grossman, M. Neubert and A.L. Kagan, JHEP **9910** (1999) 029.

[149] B. Aubert *et al.* [BaBar Collaboration], BABAR-PUB-04-005 [hep-ex/0403001].

[150] A.A. Penin and M. Steinhauser, Phys. Rev. **D65** (2002) 054006;
M. Jamin and B.O. Lange, Phys. Rev. **D65** (2002) 056005;
K. Hagiwara, S. Narison and D. Nomura, Phys. Lett. **B540** (2002) 233.

[151] I. Dunietz, Phys. Rev. **D52** (1995) 3048.

[152] R. Fleischer and I. Dunietz, Phys. Rev. **D55** (1997) 259.

[153] R. Fleischer and I. Dunietz, Phys. Lett. **B387** (1996) 361.

[154] A.S. Dighe, I. Dunietz, H.J. Lipkin and J.L. Rosner, Phys. Lett. **B369** (1996) 144.

[155] A.S. Dighe, I. Dunietz and R. Fleischer, Eur. Phys. J. **C6** (1999) 647.

[156] R. Fleischer, Phys. Rev. **D60** (1999) 073008.

[157] A. Belkov, S. Shulga, Part. Nucl. Lett. **117** (2003) 11; Comput. Phys. Commun. **156** (2004) 221.

[158] R. Fleischer, Phys. Lett. **B562** (2003) 234.

[159] R. Fleischer, Nucl. Phys. **B659** (2003) 321.

[160] M. Gronau and J.L. Rosner, Phys. Lett. **B482** (2000) 71.

[161] P.Z. Skands, JHEP **0101** (2001) 008.

[162] G. Balbi *et al.*, CERN-LHCb/2003-123 and 124;
R. Antunes Nobrega *et al.* [LHCb Collaboration], *Reoptimized LHCb Detector, Design and Performance*, Technical Design Report 9, CERN/LHCC 2003-030.

[163] A. Khodjamirian, T. Mannel and M. Melcher, Phys. Rev. **D68** (2003) 114007.

[164] M. Beneke, eConf **C0304052** (2003) FO001 [hep-ph/0308040].

[165] R. Fleischer, Eur. Phys. J. **C16** (2000) 87.

[166] A.J. Buras, F. Parodi and A. Stocchi, JHEP **0301** (2003) 029.

[167] K. Abe *et al.* [Belle Collaboration], BELLE-PREPRINT-2004-1 [hep-ex/0401029].

[168] R. Aleksan, I. Dunietz and B. Kayser, Z. Phys. **C54** (1992) 653.

[169] I. Dunietz and R.G. Sachs, Phys. Rev. **D37** (1988) 3186 [E: **D39** (1989) 3515];
I. Dunietz, Phys. Lett. **B427** (1998) 179;
D.A. Suprun, C.W. Chiang and J.L. Rosner, Phys. Rev. **D65** (2002) 054025.

[170] R. Fleischer, Nucl. Phys. **B671** (2003) 459.

[171] B. Aubert *et al.* [BaBar Collaboration], BABAR-PUB-03-033 [hep-ex/0310037].

[172] K. Abe *et al.* [Belle Collaboration], BELLE-CONF-0341 [hep-ex/0308048].

[173] A.J. Buras and M. Misiak, Acta Phys. Polon. **B33** (2002) 2597.

[174] G. Buchalla, A.J. Buras and M.K. Harlander, Nucl. Phys. **B349** (1991) 1.

[175] A.J. Buras and M.K. Harlander, Adv. Ser. Direct. High Energy Phys. **10** (1992) 58.

[176] A. Ali, CERN-TH/2002-284 [hep-ph/0210183];
T. Hurth, Rev. Mod. Phys. **75** (2003) 1159;
K. Bieri and C. Greub, hep-ph/0310214.

[177] G. Buchalla and A.J. Buras, Nucl. Phys. **B548** (1999) 309.

[178] G. Buchalla and A.J. Buras, Nucl. Phys. **B400** (1993) 225.

[179] M. Misiak and J. Urban, Phys. Lett. **B451** (1999) 161.

[180] D. Acosta *et al.* [CDF Collaboration], FERMILAB-PUB-036-E [hep-ex/0403032];
M.C. Chang *et al.* [Belle Collaboration], Phys. Rev. **D68** (2003) 111101.

[181] A.J. Buras, Phys. Lett. **B566** (2003) 115.

[182] A.J. Buras, TUM-HEP-544-04 [hep-ph/0402191].

[183] G. Buchalla and A.J. Buras, Nucl. Phys. **B398** (1993) 285.

[184] A.J. Buras and L. Silvestrini, Nucl. Phys. **B546** (1999) 299.

[185] A.J. Buras, G. Colangelo, G. Isidori, A. Romanino, L. Silvestrini, Nucl. Phys. **B566** (2000) 3;
A.J. Buras, A. Romanino and L. Silvestrini, Nucl. Phys. **B520** (1998) 3.

[186] G. Buchalla, G. Hiller and G. Isidori, Phys. Rev. **D63** (2001) 014015;
D. Atwood and G. Hiller, hep-ph/0307251.

[187] V. Barger, C.W. Chiang, P. Langacker and H.S. Lee, Phys. Lett. **B580** (2004) 186.

[188] J. Kaneko *et al.* [Belle Collaboration], Phys. Rev. Lett. **90** (2003) 021801;
B. Aubert *et al.* [BaBar Collaboration], BABAR-CONF-03-19 [hep-ex/0308016].

[189] A. Alavi-Harati *et al.* [KTeV Collaboration], FERMILAB-PUB-03-446 [hep-ex/0309072].

[190] Y. Grossman and Y. Nir, Phys. Lett. **B398** (1997) 163.

[191] G. Buchalla, G. D'Ambrosio and G. Isidori, Nucl. Phys. **B672** (2003) 387.

[192] G. Isidori, C. Smith and R. Unterdorfer, hep-ph/0404127.

[193] S.R. Choudhury, N. Gaur and A.S. Cornell, hep-ph/0402273.

[194] P.H. Chankowski, J.R. Ellis, S. Pokorski, M. Raidal and K. Turzynski, CERN-PH-TH/2004-030 [hep-ph/0403180].